Universität Bremen

Max Planck Institute for Marine Microbiology

# Oxygen dynamics of marine sediments on different spatial scales

Jan P. Fischer

Dissertation
zur Erlangung des Doktorgrades der Naturwissenschaften
- Dr. rer. nat. -

Fachbereich Biologie / Chemie
der Universität Bremen

Bremen, September 2009

Die vorliegende Arbeit wurde in der Zeit von September 2004 bis September 2009 am Max-Planck-Institut für marine Mikrobiologie in Bremen angefertigt.

**Gutachter:**
Prof. Dieter Wolf-Gladrow
Prof. Antje Boetius

**Prüfer:**
Prof. Dr. Ulrich Fischer
Dr. Frank Wenzhöfer

**Weitere Mitglieder des Prüfungsausschusses:**
Christina Bienhold
Katrin Schmidt

Datum des Promotionskolloquiums: 15. Oktober 2009

All phenomena are like a dream,
an illusion, a bubble and a shadow
Like dew and lightning.

Diamond Sūtra, ca. 100 A.D.

# Contents

# List of Figures

# List of Tables

# Zusammenfassung

Oxidation von organischem Material in marinen Sedimenten führt zu einer Zehrung von Sauerstoff und damit zu einem Sauerstofffluss über die Sediment/Wasser Grenze. Dieser Fluss kann verwendet werden um benthische Mineralisationsprozesse zu quantifizieren und er ist verhältnissmäßig leicht zu bestimmen. Die globale Verteilung des Flusses von partikulärem organischem Material zum Meeresboden ist zum großen Teil durch Messungen dieser Sauerstoffaufnahme bestimmt worden. Darüberhinaus können Messungen der Sauerstoffdynamik in photischen Sedimenten Aufschluss über das Ausmaß und die Verteilung benthischer Primärproduktion geben. Die Anzahl an *in-situ* Messungen ist jedoch immer noch relativ begrenzt und in einigen z.T. ausgedehnten Gebieten wie den oligotrophen subtropischen Ozeanen ist die Datenlage kaum ausreichend um benthische Mineralisationsraten abzuschätzen. Auch der Einfluss benthischer Photosynthese auf die Stoffumsätze in den sublitoralen Bereichen der Schelfmeere wurde bisher kaum systematisch erfasst, obwohl eine große Relevanz vermutet wird. Eine Reihe von Studien haben in den letzten Jahren darüberhinaus gezeigt, dass die Sauerstoffdynamik in Sedimenten sowohl räumlich als auch zeitlich auf verschiedenen Skalen stark variiert. Vergleiche zwischen verschiedenen Messungen und Hochrechnungen für größere Gebiete setzen Daten über diese Variabilität und die dabei relevanten Skalen vorraus.

Im Rahmen dieser Arbeit wurde benthische Sauerstoffdynamik sowohl im Labor als auch *in-situ* erforscht. Ziel war es, Mineralisationsprozesse in Sedimenten und deren treibende Kräfte besser zu verstehen. Die untersuchten Längenskalen reichten dabei von ca. 0.1 mm (lichtgetriebene Heterogenität in Respirations- und Produktionsraten in sandigen Küstensedimenten) bis zu mehreren 1000 km (Transekte auf einer Forschungsfahrt im Südpazifik). Für kleinskalige Untersuchungen in 2D wurde die Planar Optoden-Technologie weiterentwickelt. Eine zeitgleiche Messung von Sauerstoffverteilung und Lichtfeld im Sediment, sowie eine deutliche Verbesserung der räumlichen Auflösung der Sauerstoffmessungen konnte erreicht werden. In sandigen Sedimenten wurde ein stark hetereogenes Lichtfeld, hervorgerufen durch Lichtbrechung und -streuung, nachgewiesen. Lokale Photosynthese- und Respirationsraten zeigten eine deutliche Korrelation mit dem Lichtfeld, was auf eine enge und kleinskalige Kopplung zwischen autotrophen und heterotrophen Organismengemeinschaften schließen lässt.

Um Mineralisationsraten und benthische Primärproduktion in subtidalen photischen Küstensedimenten zu erforschen wurde ein *in-situ* Multi-Parameter Ansatz gewählt. Zeitgleiche Messungen mit Planar Optoden, Mikroelektroden und Inkubationskammern, zusammen montiert auf dem benthischen Crawler "C-MOVE", sowie *'Eddy-Correlation'* Messungen ermöglichten es, einen weiten Bereich an Längenskalen abzudecken. Fauna und Makroalgen dominierten die Sauer-

stoffdynamik des Sediments, während einzellige phototrophen Organismen (Mikrophytobenthos) eine weniger große Rolle spielten. Deutliche benthische Photosynthese konnte zwar nachgewiesen werden, jedoch erreichte die Sauerstoffproduktion bei natürlicher Beleuchtung zu keiner Zeit den Sauerstoffbedarf des Sediments. Nach Änderung der Lichtbedingungen oder mechanische Störungen des Sediments dauerte es relativ lange, bis ein neues Fließgleichgewicht der Sauerstoffverteilung eingestellt war. Dies lässt darauf schließen, dass Gleichgewichtszustände in diesen Sedimenten die Ausnahme sind. Ein großer Teil der räumlichen Variabilität und Dynamik der $O_2$-Verteilung im untersuchten Gebiet wurde durch benthische Fauna hervorgerufen.

Die Sedimente des zentralen subtropischen Südpazifik stellen einen deutlichen Kontrast zu den hochdynamischen und produktiven Küstensedimenten dar. Durch *in-situ* und Labormessungen von Mikrosensor-Sauerstoffprofilen konnte die benthische Mineralisationsrate in dieser nährstoffärmsten Zone der Ozeane auf 0.4 bis 1.5 $\mathrm{gC\,m^{-2}\,yr^{-1}}$ eingegrenzt werden. Eine mathematische Modellierung der Profile ergab, dass praktisch der gesamte bioverfügbare organischem Kohlenstoff innerhalb der oberen Millimeter des Sediments aufgezehrt wurde. Die Sauerstoffzehrung war insgesamt so gering dass eine Diffusion von $O_2$ in tiefere Sedimentschichten nicht aufgehalten wurde. Aus diesem Grunde konnten oxische Bedingungen bis in 8 Meter Sedimenttiefe (maximale Länge der geborgenen Kerne) nachgewiesen werden. Dies stellt die größte bisher publizierte Sauerstoffeindringtiefe in marinen Sedimenten dar. Auf zwei, mehrere tausend Kilometer langen Transekten wurden nur vergleichsweise geringe Unterschiede in der Sauerstoffverteilung gemessen und Extrapolationen der tiefen Profile lassen ein komplett oxisches Sediment sowie einen Sauerstofffluss in den darunterliegenden Basalt für weite Teile des Südpazifik vermuten.

# Thesis Abstract

The oxidation of organic material in marine sediments leads to an oxygen uptake and thereby a flux of $O_2$ across the sediment / water interface. This flux, being relatively easy to quantify, is an important parameter in order to assess benthic mineralization rates. Too date, knowledge about global fluxes of particulate organic carbon to the sediments is for the most part derived from benthic oxygen uptake studies. Furthermore, oxygen dynamics in photic sediments gives information about magnitude and distribution of benthic primary production. However, the number of *in situ* studies is still limited and in some areas (e.g., the oligotrophic Subtropical Gyres) not even sufficient to allow for reliable estimates of benthic mineralization rates. The relevance of benthic photosynthesis in shallow subtidal zones is also still largely unexplored. Furthermore, recent work indicates strong spatial variability of sediment oxygen dynamics on various spatial and temporal scales. Knowledge about scales and magnitudes of this variability is essential for site comparison and up-scaling and, again, calls for additional studies of benthic oxygen fluxes and their dynamics.

During this study, benthic oxygen distributions and fluxes were investigated in contrasting environments on very different scales - both in the laboratory and *in situ*. The aim was to improve our understanding of driving factors and distribution of benthic mineralization processes. The studied spatial scales ranged from ∼0.1 mm (light-driven heterogeneities in production- and respiration rates in coastal sandy sediment) to several 1000 km (transects in the South Pacific). For microscale studies in 2D, planar optode technology was further developed. Application of this advanced technology enhanced spatial resolution as well as accuracy, and facilitated the concurrent determination of the light field within the sediments. It was found that diffraction and light scattering in sandy sediments resulted in strong heterogeneities in the distribution of scalar irradiance. Local rates of respiration and photosynthesis were clearly correlated to the irradiance distribution, indicating a tight coupling between autotrophic and heterotrophic communities on a sub millimeter scale.

To study benthic mineralization rates and -primary production in subtidal, photic sediments in the Kattegat, an *in situ* multi-parameter approach was chosen. Using a benthic crawler ('C-MOVE') as a platform, measurements with planar optodes, profiling microelectrodes, and incubation chambers, all attached to the crawler were conducted simultaneously. Complemented with eddy correlation measurements of benthic oxygen fluxes, this approach allowed to cover different aspects of benthic oxygen dynamics on largely different spatial scales. By combining the different measurements it was possible to identify some fundamental characteristics of the chosen area. Considerable benthic primary production was found with a high contribution of macroal-

gae as opposed to microphytobenthos. However, even at high light intensities, the sediments still proved to be net heterotrophic. Changes in light regime and mechanical sediment perturbations resulted in long periods of changing oxygen distributions, indicating that non-steady-state situations are prevalent at that site. Oxygen distribution and fluxes displayed a large spatial variability and dynamics that could, to a large extent, be attributed to faunal activity.

In contrast to this highly dynamic and productive coastal sediment variability and fluxes in the South Pacific Gyre proved to be much smaller. *In situ* and *ex situ* microelectrode oxygen profiling allowed to constrain benthic mineralization rates in this most oligotrophic oceanic region to 0.4 to 1.5 $\mathrm{gC\,m^{-2}\,yr^{-1}}$, around 2% of typical values found in the Kattegat. Mathematical modeling of the microprofiles revealed that almost all bioavailable organic matter was remineralized within the first few millimeters of the sediment. However, oxygen was not used up in the upper sediment layer, diffused further downwards, and was still present at a depth of eight meter below the seafloor as measured with fiber optical sensors on piston cores. These measurements represent the deepest oxygen penetration ever reported. Along transects between the rim and the center of the gyre, little difference in the general pattern of deep oxygen penetration was found and mathematical modeling of the steady state diffusion-reaction equation suggested completely oxic sediments and a flux of oxygen to the underlying basalt, up to 70 m below the sediment surface.

# Chapter 1.

# General Introduction

---

The global cycles of carbon and oxygen are tightly linked and involve atmosphere, oceans and sediments. In the present-day Earth system, oxygenic photosynthesis is the major driving force for (almost) all biogeochemical reactions and the basis for live on earth. Organic matter is produced from inorganic carbon using sunlight as the energy source. This primary production constitutes the basis of the whole biosphere. The rate of oxygen production by photosynthesis is nearly equivalent to the rate of oxygen consumption by aerobic respiration and the oxidation of reduced substances (Fig. 1.1). Therefore, oxygen acts as ultimate electron acceptor for nearly all reduction equivalents produced. While roughly half of the global photosynthesis is conducted by organisms in the photic zone of the oceans, a relevant fraction is produced in shallow, photic sediments. Part of the marine production ultimately accumulates in marine sediments, where it is slowly recycled by an active and diverse (microbial) community. This remineralization ultimately leads to a release of $CO_2$ and nutrients back to sediment pore water and the water column. Marine sediments therefore constitute an important compartment in the global cycles of oxygen and carbon.

## 1.1. Pelagic carbon cycle

The largest marine carbon pool is comprised of dissolved inorganic carbon (DIC) and is directly coupled with the atmosphere (Fig. 1.1). This exchange of $CO_2$ across the air-sea interface is largely controlled by differences in partial pressure, sea surface temperature, circulation patterns and wind induced sea surface roughness. Carbon dioxide easily dissolves in water, forming carbonic acid, bicarbonate, and carbonate in proportions depending on pH. In the photic zone, photosynthetic organisms, mostly microalgae and cyanobacteria, fix $CO_2$ and build up biomass, thus driving the whole marine food web (Fig. 1.1). The annual mean marine primary production of 30-60 Pg of organic carbon ($1\,\mathrm{Pg} = 10 \times 10^{15}\,\mathrm{g}$, equal to a graphite cube with an edge length of 3000 m.) (Duarte and Cebrian, 1996), account for 30% (Houghton, 2007) to 48% (Field et al.,

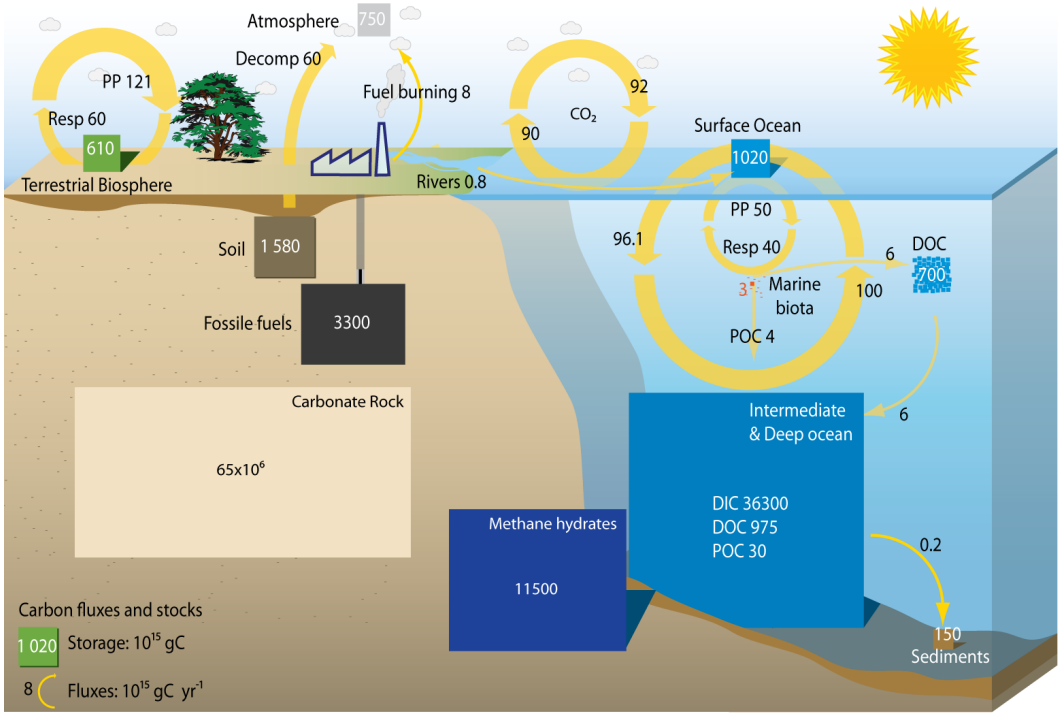


Figure 1.1.: Simplified global carbon cycle, modified after (Pravettoni, 2009). Reservoirs are given in GtC and fluxes in GtC $\mathrm{yr}^{-1}$. Primary production is indicated by PP and respiration by Resp. The global methane hydrate inventory (after MacDonald, 1990) comprises oceanic margins and permafrost soils. Partitioning of the deep ocean carbon pool after Houghton (2007). Note that the reservoir size of carbonate rock is not to scale. Gross fluxes generally have uncertainties of more than $\pm 20\%$ but fractional amounts have been retained to achieve overall balance when including estimates in fractions of GtC $\mathrm{yr}^{-1}$ for riverine transport, weathering, deep ocean burial, etc. (Denman et al., 2007). All other data: IPCC 2001.

1998) of the total primary production on earth. It is carried out by a phytoplankton biomass of only 1 Pg (Carr et al., 2006). The turnover of carbon in the oceans is therefore high, the amount of living carbon is small and the cycle between photosynthesis and respiration is rapid compared to that on land. The organic matter export to greater depths depends on the effectiveness of remineralization processes throughout the water column. Only a small fraction of the surface primary production reaches deep layers (1-3% Jahnke, 1996); (∼5% Romankevich et al., 1999). Several empirical models, mostly based on sediment trap and surface chlorophyll data, have been established to describe the (exponential) relationship between this proportion and water depth (Suess, 1980, Betzer et al., 1984, Berger et al., 1987, Pace et al., 1987, Antia et al., 2001). However, the relationship is not fixed and varies with surface productivity (Wenzhöfer and Glud, 2002). Accumulation of organic material within marine sediments stimulates an intense and highly spatially organized remineralization.

## 1.2. Early diagenesis

Steady settling of organic and mineral particles from the surface ocean form the marine sediments. They take an important regulatory function in the marine carbon cycle, since they have a large storage capacity for organic carbon and nutrients and recycle them on different time scales (Smith and Hollibaugh, 1993). Through this benthic-pelagic coupling, sediments reflect processes occurring in the water column. They thus affect not only the balance of $CO_2$ and $O_2$ in the bottom water but also nutrient concentrations (Martin and Sayles, 2006). Diagenesis is the general term for processes taking place after the deposition of sedimented material on the seafloor (Berner, 1980). The alterations of the sediments can be due to physical forces, (abiotic) chemical reactions, biologically catalyzed reactions, and transport phenomena. The chemical constitution of marine sediments is largely controlled by the remineralization of organic matter due to microorganisms, inhabiting the pore space between the sediment grains. The relevant timescales of remineralization are dependent on the depth and the activity of the benthic community and the respective compounds. They range from hours for highly active coastal sediments and microbial mats, to geological time scales for burial in sediments (Gehlen et al., 2006). However, only 0.2 - 0.4% of the marine primary production gets ultimately buried (Berner, 1982).

### 1.2.1. Pathways of organic carbon mineralization in marine sediments

The top layer of sediments is usually dominated by aerobic metabolism. The high electronegativity of molecular oxygen makes it the most favorable abundant electron acceptor. Pathways relying on other electron acceptors are thermodynamically far less efficient and are outcompeted in oxic environments. The microbial consumption of $O_2$ leads to a depletion of oxygen with depth. Below the oxic horizon, carbon oxidation may be coupled to denitrification, followed by manganese reduction, iron reduction, sulfate reduction and carbonate reduction to methane in successively deeper layers (Fig. 1.2)(e.g. Froelich et al., 1979, Bender and Heggie, 1984, Canfield

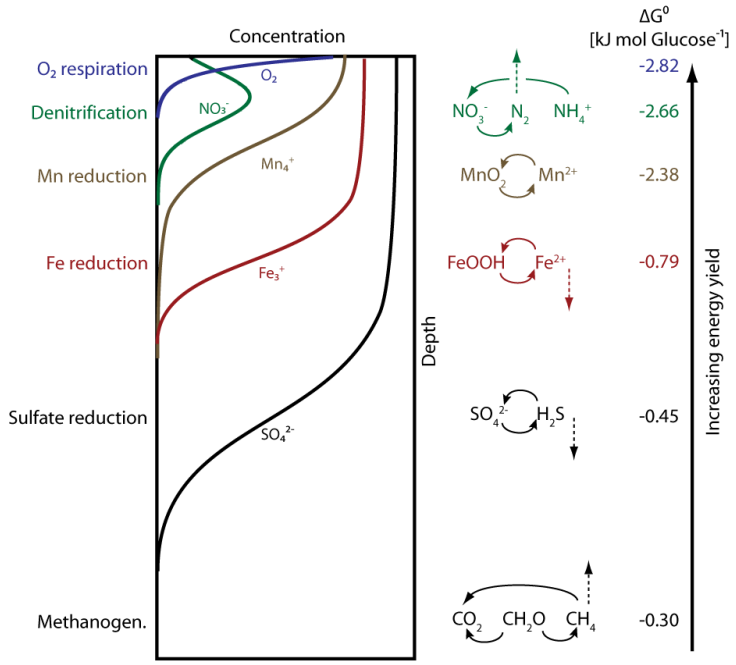


Figure 1.2.: Middle: Idealized vertical sequence of electron acceptors in marine Sediments Left: Simplified scheme of reoxidation of inorganic metabolites with oxygen. Vertical arrows indicate metabolites that escape reoxidation (modified after Canfield et al., 2005). Right: Standard free energy changes for the different remineralization processes (values after Burdige, 2006).

et al., 1993). However, up to now not all of these processes are directly experimentally accessible, different processes may overlap and the relative importance of the pathways differs regionally (Canfield et al., 1993, Wang et al., 2006) and temporally (Soetaert et al., 1996). Therefore, the ratio of aerobic to anaerobic mineralization is highly variable. In continental margin sediments, not more than 20% of total organic carbon is oxidized aerobically (Canfield et al., 1993, Jørgensen, 1996) while in open-ocean low-productivity zones aerobic oxidation increases in importance and may reach up to 100% as reported in this thesis. Due to the high sulfate concentration of seawater, sulfate reduction dominates the anaerobic oxidation of organic matter (Jørgensen, 1977). The reduced products of anaerobic metabolism (e.g. $H_2S$, $Fe^{2+}$) diffuse upwards and can act as electron donor for other microbially mediated redox reactions. Most reducing equivalents are finally reoxidized by molecular oxygen (Fig. 1.2). Hence oxygen is the terminal electron acceptor of almost all electron equivalents, released during the aerobic and anaerobic oxidation of organic matter. The benthic oxygen uptake is thus nearly equivalent to the total sediment metabolism, independent from the actual partitioning between the different pathways (Bender and Heggie, 1984, Thamdrup and Canfield, 2000, Canfield et al., 2005). Exceptions are the escape of compounds like $N_2$, $CH_4$ or $H_2S$ to the water column, and the permanent burial of reduced substances, especially pyrite. However, these processes generally do not account for more than 15% of the electron equivalents of total carbon mineralization (Canfield et al., 2005).

Furthermore, only 5% of the organic matter that reaches the seafloor is permanently buried and thus escapes remineralization (Martin and Sayles, 2006). Oxygen uptake by marine sediments therefore contains information on benthic mineralization rates and the magnitude and spatial variability of POC fluxes throughout the oceans.

Sediment traps often do not provide accurate results for the mean vertical carbon flux, since sedimentation occurs in episodic events or results are biased due to near bottom lateral currents and high turbulence (e.g. Jahnke et al., 1990, Kozerski, 1994). Hence, a considerable discrepancy between sediment trap data and sediment oxygen demand was found in a 7-year long-term study (Smith and Kaufmann, 1999). The use of benthic oxygen uptake is often a superior measure since it is unaffected by lateral currents, turbulence etc. Benthic oxygen uptake has been studied widely over the last decades and has greatly enhanced our knowledge about global ocean carbon fluxes (Cai and Sayles, 1996, Jahnke, 1996, Wenzhöfer and Glud, 2002, Seiter et al., 2005, e.g.). Recently, Glud (2008) calculated a marine global carbon mineralization rate of $\sim$1.5 Gt C yr$^{-1}$, based on benthic $O_2$ consumption estimations. However, extrapolations of oxygen fluxes for larger areas and longer periods still have to rely on very sparse data sets and values for spatial and temporal variability of oxygen fluxes are poorly constrained for many oceanic regions to date. The subtropical gyres are particularly undersampled (Daneri and Quinones, 2001) and most work in coastal areas is biased towards littoral and estuarine areas around Europe and North America.

### 1.2.2. Controlling factors of benthic oxygen dynamics

**Particulate organic carbon flux -** Rates of benthic microbial processes depend on various factors that change on different time scales. The most important driving force for carbon mineralization in sediments is the availability of organic carbon (Berner, 1980). Since the labile POC content of marine sediments below the photic zone is dominated by the rain of organic matter from the overlying water column, primary production and therefore light and nutrient availability in surface waters strongly affect sediment oxygen dynamics. A high correlation was found between sediment oxygen uptake, oxygen penetration depth, and water depth (Fig. 1.3). One reason is that primary production in the open oceans is generally smaller than in coastal areas. Additionally, a higher fraction of POC can be recycled within the water column in deeper waters. The global distribution of POC fluxes to the seafloor has been extrapolated from benthic $O_2$ fluxes assuming steady state situations (Fig. 1.4, Jahnke 1996; Seiter et al. 2005). It exhibits strong regional differences, spanning at least two orders of magnitude. Highest values are found in western coastal upwelling regions whereas the lowest fluxes are predicted for the central oceans, especially the subtropical gyres. However, the flux of POC to the seafloor is not only spatially heterogeneous, it also varies on inter- and intraanual time scales (Smith et al., 1992, Newton et al., 1994, Romankevich et al., 1999, e.g.), driven by events like algal blooms, El Niño, etc. So far, little is known about this temporal variability since the effort to capture it is enormous and technologies for long term observatories are still emerging. However, the few

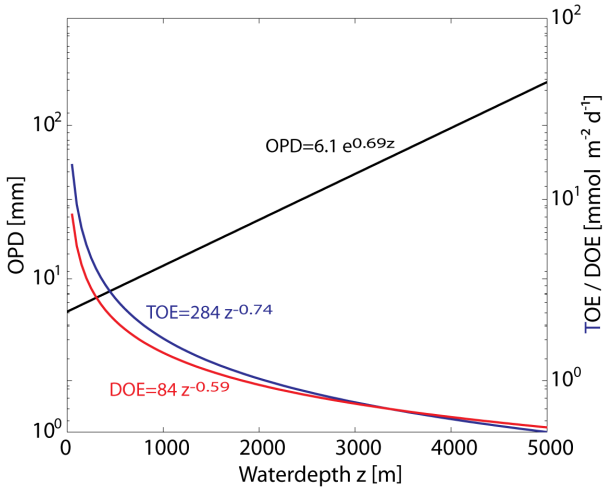


Figure 1.3.: The *in situ* oxygen penetration depth (OPD), total oxygen exchange (TOE) and diffusive oxygen exchange (DOE) plotted against water depth (modified after Glud, 2008).

long-term sediment trap studies (e.g. Smith and Kaufmann, 1999) show a pronounced temporal variability and Witte et al. (2003) report a rapid response of the benthic community to food pulses, even in the deep-sea.

**Bottom water oxygen concentration -** Bottom water oxygen concentration ($BWO_2$) is another controlling factor for the benthic respiration rate. An empirical relationship between organic carbon content in the top layer of the sediment, $BWO_2$, and sediment respiration was established by Cai and Reimers (1995). It shows increasing oxygen fluxes into the sediment with increasing $BWO_2$, following first-order reaction kinetics. Since the preservation of organic matter in marine sediments depends on the time the material is exposed to oxygen (Hartnett et al., 1998), decreasing $BWO_2$ favors a slower decay of the organic matter. This effect is especially important in oxygen-depleted continental margins. Differences in $BWO_2$ on benthic respiration rates play a minor role in the deep-sea, since the amount of labile carbon is low compared to the availability of oxygen. An exception is the northeast Pacific (Seiter et al., 2005). Here, $BWO_2$ is below $\sim$50-70 µmol $L^{-1}$ and shows a strong effect on the decay of organic matter.

**Quality of organic matter -** Particulate organic carbon is not a homogeneous pool but consists of material of different quality in terms of bioavailability that is degraded at different rates (Westrich and Berner, 1984). As a result, the reaction kinetics of organic matter oxidation as a whole is non-linear (Boudreau and Ruddick, 1991). The quality of organic matter (e.g. the bioavailability) decreases with sediment depth, since the easily degradable material is consumed first. Together with the energetically less favorable electron acceptors deeper within the sediment, this is the reason for declining respiration rates with depth. Therefore, the oxygen penetration depth (OPD) depends on quality and quantity of the rain of organic matter from the overlying water column. Sediments in highly oligotrophic regions can be expected to exhibit the deepest oxygen penetration. Wenzhöfer et al. (2001) found *in situ* OPDs of up to 260 mm in the South Atlantic,

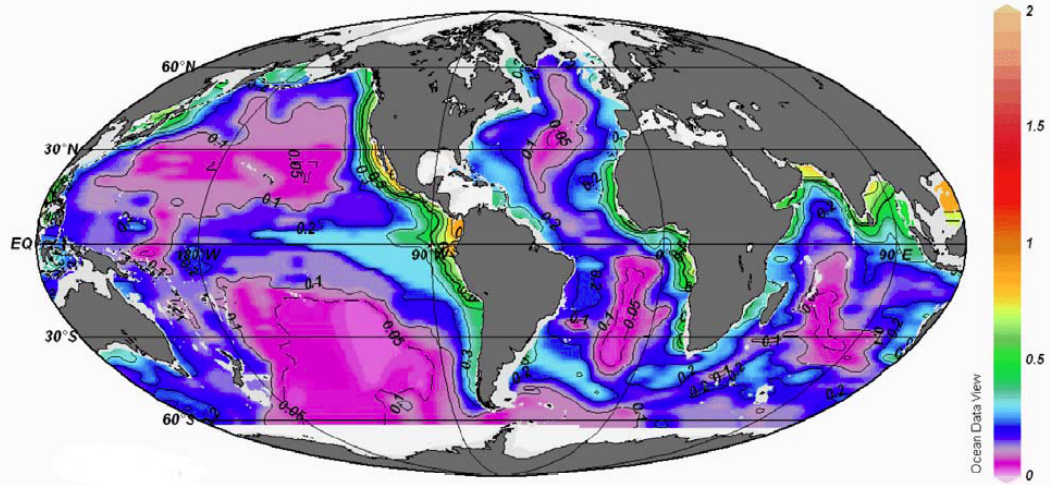


Figure 1.4.: Global benthic $O_2$ flux in mol m-2 yr-1 after Jahnke (1996). Reproduced after JGOF workshop report No. 38 (Fischer et al., 2003).

and Murray and Grundmanis (1980) report oxic conditions in the porewater of equatorial Pacific sediments up to 0.5 m below seafloor (mbsf). So far, the oligotrophic 'marine deserts' are largely understudied. Little is known about oxygen penetration depth and the magnitude of carbon mineralization in these regions where little ground-truthing data are available to calibrate models that extrapolate POC fluxes from remote-sensing ocean color data and water depth.

## 1.3. Coastal sediments

In contrast to the oligotrophic deep-sea, fluxes of organic matter to the sediment in coastal zones are high. Although shelf sediments (<1000 m water depth) cover only 7% of the total ocean surface they account for half of the benthic remineralization (Glud, 2008) and thus play a crucial role in the global carbon cycle. The high load of organic matter in coastal sediments often leads to oxygen depletion within the first millimeters. Oxygen uptake on the shelf is generally much more dynamic than in the open ocean: Effects of seasonality (algal blooms) are not buffered by the averaging effect of a deep water column. Riverine input of terrestrial organic material leads to increased respiration and the increased nutrient load stimulates primary production. Furthermore, coastal sediments often experience strong physical forcing due to wind induced surface currents and waves, leading to sediment resuspension.

### 1.3.1. Benthic photosynthesis

Heterotrophic communities in aphotic sediments depend on settled material as both a carbon source and an electron donor. In shallow, light exposed sediments, however, benthic primary production (BPP) by single-celled photosynthetic organisms (microphytobenthos, MPB) and macrophytes build up a considerable amount of organic carbon directly in the top layer of the

sediment. This has a major influence on the carbon content and oxygen budget of these sediments. Benthic primary production often exceeds the production in the overlying water column (MacIntyre et al., 1996, Underwood and Kromkamp, 1999) and it is highly dependent on light conditions (e.g. Billerbeck et al., 2007). Especially at strong irradiances, photoexudates are produced, which directly fuel heterotrophic respiration (De Brouwer and Stal, 2001). These extracellular polymeric substances (EPS) can also alter the sediments physical properties like permeability and erodability to a relevant degree (e.g. Stal, 2010). Furthermore, the $O_2$ release rate of MPB rapidly changes over time with light availability. Strong illumination leads to oxygen super-saturation of the first millimeters in addition to the possible formation of gas-bubbles. The oxygen distribution responds relatively fast upon changes in light conditions due to diel cycles, shading by clouds, etc., resulting in variable OPDs and uptake rates. Rates of benthic respiration are usually higher in the light than in the dark because the aerated sediment volume and the availability of EPS are increased (Epping and Jørgensen, 1996). So far, studies of the oxygen and carbon budgets on near-shore subtidal sediments are rare; especially given that the contribution of BPP in these areas is largely unconstrained. The intense coupling between autotrophic and heterotrophic organisms on small scales and the highly dynamic nature of these systems complicates studies related to heterogeneity. The influence of the variability in local scalar irradiance on PBB and respiration has not been addressed so far in detail, partly because of the lack of appropriate technology to assess the 2D light field within sediments.

### 1.3.2. The role of fauna

Areas with high respiration rates are also characterized by intense faunal activity. Coastal zones are especially dominated by faunal respiration, often accounting for more than 50% of the total oxygen uptake (Glud, 2008). In areas with lower availability of carbon sources such as the open ocean, microbial respiration becomes more important. Sediment mobilization by fauna (bioturbation) can be of relevance for the biogeochemistry of marine sediments, since formerly anoxic sediment may be exposed to oxygen and fresh organic carbon is mixed into deeper layers (Jørgensen et al., 2005, Meysman et al., 2006, Volkenborn et al., 2007). Furthermore, bioirrigation by pumping animals like many worms and mussels locally introduce oxygenated water into the sediment (Aller and Aller, 1998, Wenzhöfer and Glud, 2004, Polerecky et al., 2006). The idealized vertical succession of redox reactions (Fig. 1.2) can thus be completely altered into a highly structured 3D configuration.

## 1.4. Sediment oxygen dynamics on different spatial scales

Increasing evidence has shown that oxygen concentrations in marine sediments are highly variable in time and space. Benthic carbon mineralization, and therefore oxygen dynamics, strongly differ in magnitude and vertical structure on spatial scales spanning several orders of magnitude, ranging from sub-millimeter features (e.g. Jørgensen, 1977, Jahnke, 1985, Glud et al., 1999) to

basin wide differences (e.g. Jahnke, 1996, Wenzhöfer and Glud, 2002, Seiter et al., 2005). Large-scale variations in oxygen dynamics are mostly driven by the distribution of pelagic primary production and the resulting fluxes of POC. The decomposition of aggregated organic matter in sediments leads to heterogeneities on different scales since the particles themselves can strongly vary in size, ranging from sub-millimeter fecal pellets and pieces of macroalgae (Franke et al., 2006) to dead whales (Treude et al., 2009). Generally, deep-sea sediments are believed to exhibit much lower small scale variability in oxygen consumption than coastal sediments which is due to the averaging effect of the water column and lower animal densities. However, recent studies in the Sagami Bay (Japan) at water depths of >1400 m, report pronounced small-scale variability of benthic oxygen dynamics (Glud et al., 2005, 2009). Along a 175 m transect, they found diffusive oxygen exchanges (DOE) and OPD varying by factors of 10 and 6, respectively, with a characteristic patch size of only ∼2 cm, while a similar analysis in coastal sediments revealed a patch size of ∼0.5 cm (Glud et al., 2001). In other shallow, coastal sediments, horizontal heterogeneities in $O_2$ concentrations down to the millimeter scale have been found with up to 10 fold differences in oxygen exchange rate within 2 mm (Fenchel, 1996). Knowledge of relevant scales and spatial variability of benthic oxygen dynamics is a prerequisite for the calculation of accurate carbon budgets. The micro-patchiness of oxygen fluxes in marine sediments has only recently gained interest and the consequences have barely been assessed quantitatively (Glud, 2008). A recent review by Stockdale et al. (2009) focuses exclusively on sub-millimeter heterogeneities in sediments, identifying the need for more detailed studies.

## 1.5. Measuring benthic oxygen dynamics

### 1.5.1. Core / Chamber Incubations

The demand to measure oxygen dynamics in marine sediments led to the development of several analytical tools. The oldest and most widely used method to determine benthic oxygen exchange are benthic chambers. A defined sediment surface is enclosed with overlying water, in which oxygen concentrations are recorded. By the change in concentration over time, the total oxygen exchange (TOE) of the sediment can be determined. It includes not only microbial processes but also faunal respiration and reoxidation of reduced substances (Pamatmat and Fenton, 1968, Pamatmat, 1971, Smith et al., 1978). These chamber- or core incubations average over sediment areas of typically 10 $cm^2$ to 1000 $cm^2$. Smaller chambers have a larger rim to sediment-surface ratio thus tend to produce relatively stronger artifacts due to sediment disturbance and disturbed macrobenthos. Furthermore, spatial variability in faunal distribution might bias the results. Therefore, larger chambers usually give more reliable results (Glud and Blackburn, 2002). These incubation methods integrate over the whole sediment depth without resolving vertical patterns of benthic respiration, small scale horizontal variability, and fast changes.

### 1.5.2. Microsensor profiling

Electrochemical oxygen microsensors are Clark-Type electrodes with an additional guard cathode and tip diameters of typically ∼5 to 20 µm (Revsbech, 1989). The reduction of oxygen on the measurement cathode creates a current in the range of $10 \times 10^{-12}$ to $10 \times 10^{-9}$ A that is inherently proportional to the oxygen partial pressure in the surrounding medium. The corresponding oxygen consumption at the electrode itself is insignificant, there is virtually no stirring-sensitivity and the sensor exhibits a spherical measuring characteristic. These sensors allow the determination of high-resolution vertical profiles of oxygen. Since their introduction into the field of marine research by Revsbech et al. (1980), numerous studies based on this technology were published (for an overview see Reimers (2007)) and the use of microsensors in sediments greatly enhanced the knowledge about magnitude and spatial organization of benthic mineralization processes. In most profiling measurements, the sensor is moved from the water column into the sediment in increments of 50 - 200 µm, depending on the desired resolution. Oxygen values at each position are determined and a profile is thus recorded. A typical profile can be divided into three horizons: (I) the water column, (II) the diffusive boundary layer (DBL) and (III) the sediment. Within the water column oxygen concentrations are virtually constant due to turbulent mixing. Approaching the surface, hydrodynamic energy decreases until, close to the sediment surface (0.1-1mm), molecular diffusion becomes the dominant transport process. In this DBL oxygen concentrations decrease almost linearly since the oxygen uptake in this zone is small compared to the sediment's oxygen demand and hence can be used to quantify the DOE of the sediment according to Fick's first law of diffusion (Fig. 1.5).:

$$DOE = -D_0 \left. \frac{\partial C}{\partial z} \right|_{z=0} \tag{1.1}$$

where $D_0$ is the molecular diffusion coefficient of oxygen in seawater at the respective conditions, $C$ is the oxygen concentration and $z$ the depth.

Within sediments, diffusive transport is limited to the pore spaces. Due to the sudden decrease in the effective diffusion coefficient at the sediment surface, a distinct bend in the profile can be observed. The much higher respiration rates within the sediment compared to the water column lead to strongly declining profiles. The DOE is generally smaller than the TOE since it does not account for faunal respiration. The difference is largest in shallow shelf sediments with high faunal activity and decreases with increasing water depth (Fig. 1.3). The second derivative of an oxygen concentration profile represents the local oxygen uptake. Hence, in steady state situations, microelectrode profiling can also be used to determine depth-resolving volumetric respiration rates (Rasmussen, 1992). An iterative approach was used by Berg et al. (1998) to identify the number of statistically significant different zones of respiration rates. Revsbech et al. (1981) introduced a method to assess the vertical organization of benthic primary production using oxygen microelectrodes. They recorded the initial decline in oxygen concentration immediately after a sudden darkening of the sediment. Under the assumption of initially unchanged respiration rate and diffusion, the rate of oxygen disappearance in the dark is equal to the photosynthesis

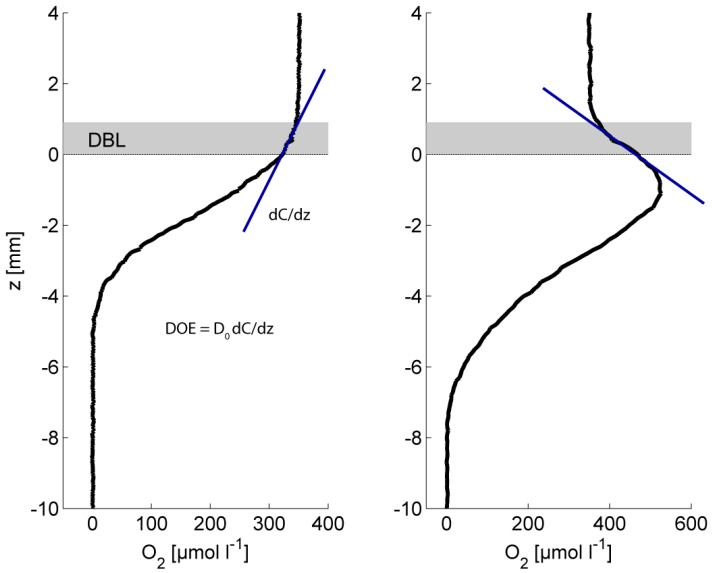


Figure 1.5.: Oxygen profiles in a shallow phototrophic marine sediment at darkness (left panel) and during daytime (right) (own data).

rate in the light. By repeating this measurement scheme at different sediment depths, profiles of benthic gross photosynthesis can be determined. To obtain high spatial resolution (∼0.1 mm), it is necessary to measure the oxygen decline within the first few seconds of the dark period (Revsbech and Jørgensen, 1983). Very fast-responding electrodes are thus required. Fiber optic oxygen microsensors represent an alternative to electrochemical microsensors (Klimant et al., 1995). They consist of a light-guiding fiber with an oxygen sensitive fluorescent dye immobilized in a polymer matrix on the tip. Oxygen diffuses into this sensing layer and the dye is excited by illumination with suitable wavelengths. The fluorophore molecules return from the excited state into the ground state by emitting light of longer wavelength over a short period of time. Some of the excited dye molecules transfer their energy to oxygen molecules, where the energy is dissipated non-radiatively ('fluorescence quenching'). Thus, higher concentrations of oxygen within the sensing layer result in weaker fluorescence with shorter lifetime. The fluorescent light travels back through the fiber, passes an emission filter to suppress the excitation light, and is captured by a photodiode or photomultiplier. The relationship between oxygen concentration and fluorescence intensity or lifetime can be described by a Stern-Vollmer equation with two fluorescent components, one being non-quenchable (Klimant et al., 1995):

$$\frac{I}{I_0} = \frac{\tau}{\tau_0} = \frac{\alpha}{(1 - K_{SV}[O_2])} + (1 - \alpha) \tag{1.2}$$

$I$ and $\tau$ are the fluorescence intensity and lifetime, in the presence of oxygen, $I_0$ and $\tau_0$ are the respective values in the absence of oxygen. The fraction of quenchable fluorescence is $\alpha$. The quenching coefficient $K_{sv}$ has to be determined by calibration at different oxygen concentrations

($[O_2]$). The use of lifetime is preferred over intensity measurements since it is more robust against different disruptive factors (Borisov and Wolfbeis, 2008).

### 1.5.3. Planar optodes

Profiling measurements with microsensors are not able to resolve high lateral and temporal variability. The possibility of two-dimensional imaging of oxygen concentrations with planar optodes (PO) represents a great advancement in this respect. They consist of a transparent support material with a thin layer of the same fluorescent dye, which is used for fiber optodes. In laboratory setups the planar sensor unit is part of the inner wall of an aquarium (Fig. 1.6A). The dye is excited by blue LEDs and fluorescence is recorded with a specialized camera setup. To image the distribution of fluorescence lifetime, the camera shutter needs to be synchronized with the pulses of excitation light. Two images are taken at different times after the excitation ended (Fig. 1.6B). These images can be used to calculate the fluorescence lifetime for every pixel, which can then be converted to oxygen values according to Equation 1.2 (Holst and Grunwald, 2001).

The ability to image oxygen distribution in two dimensions greatly enhanced the understanding of spatial organization of benthic biogeochemical processes which can hardly be resolved by microsensor measurements (Glud et al., 1999, Solan et al., 2003, Viollier et al., 2003, Frederiksen and Glud, 2006, Oguri et al., 2006). The highly heterogenic and dynamic oxygen distribution in fauna inhabited sediments for example, has been clearly shown (Wenzhöfer and Glud, 2004). The extent to which local accumulation of labile organic matter may lead to spatial and temporal heterogeneities in aerobic respiration and therefore oxygen distribution was also assessed with planar optodes (Franke et al., 2006). The PO principle has been adapted for *in situ* measurements by Glud et al. (2001), who used an inverted periscope to obtain images within the sediment (Fig. 1.7).

Planar optodes have not only been used in marine science but found applications in physiology and in biomedical imaging of oxygen concentrations (Kimura et al., 2007, Lochmann et al., 2008). Recently, POs were adapted to measure pH (Stahl et al., 2006), $CO_2$ (Zhu et al., 2005) and $NH_4^+$ (Strömberg and Hulth, 2005).

However, POs also entail some disadvantages since measurements are carried out along an impermeable wall. This might not only disturb the faunal community but it also alters the three-dimensional oxygen distribution (Polerecky et al., 2006). Furthermore, light guiding effects in the planar optode foil and support window lower the precision and spatial resolution of planar optodes in an unpredictable way (Franke, 2005) and thus hinder the calculation of accurate fluxes and respiration rates.

### 1.5.4. Eddy correlation

The most recent addition to the pool of methods used to determine benthic oxygen exchange rates is Eddy Correlation. Originally developed to measure fluxes of gasses in the atmosphere,

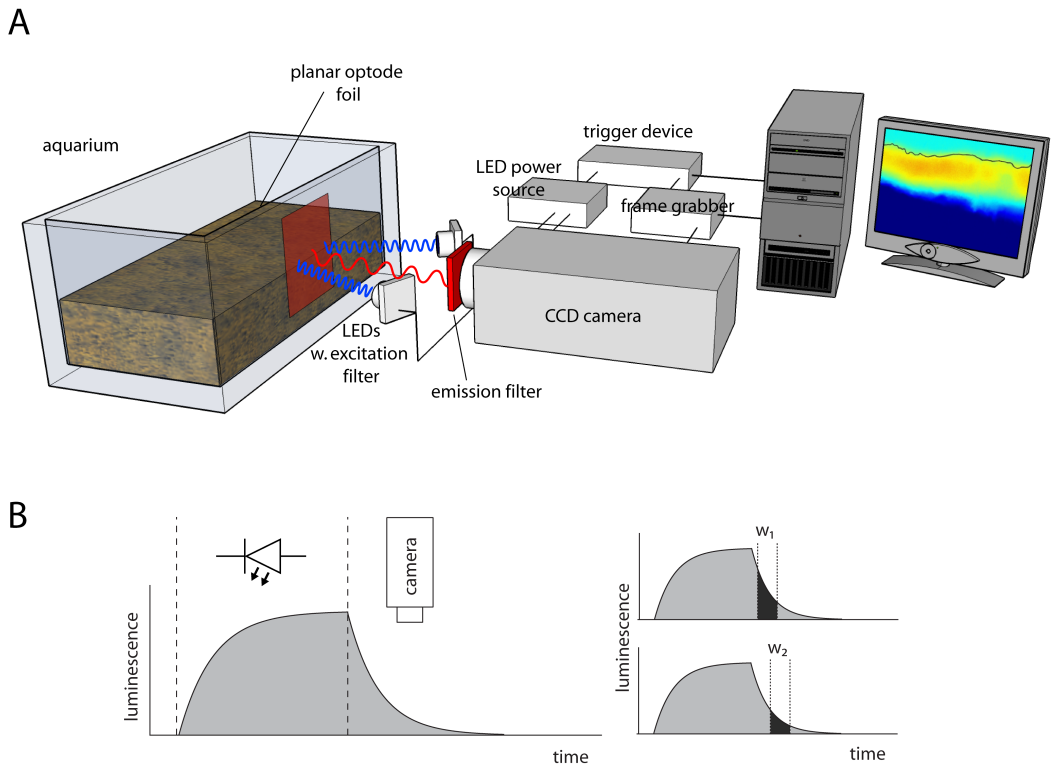


Figure 1.6.: (A) Sketch of a planar optode laboratory setup (not to scale). The planar optode foil is placed on the inside of a wall of an aquarium. Blue LEDs are used to excite the dye on the foil. Time-resolved fluorescence images of the foil are acquired by precise triggering of the fast gateable highly sensitive camera and the LEDs. (B) Scheme for lifetime imaging. Two images are taken during the fluorescence decay ($w_1$ and $w_2$). The quotient of the intensities is used to calculate fluorescence lifetime for every pixel of the image.

eddy correlation was adapted for marine *in situ* $O_2$ measurements (Berg et al., 2003). Oxygen concentrations in a small volume above the sediment are measured with a fast microsensor at high frequency. Synchronously, the local flow velocity is determined with an acoustic doppler velocity-meter. By correlating oxygen concentrations and the vertical component of the turbulent velocity field, the average flux of oxygen can be determined in this direction. For example, if downward moving water parcels contain on average more oxygen than upward moving parcels, there is a net downward flux of oxygen. If the instrument is located close to the sediment surface, the flux across the sediment / water interface can thus be determined. Eddy correlation measurements are the only truly non-invasive technique to assess vertical fluxes. They provide spatially averaged flux information, over areas up to several hundred square meters, depending on hydrodynamic conditions (Berg et al., 2007). Therefore, eddy correlation is an excellent tool for average oxygen budgets but it conceals spatial variability (McGinnis et al., 2008). Few measurements have been carried out so far, directly comparing eddy diffusion fluxes to TOE values from chamber measurements and DOE from microprofiles. Therefore, the true potential of the method remains to be shown.

The different methods for benthic $O_2$ exchange measurements with their advantages and drawbacks are summarized in Table 1.1.

### 1.5.5. *In situ* measurements

All the techniques mentioned above were originally developed for laboratory use. However, evidence was found that differences between *in situ* and ex-situ oxygen measurements exist (Reimers et al., 1986) and consequently, instruments for *in situ* measurements were developed (Reimers and Glud, 2000) (Fig. 1.7). Ex-situ oxygen profiling tends to overestimate DOE and underestimate OPDs. The effect can lead to 3.5 fold increases in DOE and OPDs reduced to 20% (Glud et al., 1994). Different explanations have been proposed, including up-mixing of reduced compounds and transient heating during the core retrieval process, enhanced respiration caused by lysis of barophilic or psycrophilic cells and lysis due to $CO_2$ oversaturation within cells (Glud, 2008, Sachs et al., 2009). Similar problems arise with core incubations. Additionally, the effect of the relatively small diameter of retrieved sediment cores, compared to benthic incubation chambers has to be noted here. Especially in systems with pronounced heterogeneity and high faunal densities, small cores might not yield representative results. Therefore, *in situ* measurements are considered crucial for reliable results. Three principally different methods of deployment are commonly used: autonomous benthic landers, remotely operated vehicles (ROV), and moored instruments. While the first sink to the sediment and start their measurements unattended, ROVs place the measuring devices (*in situ* profiler, benthic chamber etc.) remotely controlled from the ship (Boetius and Wenzhöfer, 2009). Most ROVs float in the water and are being positioned by thrusters. However, a few benthic crawlers exist, which traverse the seafloor with the measuring equipment fixed to them (Smith et al., 1997). They allow very precise positioning and -at the same time- high areal coverage. *In situ* methods enabled fundamental

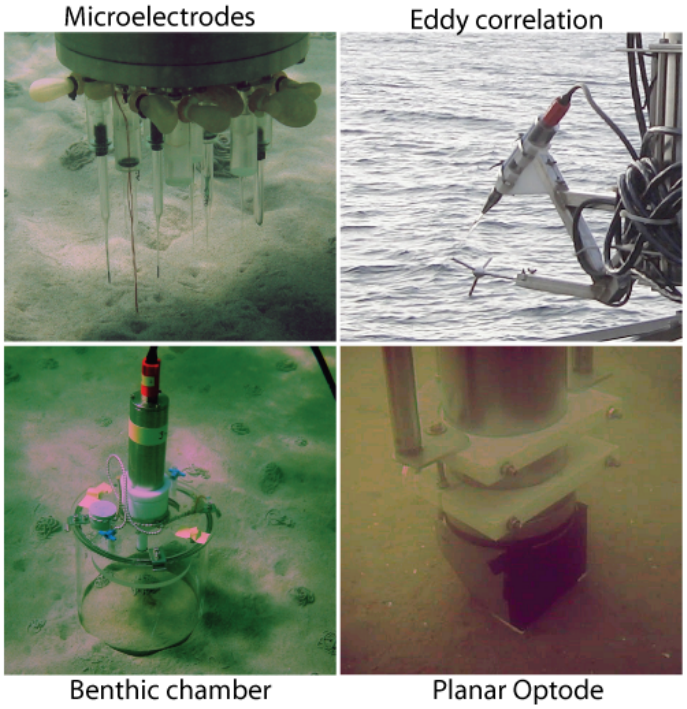


Figure 1.7.: Methods to determine sediment oxygen dynamics *in situ*. The eddy-correlation device is show before deployment. The figures on the left are courtesy of Frank Wenzhöfer.

insights into the functioning of benthic microbial ecosystems. However, the technology is complex and costly and their use is time consuming. Therefore, only a limited number of studies is available, large areas are undersampled, and the quantification of heterogeneity is at its infancy.

## 1.6. Objectives and outline of the thesis

The aim of this thesis is to quantify marine sediment oxygen turnover as a measure of overall carbon mineralization in so far undersampled areas, covering a large range of spatial scales. To study 2D oxygen dynamics in highly active photic sediments together with the light field as the most important driving force at the sub-millimeter level, a specialized planar optode setup was developed and applied in the laboratory. The other end of the scale is marked by several thousand kilometer long transects in the extremely oligotrophic South Pacific Gyre, where meter-long oxygen profiles were measured in almost inert sediments. A multi-method multi-scale approach was taken for measurements in shallow subtidal shelf sediments in the Kattegat, using planar optodes, microelectrodes and benthic chambers simultaneously. For all studies, appropriate techniques / technologies needed to be developed and / or adapted.

Table 1.1.: Overview and comparison of the different methods used to quantify benthic oxygen dynamics

| Method | Parameters | Advantages | Drawbacks |
|---|---|---|---|
| Core- / Chamber incubation | total oxygen exchange (TOE) | relatively easy; porewater advection can be simulated; includes fauna respiration | little spatial information; long duration of measurements; dependend on chamber size |
| Electrochemical Microsensors | diffusive oxygen exchange (DOE); oxygen penetration depth (OPD); depth resolved respiration rates; depth resolved photosynthesis rates | information about vertical structure; minimal invasive; high resolution | complex setup; delicate sensors; 15-30 min per profile |
| Fiber optic Sensors | DOE; OPD | information about vertical structure; minimal invasive; high resolution; low drift | slower than electrochemical sensors |
| Planar Optodes | 2D oxygen images; spatially resolved rates | fast data acquisition information about heterogeneity | measurements along a wall; complicated setup; expensive |
| Eddy correlation | total vertical oxygen flux | non-invasive, averages over large area | highly experimental; complex setup; no spatial information |

### 1.6.1. Overview of the manuscripts

This thesis comprises four manuscripts, presented as chapters 2-5. Chapter 2 has been submitted to Limnology and Oceanography - Methods, chapter 3 is in preparation for Limnology and Oceanography. Chapter 4 comprises a co-authorship and has been published in Proceedings of the National Academy of Science (PNAS); chapter 5 has been published in Biogeoscience. A fifth manuscript, comprising another co-authorship, has been published in FEMS Microbiology Ecology. Only the abstract appears in the appendix, since it is not directly focused on the subject of this thesis.

**Chapter 2**

*A novel high resolution Planar Optode for two-dimensional oxygen imaging and light field sensing*

Jan P. Fischer and Frank Wenzhöfer

Since local light availability is a key driving force for benthic metabolism in euphotic sediments, a method to measure both, oxygen concentration dynamics and irradiance at high spatial resolution in 2D was desired. However, optical cross-talk in conventional planar optode imaging setups constitutes a relevant problem at high gradients and if small features should be observed, it leads to smeared images. The newly developed High Resolution Planar Optode resolves both problems. It allows for reliable 2D-oxygen measurements with simultaneous estimations of the light field down to a scale of ∼50-100 µm. Local noise in oxygen images counteracts a direct calculation of spatial derivatives and thus fluxes and respiration rates from planar optode images. A method, analogue to the 1D-approach described by Epping et al. (1999), calculating local oxygen uptake rates and benthic primary production in photosynthetically active sediments based on perturbations in the light conditions was developed and applied to oxygen image series captured with the High Resolution Planar Optode. The new device was developed, assembled and applied by Jan Fischer; all experiments and calculations were carried out, and the manuscript was written by Jan Fischer with conceptual and editorial input from Frank Wenzhöfer.

**Chapter 3**

*Sediment oxygen dynamics in the Kategatt:* in situ *studies using the benthic crawler MOVE*

Jan P. Fischer, Hans Røy, Felix Janssen, Christoph Waldmann, Frank Wenzhöfer

Most measurements of total oxygen exchange (TOE) and diffusive oxygen exchange (DOE) were performed along ocean margins and in intertidal zones. Measurements in the open ocean are sparse, but, astonishingly, little work has also been done on shallow intertidal sediments. The relative importance of microphytobenthos and macrophytes for benthic oxygen dynamics in these highly dynamic nutrient rich and strongly fauna inhabited sediments is therefore highly unconstrained. Spatial variability of benthic carbon mineralization can be expected to extend over several orders of magnitude and few attempts have been made to tackle the issue of scaling in

these habitats. The benthic crawler C-MOVE enabled us to approach this question and allowed to carry out a multi-scale measuring campaign, ranging from sub-millimeter to kilometer scales. Additional *in situ* experiments with measurements under artificially controlled light conditions were performed to assess the temporal response of the system under perturbations. The study was accompanied by eddy-correlation measurements which yielded average oxygen fluxes over larger sediment surface areas. This study was initiated and planed by Frank Wenzhöfer and Jan Fischer. The field study was conducted by all co-authors and the manuscript was written by Jan Fischer with input and editorial help from the co-authors.

**Chapter 4**

*Subseafloor sedimentary life in the South Pacific Gyre*

Steven D'Hondt, Arthur J. Spivack, Robert Pockalny, Timothy G. Ferdelman, Jan P. Fischer, Jens Kallmeyer, Lewis J. Abrams, David C. Smith, Dennis Graham, Franciszek Hasiuk, Heather Schrum, and Andrea M. Stancin

Microbial communities in the South Pacific Gyre are characterized by very low biomass and metabolic activity. Cell numbers are 3 orders of magnitude lower and net respiration rates are 1-3 orders of magnitude lower than in the respective depth in previously described marine sediments. The relatively thin sediment cover is oxic throughout the whole sediment column (s. Chapter 4), and the generation of $H_2$ by radiolysis potentially constitutes a significant source of reduction equivalents. Although the South Pacific Gyre most likely represents the most oligotrophic oceanic region, extrapolations suggest that almost half of the worlds ocean sediments may approach these low cell abundances and respiration rates. This study was initiated by Steve D'Hondt, Bo Barker Jørgensen and Tim Ferdelman. The method for the oxygen measurements on piston cores was developed and measurements were performed and processed by Jan Fischer. The manuscript was written by Steven D'Hondt with input and editorial comments by the co-authors.

**Chapter 5**

*Oxygen penetration deep into the sediment of the South Pacific gyre*

Jan P. Fischer, Timothy G. Ferdelman, Steven D'Hondt, Hans Røy, Frank Wenzhöfer

Since the South Pacific gyre constitutes the ultimate oceanic desert with surface chlorophyll concentrations below $0.02\,\mathrm{mg\,m^{-3}}$ and sedimentation rates smaller than $1\,\mathrm{mm\,kyr^{-1}}$, deep penetration of oxygen can be expected here. However, no measurements of benthic carbon mineralization in this gigantic region have been presented so far. Furthermore, these measurements are missing for most other highly oligotrophic oceanic regions. We measured the highest oxygen penetration depth ever reported for marine sediments and confined the total flux of oxygen to the seafloor in this region experimentally by the use of ex-situ and *in situ* techniques for the first time. Reaction-Diffusion models indicate that the labile fraction of organic carbon is used up within the first few millimeters of the sediment and respiration rates thus strongly drop with

depth. Oxygen that is not used up in this surface layer of the sediment is free to diffuse downwards, leading to oxic conditions throughout the whole sediment and down to the basalt for a large area in the South Pacific. This study was initiated by Bo Barker Jørgensen and Steven D'Hondt. Jan Fischer planned and carried out all oxygen measurements, data analysis and modeling as well as the writing of the manuscript with input from Frank Wenzhöfer and editorial help of the co-authors.

# References


Aller, R. C., Aller, J. Y., 1998. The effect of biogenic irrigation intensity and solute exchange on diagenetic reaction rates in marine sediments. J. Mar. Res. 56 (4), 905–936.

Antia, A., Koeve, W., Fischer, G., Blanz, T., Schulz-Bull, D., Scholten, J., Neuer, S., Kremling, K., Kuss, J., Peinert, R., 2001. Basin-wide particulate carbon flux in the Atlantic Ocean: Regional export patterns and potential for atmospheric $CO_2$ sequestration. Glob. Biogeochem. Cycles 15 (4), 845–862.

Bender, M. L., Heggie, D. T., 1984. Fate of organic carbon reaching the deep sea floor: a status report. Geochim. Cosmochim. Acta 48 (5), 977–986.

Berg, P., Risgaard-Petersen, N., Rysgaard, S., 1998. Interpretation of measured concentration profiles in sediment pore water. Limnol. Oceanogr. 43 (7), 1500–1510.

Berg, P., Røy, H., Janssen, F., Meyer, V., Jørgensen, B. B., Huettel, M., de Beer, D., 2003. Oxygen uptake by aquatic sediments measured with a novel non-invasive eddy-correlation technique. Mar. Ecol. Prog. Ser. 262, 75–83.

Berg, P., Røy, H., Wiberg, P. L., 2007. Eddy correlation flux measurements: The sediment surface area that contributes to the flux. Limnol. Oceanogr. 52 (4), 1672 – 1684.

Berger, W. H., Fischer, K., Lai, C., Wu, G., 1987. Ocean productivity and organic carbon flux. i. overview and maps of primary production and export production. University of California, San Diego, SIO Reference 87-30, 67pp.

Berner, R., 1980. Early Diagenesis: A Theoretical Approach, 1st Edition. Princeton Series in Geochemistry. Princeton University Press.

Berner, R. A., 1982. Burial of organic carbon and pyrite sulfur in the modern ocean; its geochemical and environmental significance. Am. J. Sci. 282 (4), 451 – 473.

Betzer, P., Showers, W., Laws, E., Winn, C., Ditullio, G., Kroopnick, P., 1984. Primary productivity and particle fluxes on a transect of the equator at 153°w in the Pacific Ocean. Deep-sea research. Part A 31 (1), 1–11.

Billerbeck, M., Røy, H., Bosselmann, K., Huettel, M., 2007. Benthic photosynthesis in submerged wadden sea intertidal flats. Estuarine Coastal Shelf Sci. 71 (3-4), 704–716.

Boetius, A., Wenzhöfer, F., 2009. In situ technologies for studying deep-sea hotspot ecosystems. Oceanography 22 (1), 177.

Borisov, S. M., Wolfbeis, O. S., 2008. Optical biosensors. Chem. Rev. 108 (2), 423–461.

Boudreau, B. P., Ruddick, B. R., 1991. On a reactive continuum representation of organic matter diagenesis. Am. J. Sci. 291 (5), 507–538.

Burdige, D. J., 2006. Geochemistry of marine sediments. Princeton University Press.

Cai, W.-J., Reimers, C. E., 1995. Benthic oxygen flux, bottom water oxygen concentration and core top organic carbon content in the deep northeast Pacific Ocean. Deep Sea Res. Part I 42 (10), 1681–1699.

Cai, W.-J., Sayles, F. L., 1996. Oxygen penetration depths and fluxes in marine sediments. Mar. Chem. 52 (2), 123–131.

Canfield, D. E., Jørgensen, B. B., Fossing, H., Glud, R. N., Gundersen, J., Ramsing, N. B., Thamdrup, B., Hansen, J. W., Nielsen, L. P., Hall, P. O. J., 1993. Pathways of organic carbon oxidation in three continental margin sediments. Mar. Geol. 113 (1-2), 27–40.

Canfield, D. E., Kristensen, E., Thamdrup, B., 2005. Aquatic geomicrobiology, 1st Edition. Vol. 48 of Advances in Marine Biology. Elsevier.

Carr, M.-E., et al., 2006. A comparison of global estimates of marine primary production from ocean color. Deep Sea Res. Part II 53 (5-7), 741–770.

Daneri, G., Quinones, R., 2001. Undersampled ocean systems: a plea for an international study of biogeochemical cycles in the Southern Pacific Gyre and its boundaries. US JGOFS Newsletter January 11 (1), 9.

De Brouwer, J. F. C., Stal, L. J., 2001. Short-term dynamics in microphytobenthos distribution and associated extracellular carbohydrates in surface sediments of an intertidal mudflat. Mar. Ecol. Prog. Ser. 218, 33–44.

Denman, K., Brasseur, G., Chidthaisong, A., Ciais, P., Cox, P., Dickinson, R., Hauglustaine, D., Heinze, C., Holland, E., Jacob, D., Lohmann, U., Ramachandran, S., da Silva Dias, P., Wofsy, S., Zhang, X. (Eds.), 2007. Couplings Between Changes in the Climate System and Biogeochemistry. Climate Change 2007: The Physical Science Basis. Contribution of Working Group I to the Fourth Assessment Report of the Intergovernmental Panel on Climate Change. Cambridge University Press, Cambridge, New York.

Duarte, C. M., Cebrian, J., 1996. The fate of marine autotrophic production. Limnol. Oceanogr. 41 (8), 1758–1766.

Epping, E., Jørgensen, B., 1996. Light-enhanced oxygen respiration in benthic phototrophic communities. Mar. Ecol. Prog. Ser. 139 (1), 193–203.

Epping, E. H. G., Khalili, A., Thar, R., 1999. Photosynthesis and the dynamics of oxygen consumption in a microbial mat as calculated from transient oxygen microprofiles. Limnol. Oceanogr. 44 (8), 1936–1948.

Fenchel, T., 1996. Worm burrows and oxic microniches in marine sediments. 1. spatial and temporal scales. Marine Biology 127 (2), 289–295.

Field, C. B., Behrenfeld, M. J., Randerson, J. T., Falkowski, P., 1998. Primary production of the biosphere: Integrating terrestrial and oceanic components. Science 281 (5374), 237–240.

Fischer, G., Gruber, N., Lampitt, R., Lévy, M., Laws, E., Platt, T., Spall, S., Steele, J., 2003. Global ocean productivity and the fluxes of carbon and nutrients: Combining observations and models. JGOFS Report (38).

Franke, U., 2005. Applications of planar oxygen optodes in biological aquatic systems. PhD thesis, University Bremen.

Franke, U., Polerecky, L., Precht, E., Huettel, M., 2006. Wave tank study of particulate organic matter degradation in permeable sediments. Limnol. Oceanogr. 51 (2), 1084–1096.

Frederiksen, M. S., Glud, R. N., 2006. Oxygen dynamics in the rhizosphere of zostera marina: A two-dimensional planar optode study. Limnol. Oceanogr 51 (2), 1072–1083.

Froelich, P. N., Klinkhammer, G. P., Bender, M. L., Luedtke, N. A., Heath, G. R., Cullen, D., Dauphin, P., Hammond, D., Hartman, B., Maynard, V., 1979. Early oxidation of organic matter in pelagic sediments of the eastern equatorial Atlantic: suboxic diagenesis. Geochim. Cosmochim. Acta 43 (7), 1075–1090.

Gehlen, M., Bopp, L., Emprin, N., Aumont, O., Heinze, C., Ragueneau, O., 2006. Reconciling surface ocean productivity, export fluxes and sediment composition in a global biogeochemical ocean model. Biogeosciences 3 (4), 521–537.

Glud, R. N., 2008. Oxygen dynamics of marine sediments. Marine Biology Research 4 (4), 243 – 289.

Glud, R. N., Blackburn, N., 2002. The effects of chamber size on benthic oxygen uptake measurements: a simulation study. Ophelia 56 (1), 23–31.

Glud, R. N., Gundersen, J. K., Jørgensen, B. B., Revsbech, N. P., Schulz, H. D., 1994. Diffusive and total oxygen uptake of deep-sea sediments in the eastern South Atlantic Ocean:in situ and laboratory measurements. Deep Sea Res. Part I 41 (11-12), 1767–1788.

Glud, R. N., Kühl, M., Kohls, O., Ramsing, N. B., 1999. Heterogeneity of oxygen production and consumption in a photosynthetic microbial mat as studied by planar optodes. Journal of Phycology 35 (2), 270–279.

Glud, R. N., Stahl, H., Berg, P., Wenzhöfer, F., Oguri, K., Kitazato, H., 2009. In situ microscale variation in distribution and consumption of $O_2$: A case study from a deep ocean margin sediment (Sagami Bay, Japan). Limnol. Oceanogr. 54 (1), 1–12.

Glud, R. N., Tengberg, A., Kühl, M., Hall, P. O. J., Klimant, I., Holst, G., 2001. An in situ instrument for planar $O_2$ optode measurements at benthic interfaces. Limnol. Oceanogr. 46 (8), 2073–2080.

Glud, R. N., Wenzhöfer, F., Tengberg, A., Middelboe, M., Oguri, K., Kitazato, H., 2005. Distribution of oxygen in surface sediments from central Sagami Bay, Japan: In situ measurements by microelectrodes and planar optodes. Deep-Sea Res. Part I Oceanogr. Res. Pap. 52 (10), 1974–1987.

Hartnett, H. E., Keil, R. G., Hedges, J. I., Devol, A. H., 1998. Influence of oxygen exposure time on organic carbon preservation in continental margin sediments. Nature 391 (6667), 572–575.

Holst, G., Grunwald, B., 2001. Luminescence lifetime imaging with transparent oxygen optodes. Sensors and Actuators B: Chemical 74 (1-3), 78–90.

Houghton, R. A., 2007. Balancing the global carbon budget. Annual Review of Earth and Planetary Sciences 35 (1), 313–347.

Jahnke, R., 1985. A model of microenvironments in deep-sea sediments: Formation and effects on porewater profiles. Limnol. Oceanogr. 30 (5), 956–965.

Jahnke, R., 1996. The global ocean flux of particulate organic carbon: Areal distribution and magnitude. Global Biogeochem. Cycles 10, 71–88.

Jahnke, R. A., Reimers, C. E., Craven, D. B., 1990. Intensification of recycling of organic matter at the sea floor near ocean margins. Nature 348 (6296), 50–54.

Jørgensen, B., 1977. Bacterial sulfate reduction within reduced microniches of oxidized marine sediments. Marine Biology 41 (1), 7–17.

Jørgensen, B. B., 1996. Case study - Aarhus Bay. In: Jørgensen, B. B., Richardson, K. (Eds.), Eutophication in Coastal Marine Ecosystems - Coastal and Estuarine Studies. Vol. 52. American Geophysical Union, Washington DC.

Jørgensen, B. B., Glud, R. N., Holby, O., 2005. Oxygen distribution and bioirrigation in arctic fjord sediments (Svalbard, Barents Sea). Mar. Ecol. Prog. Ser. 292, 85–95.

Kimura, S., Matsumoto, K., Mineura, K., Itoh, T., 2007. A new technique for the mapping of oxygen tension on the brain surface. Journal of the Neurological Sciences 258 (1-2), 60–68.

Klimant, I., Meyer, V., Kühl, M., 1995. Fiber-optic oxygen microsensors, a new tool in aquatic biology. Limnol. Oceanogr. 40 (6), 1159 – 1165.

Kozerski, H.-P., 1994. Possibilities and limitations of sediment traps to measure sedimentation and resuspension. Hydrobiologia 284 (1), 93–100.

Lochmann, C., Haupl, T., Beuthan, J., 2008. Luminescence lifetime determination for oxygen imaging in human tissue. Laser Phys. Letters 5 (2), 151.

MacDonald, G. J., 1990. Role of methane clathrates in past and future climates. Climatic Change 16 (3), 247–281.

MacIntyre, H., Geider, R., Miller, D., 1996. Microphytobenthos: The ecological role of the "secret garden" of unvegetated, shallow-water marine habitats. i. distribution, abundance and primary production. Estuaries and Coasts 19 (2), 186–201.

Martin, W. R., Sayles, F. L., 2006. Organic matter oxidation in deep-sea sediments: Distribution in the sediment column and implications for calcite dissolution. Deep Sea Res. Part II 53 (5-7), 771–792.

McGinnis, D. F., Berg, P., Brand, A., Lorrai, C., Edmonds, T. J., Wüest, A., 2008. Measurements of eddy correlation oxygen fluxes in shallow freshwaters: Towards routine applications and analysis. Geophys. Res. Letters 35, L04403.

Meysman, F. J. R., Middelburg, J. J., Heip, C. H. R., 2006. Bioturbation: a fresh look at Darwin's last idea. Trends Ecol. Evol. 21 (12), 688–695.

Murray, J. W., Grundmanis, V., 1980. Oxygen consumption in pelagic marine sediments. Science 209 (4464), 1527–1530.

Newton, P. P., Lampitt, R. S., Jickells, T. D., King, P., Boutle, C., 1994. Temporal and spatial variability of biogenic particles fluxes during the JGOFS northeast Atlantic process studies at 47°N, 20°W. Deep Sea Res. Part I 41 (11-12), 1617–1642.

Oguri, K., Kitazato, H., Glud, R. N., 2006. Platinum octaetylporphyrin based planar optodes combined with an UV-LED excitation light source: An ideal tool for high-resolution $o_2$ imaging in $o_2$ depleted environments. Mar. Chem. 100 (1-2), 95–107.

Pace, M. L., Knauer, G. A., Karl, D. M., Martin, J. H., 1987. Primary production, new production and vertical flux in the eastern Pacific Ocean. Nature 325 (6107), 803–804.

Pamatmat, M. M., 1971. Oxygen consumption by the seabed. iv. shipboard and laboratory experiments. Limnol. Oceanogr. 16 (3), 536–550.

Pamatmat, M. M., Fenton, D., 1968. An instrument for measuring subtidal benthic metabolism in situ. Limnol. Oceanogr. 13 (3), 537–540.

Polerecky, L., Volkenborn, N., Stief, P., 2006. High temporal resolution oxygen imaging in bioirrigated sediments. Environ. Sci. Technol. 40 (18), 5763–5769.

Pravettoni, R., 2009. Carbon cycle. `http://maps.grida.no/go/graphic/carbon-cycle`, [Online; accessed 02-September-2009].

Rasmussen, H., J. B. B., 1992. Microelectrode studies of seasonal oxygen uptake in a coastal sediment: Role of molecular diffusion. Mar. Ecol. Prog. Ser. 81 (3), 289–303.

Reimers, C. E., 2007. Applications of microelectrodes to problems in chemical oceanography. Chemical Reviews 107 (2), 590–600.

Reimers, C. E., Fischer, K. M., Merewether, R., Smith, K. L., Jahnke, R. A., 1986. Oxygen microprofiles measured in situ in deep ocean sediments. Nature 320 (6064), 741–744.

Reimers, C. E., Glud, R. N., 2000. In situ chemical sensor measurements at the sediment water interface. In: Varney, M. (Ed.), Chemical sensors in oceanography. Gordon and Breach Science, Gordon and Breach Science Publishers, pp. 249–282.

Revsbech, N., 1989. An oxygen microsensor with a guard cathode. Limnol. Oceanogr. 34 (2), 474–478.

Revsbech, N., Jørgensen, B., Brix, O., 1981. Primary production of microalgae in sediments measured by oxygen microprofile, $H^{14}CO_3^-$ fixation, and oxygen exchange methods. Limnol. Oceanogr. 26 (4), 717–730.

Revsbech, N., Sørensen, J., Blackburn, H., Lomholt, J., 1980. Distribution of oxygen in marine sediments measured with microelectrodes. Limnol. Oceanogr. 25 (3), 403–411.

Revsbech, N. P., Jørgensen, B. B., 1983. Photosynthesis of benthic microflora measured with high spatial resolution by the oxygen microprofile method: capabilities and limitations of the method. Limnol. Oceanogr. 28 (4), 749–756.

Romankevich, E., Vetrov, A., Korneeva, G. (Eds.), 1999. Geochemistry of organic carbon in the ocean. Vol. 59 of Biogeochemical Cycling and Sediment Ecology NATO ASI Series. Kluwer Academic Publishers, Dordrecht / Boston / London.

Sachs, O., Sauter, E. J., Schlüter, M., Rutgers van der Loeff, M. M., Jerosch, K., Holby, O., 2009. Benthic organic carbon flux and oxygen penetration reflect different plankton provinces in the southern ocean. Deep-sea research. Part 1. Oceanographic research papers 56 (8), 1319–1335.

Seiter, K., Hensen, C., Zabel, M., 2005. Benthic carbon mineralization on a global scale. Global Biogeochem. Cycles 19 (1).

Smith, K. L., J., White, G. A., Laver, M. B., Haugsness, J. A., 1978. Nutrient exchange and oxygen consumption by deep-sea benthic communities: Preliminary in situ measurements. Limnol. Oceanogr. 23 (5), 997–1005.

Smith, Kenneth L., J., Kaufmann, R. S., 1999. Long-term discrepancy between food supply and demand in the deep eastern North Pacific. Science 284 (5417), 1174–1177.

Smith, K. L., Baldwin, R. J., Williams, P. M., 1992. Reconciling particulate organic carbon flux and sediment community oxygen consumption in the deep North Pacific 359 (6393), 313–316.

Smith, K. L., Glatts, R. C., Baldwin, R. J., Beaulieu, S. E., Uhlman, A. H., Horn, R. C., Reimers, C. E., 1997. An autonomous, bottom-transecting vehicle for making long time-series measurements of sediment community oxygen consumption to abyssal depths. Limnol. Oceanogr. 42 (7), 1601–1612.

Smith, S. V., Hollibaugh, J. T., 1993. Coastal metabolism and the oceanic organic carbon balance. Reviews of Geophysics 31.

Soetaert, K., Herman, P. M. J., Middelburg, J. J., 1996. Dynamic response of deep-sea sediments to seasonal variations: A model. Limnol. Oceanogr. 41 (8), 1651–1668.

Solan, M., Germano, J. D., Rhoads, D. C., Smith, C., Michaud, E., Parry, D., Wenzhöfer, F., Kennedy, B., Henriques, C., Battle, E., Carey, D., Iocco, L., Valente, R., Watson, J., Rosenberg, R., 2003. Towards a greater understanding of pattern, scale and process in marine benthic systems: a picture is worth a thousand worms. Journal of Experimental Marine Biology and Ecology 285-286, 313–338.

Stahl, H., Glud, A., Schröder, C. R., Klimant, I., Tengberg, A., Glud, R. N., 2006. Time-resolved pH imaging in marine sediments with a luminescent planar optode. Limnol. Oceanogr.: Methods 4 (51), 336–345.

Stal, L. J., 2010. Microphytobenthos as a biogeomorphological force in intertidal sediment stabilization. Ecological Engineering 36 (2), 236–245.

Stockdale, A., Davison, W., Zhang, H., 2009. Micro-scale biogeochemical heterogeneity in sediments: A review of available technology and observed evidence. Earth-Science Reviews 92 (1), 81–97.

Strömberg, N., Hulth, S., 2005. Assessing an imaging ammonium sensor using time correlated pixel-by-pixel calibration. Anal. Chim. Acta 550 (1-2), 61–68.

Suess, E., 1980. Particulate organic carbon flux in the oceans - surface productivity and oxygen utilization. Nature 288 (5788), 260–263.

Thamdrup, B., Canfield, D. E. (Eds.), 2000. Benthic Respiration in Aquatic Sediments, 1st Edition. Methods in Ecosystem Science. Springer-Verlag, New York.

Treude, T., Smith, C. R., Wenzhöfer, F., Carney, E., Bernardino, A. F., Hannides, A. K., Krüger, M., Boetius, A., 2009. Biogeochemistry of a deep-sea whale fall: sulfate reduction, sulfide efflux and methanogenesis. Mar. Ecol. Prog. Ser. 382, 1–21.

Underwood, G. J. C., Kromkamp, J., 1999. Primary production by phytoplankton and microphytobenthos in estuaries. In: Advances in Ecological Research. Vol. 29. Academic Press, pp. 93–153.

Viollier, E., Rabouille, C., Apitz, S. E., Breuer, E., Chaillou, G., Dedieu, K., Furukawa, Y., Grenz, C., Hall, P., Janssen, F., 2003. Benthic biogeochemistry: state of the art technologies and guidelines for the future of in situ survey. Journal of Experimental Marine Biology and Ecology 285, 5–31.

Volkenborn, N., Polerecky, L., Hedtkamp, S. I. C., Van Beusekom, J. E. E., De Beer, D., 2007. Bioturbation and bioirrigation extend the open exchange regions in permeable sediments. Limnol. Oceanogr. 52 (5), 1898–1909.

Wang, G., Spivack, A. J., D'Hondt, S., 2006. Identification of respiration pathways in deep subseafloor sediments using a $CO_2$ mass-balance model. Astrobiol. 6, 230.

Wenzhöfer, F., Glud, R. N., 2002. Benthic carbon mineralization in the Atlantic: a synthesis based on in situ data from the last decade. Deep Sea Res. Part I 49 (7), 1255–1279.

Wenzhöfer, F., Glud, R. N., 2004. Small-scale spatial and temporal variability in benthic $O_2$ dynamics of coastal sediments: Effects of fauna activity. Limnol. Oceanogr 49 (5), 1471–1481.

Wenzhöfer, F., Holby, O., Kohls, O., 2001. Deep penetrating benthic oxygen profiles measured in situ by oxygen optodes. Deep Sea Res. Part I 48 (7), 1741–1755.

Westrich, J., Berner, R., 1984. The role of sedimentary organic matter in bacterial sulfate reduction: The G model tested. Limnol. Oceanogr. 29 (2), 236–249.

Witte, U., Wenzhöfer, F., Sommer, S., Boetius, A., Heinz, P., Aberle, N., Sand, M., Cremer, A., Abraham, W. R., Jørgensen, B. B., 2003. In situ experimental evidence of the fate of a phytodetritus pulse at the abyssal sea floor. Nature 424 (6950), 763–766.

Zhu, Q. Z., Aller, R. C., Fan, Y. Z., 2005. High-performance planar pH fluorosensor for two-dimensional pH measurements in marine sediment and water. Environ. Sci. Tech. 39 (22), 8906–8911.

# Chapter 2.

# Insight into benthic photosynthesis: A novel planar optode setup for concurrent oxygen and light field imaging

---

Jan P. Fischer[1], Frank Wenzhöfer[1]

Submitted to Limnology and Oceanography: Methods

[1]Max Planck Institute for Marine Microbiology, Bremen, Germany

## 2.1. Abstract

A novel High Resolution Planar Optode (HiPO) for 2D oxygen and light field imaging is presented. Optical cross-talk effects, limiting the precision and resolution of conventional planar optode setups, could be strongly reduced by the use of a Fiber Optic Faceplate as sensing window. The new device therefore allows for accurate calculation of oxygen fluxes and respiration rates from oxygen concentration images, especially for strong and small-scale concentration gradients in sediments and microbial mats. In addition, the setup can be used to estimate the distribution of scalar irradiance within illuminated sediments or mats, thus directly linking local light availability to oxygen dynamics at high resolution. Irradiance values obtained with the HiPO were found to be in good agreement with scalar irradiance microsensor measurements in sandy sediment and a spatial resolution of ∼120 µm could be achieved. The performance of the HiPO for oxygen measurements was tested experimentally and the theoretical limit of spatial (∼100 µm) and temporal (∼10 s) resolution, governed by oxygen diffusion within the sensing layer, was determined by mathematical modeling. Rates of primary production and respiration in sandy sediments, as calculated from the transient oxygen concentrations after perturbations in light condition, showed a highly patchy distribution on sub-millimeter scale. These heterogeneities were clearly correlated to local irradiance within the sediment. Spatial correlations of photosynthesis and respiration were strongly dependent on incident irradiance.

## 2.2. Introduction

The dynamic change of oxygen concentrations within sediments and microbial mats contains information about community respiration, carbon mineralization rates and benthic primary production, and has therefore been widely studied since decades (Pamatmat, 1971, Hargrave, 1972, Jørgensen and Revsbech, 1985). In many phototrophic ecosystems like microbial mats or coastal sediments, the availability of light is the major driving force of benthic oxygen dynamics since the activity of primary producers depends on the local availability of light to the organisms within the sediment strata (Jørgensen and des Marais, 1986). The light field within sediments exhibits a great spatial (vertical penetration of light, lateral differences due to inhomogeneities in the sediment) and temporal (e.g. dial light cycle, clouds, surface waves) variability, often causing small scale heterogeneities in zones of oxygen production and consumption (Glud et al., 1999, Glud, 2008). Lassen et al. (1992a) and Dodds (1992) introduced micro scale sensors with a close to spherical light acceptance characteristic, using a scattering translucent sphere with a diameter between 70 and 250 µm glued to the end of a light guiding fiber. These sensors allow to measure scalar irradiance, i.e. the integrated light from all directions that is available for algal cells (Kühl and Jørgensen, 1992).

To assess the vertical organization of photosynthesis, Revsbech et al. (1981) introduced the light-dark shift method. They recorded the initial decline in oxygen concentration immediately after a sudden darkening of the sediment using fast responding microelectrodes (Revsbech and

Jørgensen, 1983). Under the assumption of initially unchanged respiration rate and diffusion, the rate of oxygen disappearance in the dark is equal to the photosynthesis rate in the light. By repeating this measurement scheme at different sediment depth, profiles of benthic gross photosynthesis can be determined, which is however a time consuming procedure. Epping et al. (1999) measured profiles of benthic photosynthesis and respiration rates in sediments, combining oxygen measurements and numerical simulations of the transient oxygen field ('light-dark cycle method'). While also based on perturbations in the light condition, this method does not only consider the first few seconds after darkening, but allows to follow the changes in community respiration over time. To study the relation between local light availability and gross photosynthesis at the respective depths, scalar irradiance microsensors and the light-dark shift method have been used together by Lassen et al. (1992a). They found that the horizontal distance of 120 µm between the tip of oxygen and light microsensors resulted in an uncertain relationship between the two measured parameters in individual profiles.

It is known that the lateral heterogeneity within sediment and microbial mats can be very high (Revsbech and Jørgensen, 1983, Wenzhöfer and Glud, 2004, Stockdale et al., 2009). To approach the whole, three-dimensional, dynamic picture in sediments and microbial mats, planar optodes (PO) have been introduced to the field of marine research (e.g. Glud et al., 1996). This imaging technology allows for mapping of oxygen distributions in space and time, and has become an important tool in marine research. Main part of the 'conventional' system is a transparent support foil with a fluorescent coating, which changes its fluorescence intensity and lifetime depending on the oxygen concentration (Holst et al., 1998). Planar optodes have been applied in numerous studies of many different habitats like coastal sands (Glud et al., 2001, Wenzhöfer and Glud, 2004, Franke et al., 2006, Behrens et al., 2007), deep-sea sediments (Glud et al., 2005), microbial mats (e.g. Glud et al., 1999), rhizospheres (Jensen, 2005, Frederiksen and Glud, 2006) and endolithic algal communities (Kühl et al., 2008). First used in the laboratory, this technology was later also incorporated into *in situ* modules to study shallow-water (Glud et al., 2001) and deep-sea (Glud et al., 2001, 2005) sediments under natural conditions. Subsequent modifications of the imaging technology, going from intensity to lifetime imaging (Holst et al., 1998), but also of the sensor chemistry (e.g. König et al., 2005) further improved the solute imaging. Holst et al. (2001) used a transparent PO to image oxygen distributions as well as the structures behind the optode. Recently, a special setup for low oxygen concentrations was developed (Oguri et al., 2006) and planar optodes were used together with hyperspectral imaging of pigments (Bachar et al., 2008, Kühl and Polerecky, 2008).

Glud et al. (1999) combined light-dark shift measurements with microsensors with planar optode technology to assess 2D distributions of respiration rates and photosynthesis and found pronounced small-scale variability in respiration and production. To obtain the data, they calculated the second spatial derivative of an oxygen image. However, this approach needs some caution, since noise in the image is being strongly amplified by derivation.

The benefit of imaging technologies is obvious in spatially heterogeneous systems like microbial mats or sediments which are intensely influenced by bioturbation or bioirrigation. However, also

in cases where the oxygen distribution is rapidly changing, the use of POs can be superior over profiling methods using microelectrodes or fiber optodes since the time required to get one microsensor profile is in the order of 15-30 min. In contrast, recording one oxygen image with a PO setup (comprising hundreds of profiles) is done typically in less then one second. Hence, it is possible to obtain time series of oxygen images in high frequency. However, the response time of the sensing foil itself may be in the order of 10-20 s, which is too slow to apply the light-dark shift method, where response times below 1 s are desirable (Revsbech and Jørgensen, 1983).

Recent studies showed that the accuracy of conventional PO measurements on small scales and in high gradients is reduced by an optical cross-talk effect in the window and the support foil of the PO (Franke, 2005). Values in the oxic regions are underestimated and oxygen gradients in the oxic/anoxic transition zone are flattened. This decreases the significance of calculations of fluxes and respiration rates, especially if the heterogeneity on small scales is high. Another resolution limiting factor for PO measurements that is evaluated in this study is the diffusion of oxygen within the sensing layer and support foil. Recently, Kühl et al. (2007) presented a PO system for simultaneous microscopic imaging of biofilms and oxygen concentrations. They addressed this problem by decreasing the thickness of the sensing layer to 1-2 µm. This system, however, is restricted to artificial biofilms on microscopic slides.

The light-guidance effect within the sensor foil and window not only limits the resolution of PO measurements, it also prevents the accurate imaging of light fields in sediments or microbial mats which are illuminated from the top. Here, we describe and demonstrate a new type of planar optode setup for high resolution analysis of oxygen concentration distributions as well as light intensities, using a fiber optic faceplate. The system allows correlating oxygen distributions to locally available irradiances. Sensor characteristics such as response time and spatial resolution were assessed, and the acceptance angle for local scalar irradiance measurements was determined. Two-dimensional light field data were compared to profiles obtained with a light microsensor. To calculate rates of benthic photosynthesis and respiration, we adapted the light-dark cycle method of Epping et al. (1999), combining oxygen measurements with numerical simulation of the diffusion equation for 2D, applied the system in sandy sediments and discussed the data in respect to spatial heterogeneities.

## 2.3. Materials and Procedures

### 2.3.1. Manufacturing of the High Resolution Planar Optode (HiPO)

In contrast to the conventional PO, using a polymer support foil, the HiPO described here consists of an oxygen sensitive layer, coated directly onto a fiber optic faceplate, FOFP (SCHOTT North America, Inc.; Fig. 2.1b). The FOFP itself was custom made of light guiding glass fibers, which are fused together perpendicular to the surface of the plate with the dimensions 50 × 50 × 10 $mm^3$ (Fig. 2.1b). Each single fiber has a core diameter of 6 µm with a center to center distance of 10 µm. The space between the fibers is filled with black light absorbing glass. This

assembly leads to the transportation of an image from one side of the plate, pixel by pixel, to the other. The FOFP is therefore an optically anisotropic material, where light guidance is only possible perpendicular to the plane surfaces.

The oxygen sensing layer consisted of platinum(II)mesotetra(pentafluorophenyl)porphyrin (Frontier Scientific, Inc.), dissolved together with polystyrene in chloroform (Precht et al., 2004). To increase the amount of excitation light within the sensing layer, titanium dioxide particles (5 µm, Aldrich) were added (König et al., 2005). These particles do not interfere with the quenching, but enhance the signal by scattering up to 10-fold, depending on their concentration (Zhou et al., 2007). While not mandatory for oxygen measurements, they strongly widen the acceptance angle for light field measurements. The fluorophore was applied by knife coating with a gap of 50 µm (KControl Coater, RK Print Coat Instruments, LTD). After slow evaporation of the chloroform, the resulting sensing layer (phorphyrin in polystyrene matrix) had a thickness of 15-20 µm.

### 2.3.2. Flow-through aquarium and HiPO setup

The FOFP was fitted into an aperture in a wall of a small polystyrene box ($20 \times 10 \times 8\,\mathrm{cm}^3$), with the sensing layer facing inside and being flush with the aquarium wall (Fig. 2.2). For experiments with sandy sediments and microbial mats the box was designed like a small flume with in- and outlets in the short side walls and flow laminarizing honeycomb structures on both sides. A small aquarium pump circulated the seawater, using a 10 L container as reservoir. To prevent porewater advection in the permeable sandy sediment, the sediment topography was flat and the flow rate was adjusted to a minimum, necessary to create a stable diffusive boundary layer. The fluorophore of the HiPO was excited with 2 blue LEDs with collimating optics (LUXEON Star Royal Blue 5 W LXHL-MRRC, $\lambda_{max} = 455\,\mathrm{nm}$, Lumiled) regulated by a homemade fast switchable current source (adjustable between 10 mA and 1000 mA). The emitted red luminescent light ($\lambda_{max} = 647$ nm) was imaged with a peltier-cooled, highly sensitive, fast gateable, 12 bit b/w, 1280×1024 pixel CCD camera (SensiMod, PCO Computer Optics GmbH) with a macro objective (SKR Componon 12 35 / 2.8, Stemmer Imaging in reverse mounting). The objective was chosen to ensure a distortion-free projection of the image with a small object-to-objective distance to keep the setup compact (Fig. 2.2). A long-pass filter (Kodak red wratten gelatine filter Nr. 29 (deep-red), Kodak, Inc., cut-off wavelength ∼580 nm) was installed between the objective and the CCD chip of the camera to block all blue light from the LEDs. This setup allowed distortion-free imaging with a resolution down to $5\,\mu\mathrm{m\,pixel}^{-1}$. A homemade trigger source was used to synchronize camera and LED excitation. Illumination of the sediment (to stimulate photosynthesis) was switched off for <1 s during the oxygen concentration imaging to avoid interferences with the light field. A lifetime-based measuring scheme was applied for the calculation of the oxygen field in front of the HiPO (Holst et al., 1998). Assuming a mono-exponential decay of the luminescence, the fluorescence lifetime can be calculated for each pixel. The resulting lifetime image was calibrated into an oxygen image using a modified version of the Stern-Vollmer equation, assuming a fraction of non-quenchable fluorescence of

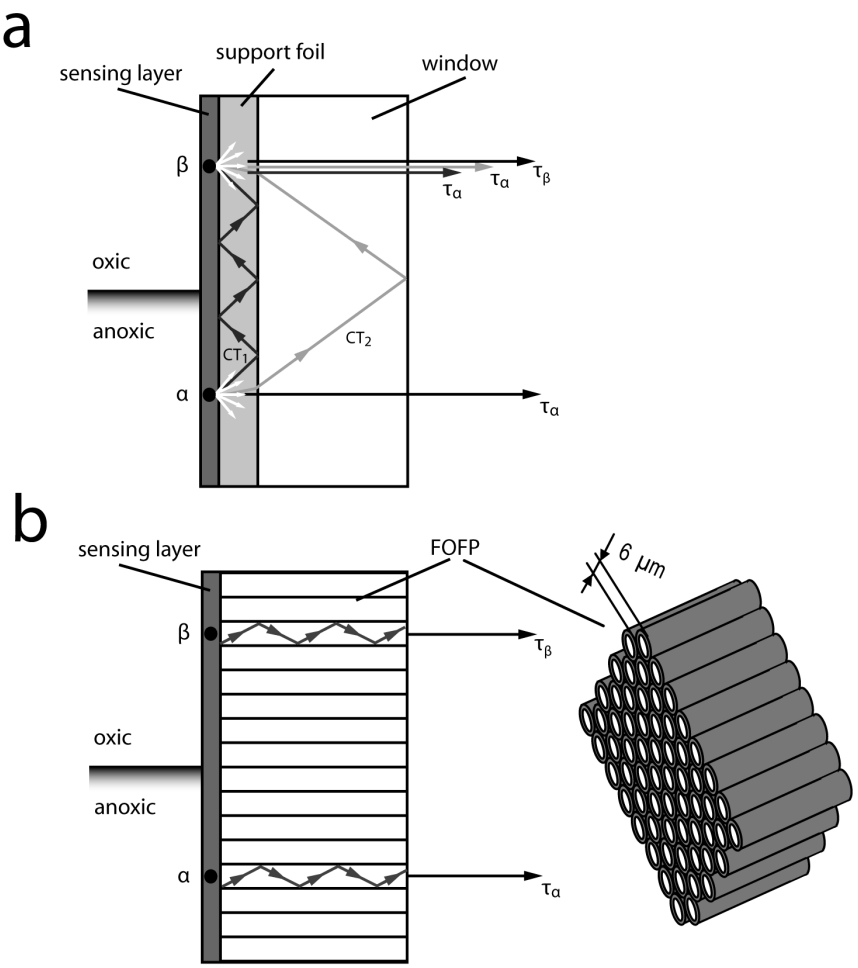


Figure 2.1.: (a) Cross-section of the conventional planar optode. Light travelling within the support foil ($CT_1$) and the window ($CT_2$) leads to optical cross-talk and mixing of fluorescence information. Light with the lifetime $\tau_\alpha$ therefore also contributes to the fluorescence, measured for point $\beta$ (modified after Franke, 2005) (b) Cross-section through the High Resolution Planar Optode (HiPO). A Fiber Optic Faceplate (FOFP), consisting of millions of light guiding fibers prevents optical cross-talk. The dimension of the plate itself is $50 \times 50 \times 10\,\mathrm{mm}^3$. The diameter of the single fibers is 6 µm; the distance between the centerlines of the fibers is 10 µm.

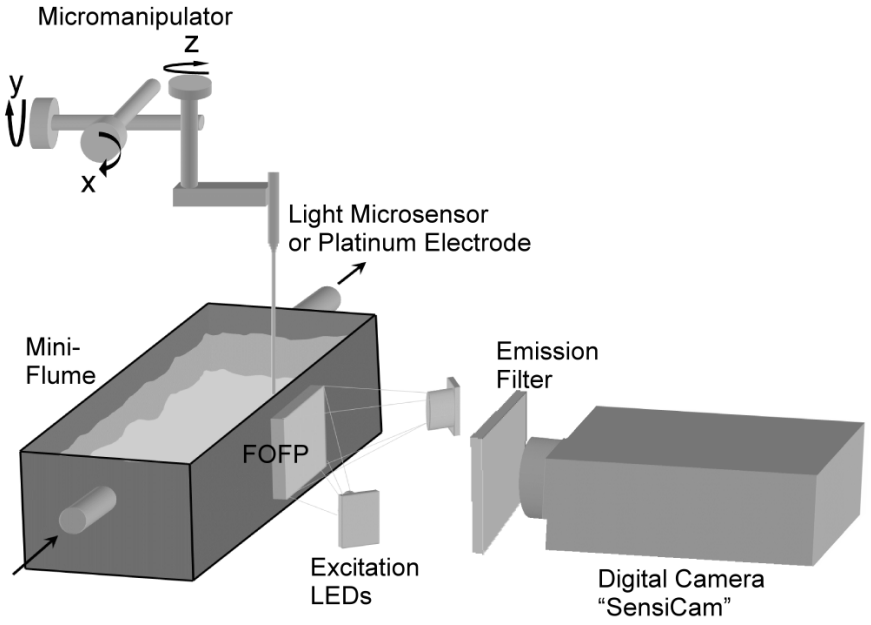


Figure 2.2.: Setup of the High Resolution Planar Optode. A Fiber Optic Faceplate inserted in a miniaturized flume and coated with a fluorophore is illuminated by blue LEDs. The resulting fluorescence is recorded with a specialized camera system. A micromanipulator is used to position a scalar irradiance microsensor for calibration of light measurements with the HiPO.

0.15, which has been found typical for this sensing complex (e.g. Holst and Grunwald, 2001). A 2-point calibration at 0% oxygen and air saturation was carried out (Glud et al., 1996). Image acquisition and trigger control were performed with custom made software (Look@Molli v1.84). The subsequent image analysis and the calculations of lifetime and oxygen images were carried out with homemade software using MATLAB 6.5 (MathWorks Inc.).

### 2.3.3. Light field measurements

Above the flume, a line of 4 white power LEDs (LUXEON Star Warm White, 1 W, LXHL-MWGC, Lumiled) with collimating optics was mounted to create a homogeneous light field at the surface of the sediment, stimulating benthic photosynthesis. These LEDs emit a continuous spectrum from ∼400 nm to ∼780 nm. Compared to sunlight, the LED spectrum contains virtually no UV- and IR-light. The peak wavelength of 630 nm is higher compared to the 520 nm of sunlight (Luxeon technical data sheet DS47, www.philipslumileds.com/pdfs/DS47.pdf). However, the LED spectrum is closer to natural conditions than most other artificial light sources. The irradiance at the sediment surface was adjusted from 0 to ∼300 µmol photons $m^{-2}$ $s^{-1}$ as measured with a spherical quantum sensor (US-SQS/L and LI 250A, Walz GmbH). Light profiles within the sediment were measured using a self made fiber optic light microsensor, consisting of a light guiding fiber with a polystyrene sphere (diameter ∼200 µm) with suspended titanium

dioxide particles for light scattering at its end (Lassen et al., 1992a). Data acquisition to a PC was done with a 12 bit A/D converter (DAQPad 6020E, National Instruments). The light microsensor was calibrated against the above mentioned quantum sensor. For this purpose, the downward scalar irradiance of a white power LED at different operating currents was measured with the factory-calibrated quantum sensor and the self-made microsensor, both mounted above a black anodized aluminum tube as light trap (data not shown). For light intensity profiles the microsensor was mounted in a micromanipulator, fixed to a motorized stage (VT-80, Micos GmbH) to allow for automated profiling. Since the light acceptance of the microsensor is lowest in the direction of the fiber, profiling (step width 100 µm) was done in an angle of 60° to the sediment surface.

To calibrate the light measurements performed with the HiPO, a light field image was averaged over all columns. Two points of the resulting profile were related to light measurements, made at the same depth with the light microsensor. All measured pixel intensities were scaled accordingly, assuming a linear relationship. Since the camera was equipped with a long-pass filter only red light was imaged.

The light acceptance of the setup depends on the numerical aperture of the fibers and the light-scattering properties of the sensing chemistry. We measured the light acceptance at different angles, ranging from 20° to 160°. A laser line was projected from different angles onto the sensing layer under artificial seawater (salt content 35 ‰). The captured light was imaged with the CCD-camera from the other side. After averaging over all lines, the total peak area was integrated to correct for the wider peaks at more acute angles. Values were normalized to the measurement at 90°.

### 2.3.4. Modeling of oxygen diffusion within the sensing chemistry

Diffusion of oxygen within the sensing chemistry leads to reduced measurements of the actual gradients and sets an upper boundary for the differentiation of adjacent features in the oxygen concentration field. To quantify this effect, finite-element numerical modeling of oxygen diffusion within a planar optode sensing layer was carried out, using the software COMSOL (COMSOL AB, Stockholm). The sensing chemistry was modeled as a 20 µm thick layer of polystyrene ($D_{O_2} = 4 \times 10^{-11}\,\mathrm{m^2\,s^{-1}}$ Poulsen and Ogilby, 2000). Initially completely anoxic, half of it was modeled to be exposed to a step change to 100% air saturation while all other boundaries were set to isolation conditions (Fig. 2.1). The transient solution of the diffusion equation for two dimensions (Crank, 1979) was solved on a domain that represented a cross-section through the sensing layer. To calculate the response of the sensing chemistry, we assumed that the fluorescence signal for each point on the HiPO surface is the sum of calculated responses throughout the thickness of the sensing layer.

### 2.3.5. Combined measurements in sandy sediments

The HiPO was applied for combined oxygen and light field sensing on sandy sediment from the subtidal zone of the island Sylt. The sediment was sieved with a 500 µm mesh to exclude macrofauna and pre-incubated in the measurement setup for one week with a light-dark cycle of 12 h at 100 µmol photons $m^{-2}$ $s^{-1}$. The apparent sediment diffusion coefficient $D_s$ =8.6 × $10^{-10}$ $m^2$ $s^{-1}$ was estimated from the oxygen diffusion coefficient in seawater with a salinity of 35 at 20°C ($D_0$ =1.99 × $10^{-9}$ $m^2$ $s^{-1}$), calculated after Boudreau (1997), and a sediment porosity of 0.43 as determined by 48 h drying at 60°C, using Archie's Law (e.g. Berner, 1980). Benthic photosynthesis measurements were carried out at three different incident irradiances ($I_d$), identified throughout the manuscript as $I_d(A)$ = 280, $I_d(B)$ = 100 and $I_d(C)$ = 40 µmol photons $m^{-2}$ $s^{-1}$. Each illumination period lasted for 3 h, followed by 3 h of darkness (Fig. 2.3). Images for scalar irradiance estimations were taken for the three light conditions at the beginning and at the end of the experiment.

### 2.3.6. Calculation of respiration and photosynthesis rates

The distribution of oxygen concentration within sediments is governed by production, respiration, chemical oxidation and diffusion. The reaction-diffusion equation describing these processes for two dimensions reads as:

$$\frac{\partial C}{\partial t} = -\phi D_s \left[ \frac{\partial^2 C}{\partial x^2} + \frac{\partial^2 C}{\partial z^2} \right] + (P - R) \tag{2.1}$$

where $C$ is oxygen concentration, $x$ is the horizontal dimension, $z$ is depth within the sediment and $t$ is time. $P$ and $R$ are time and space dependent oxygen production and uptake terms, respectively, and $D_s$ is the sediment diffusion coefficient. After a minimum of 2 h with constant irradiance, a steady-state situation established, where $\partial C/\partial t = 0$. For any given point within the sediment, the loss of oxygen by diffusion, respiration and chemical oxidation is balanced by production of oxygenic photosynthesis. After darkening, photosynthesis stops instantaneously resulting in a non-steady-state situation. Since the reaction time of the optode was not sufficient to carry out light-dark shift measurements (taken only the decline in oxygen concentration within the first few seconds after darkening into account), we adapted the method developed by Epping et al. (1999) for 2D, using transient oxygen images rather than oxygen profiles.

While the light-dark shift technique uses the initial decline at each sediment depth to estimate gross photosynthesis rate profiles, neglecting the change in diffusion over time, we compare the numerically calculated effect of diffusion alone to the measured effect of diffusion plus oxygen consumption. In order to calculate oxygen consumption rates, the following procedure was used: Oxygen images were taken during illumination at steady-state (light image; LI) and 2 min after the light was switched off (dark image; DI, Fig. 2.3). We then assumed that after the light was switched off, the two remaining processes affecting the oxygen concentration distribution are diffusion and $O_2$ consumption. To determine the change in oxygen concentration solely driven by diffusion the LI was blurred by filtering (convoluting) it with a Gaussian kernel (Koenderink,

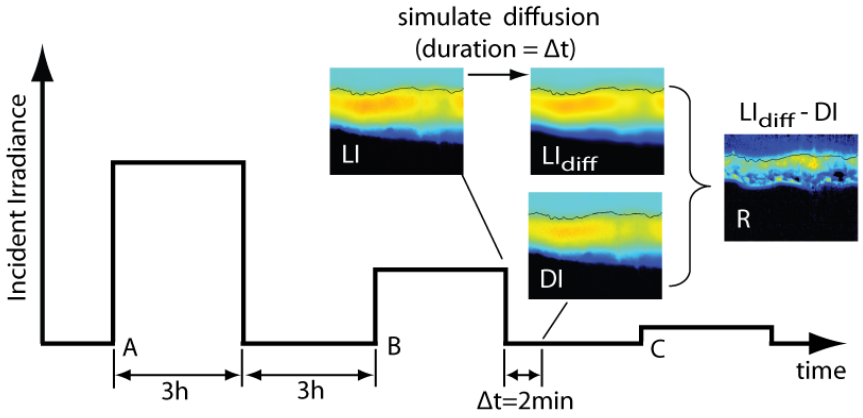


Figure 2.3.: Calculation of 2D respiration rates from transient oxygen images after changes in incident irradiance. A light image (LI) is taken at steady-state and the effect of 2 min of diffusion alone is calculated ($LI_{diff}$). Two minutes after the light was switched off, the dark image (DI) is recorded. The difference between $LI_{diff}$ and DI is an estimate of the spatial distribution of respiration rates within the sediment ($R$). The calculation of net photosynthesis was carried out in a similar way but after the onset of illumination. The letters A, B and C represent the three different light conditions used subsequently in this study. The duration of each light and dark period was 3 h.

1984); standard deviation: 45 pixels). This operation simulates 120 s of diffusion, assuming a sediment diffusion coefficient of $D_s$ =8.6 × $10^{-10}$ $m^2$ $s^{-1}$ with the LI oxygen concentrations as initial condition and zero-flux boundary conditions. This numerical solution of the diffusion equation is commonly used in image analysis (Koenderink, 1984, Cai, 1988). To ensure the applicability and precision of this method for our application, it was tested against an explicit numerical diffusion scheme, resulting in differences $< 2\%$ (pers. communication Dieter Wolf-Gladrow). The calculated image ($LI_{diff}$) was then compared to the measured DI where diffusion and respiration influenced the oxygen concentration distribution. Thus, the pixel-by-pixel difference between these two images represents an estimation of the spatial distribution of respiration (Fig. 2.3). A similar approach was used to estimate primary production. Here, the first image was taken in the dark after steady-state was reached. A diffusion step was calculated and the obtained image was compared to a measured image taken after 2 min of illumination. It has to be noted, that the resulting photosynthetic rate represents the net photosynthesis, thus production minus respiration ((P - R) in Eq. 2.1). The relatively long time step of 2 min was necessary because of the low production- and respiration rates of the studied sediment.

### 2.3.7. Calculating profiles and integrating respiration and production rates

Quantitative comparison of scalar irradiance, respiration rates and photosynthesis was done by averaging 2D data to 1D profiles of oxygen, represented by every column of the respective images,

taking the different positions of the sediment surface into account. Diffusive exchange of oxygen (DOE) across the sediment-water interface ($z = 0$) was calculated from the mean oxygen profiles using Fick's 1st law of diffusion

$$DOE = -D_0 \left.\frac{\partial C}{\partial z}\right|_{z=0} \tag{2.2}$$

with the molecular diffusion coefficient $D_0$ =1.99 $\times 10^{-9}\,\mathrm{m^2\,s^{-1}}$. Local rates of respiration and net primary production were integrated over depth ($z$) and averaged over all columns of the image, resulting in areal oxygen fluxes:

$$J_R = \frac{\Delta z}{n} \sum_{n=1}^{n_{max}} \sum_{z=0}^{z_{max}} R_{n,z} \qquad \text{and} \qquad \mathrm{J_P} = \frac{\Delta \mathrm{z}}{\mathrm{n}} \sum_{\mathrm{n=1}}^{\mathrm{n_{max}}} \sum_{\mathrm{z=0}}^{\mathrm{z_{max}}} \mathrm{P_{n,z}} \tag{2.3}$$

with $J_R$ and $J_P$ being the fluxes across the sediment-water interface, $\Delta z$ the pixelsize ($\Delta$z=10.1 µm), $n$ the numbers of columns ($n_{max} = 1280$) and $R_{n,z}$ and $P_{n,z}$ the respiration and production rates at column $n$ and depth $z$ as calculated above. The mean vertical light attenuation coefficient $K$ was calculated from the average scalar irradiance profiles $I(z)$ below 0.5 mm by fitting an exponential function to the profiles (Kühl et al., 1994): $I(z) = \alpha e^{-Kz}$, with $\alpha$ as arbitrary fit parameter.

**Local photosynthesis/irradiance relationship and photosynthetic efficiency -** The availability of scalar irradiance and photosynthesis distributions allowed calculating local photosynthesis/irradiance relationships for each of the three light conditions. These curves differ from conventional P-I curves, since they consider the local effect of scalar irradiance on photosynthesis rather than providing the averaged budget for the sediment (Dodds et al., 1999, for the 1D case). The curves were constructed by binning the scalar irradiances with a bin-width of 10 µmol photons $\mathrm{m^{-2}\,s^{-1}}$. The corresponding photosynthesis rates of all pixels that fell into one bin were averaged and plotted against the mean irradiance of the respective bin.

To assess the relative efficiency of light utilization by the phototrophic community and its variation with sediment depth, the quotient of photosynthetic rate and scalar irradiance was calculated, resulting in photosynthetic efficiencies in units of [mmol $\mathrm{O_2}$ $(\mathrm{mol\,photons})^{-1}\,\mathrm{mm^{-1}}$] (Lassen et al., 1992b).

## 2.4. Assessment and Discussion

### 2.4.1. Optical Cross-Talk effect

Light travels within the support foil and the window of conventional planar optode setups by reflection on the surfaces (Fig. 2.1a). Part of this light is decoupled on other sites of the foil and contributes to the fluorescence, originating from these spots. The overall fluorescence intensity is therefore altered, as well as the fluorescence lifetime ($\tau$) (Franke, 2005). Since the fluorescence is quenched by oxygen, light emission is stronger in anoxic regions than in oxic regions. The

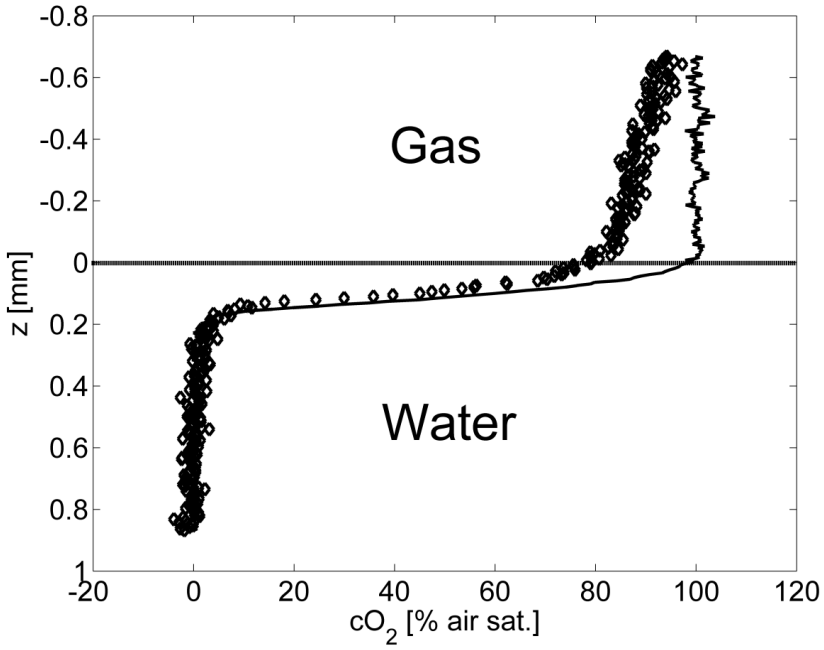


Figure 2.4.: Extracted vertical profiles of oxygen concentration after changing the gas phase over anoxic water from nitrogen to air, measured with the HiPO (solid line) and a conventional PO (open symbols).

anoxic parts of the sediment thus influence the measurements in oxic areas stronger than vice-versa. Overall, this artifact results in smeared images and flattened gradients, decreasing the significance of calculations of fluxes and respiration rates, especially if the heterogeneity on small scales is high.

The HiPO was compared against a conventional PO setup to test if this optical cross-talk could be reduced. A small flume comprising HiPO and conventional PO was half-filled with anoxic distilled water. The overlying gas phase was initially nitrogen and then rapidly changed to air, leading to highly reproducible sharp oxygen gradients across the water-air interface. In contrast to the conventional PO, no erroneously low oxygen concentration was measured above the interface with the HiPO (Fig. 2.4), indicating an effective suppression of the cross-talk effect. Hence, the recorded gradient appeared much steeper with the HiPO, as it was with the conventional setup. For practical purposes, cross-talk artifacts at the sediment-water interface can be taken into account, using the a-priori knowledge about the oxygen concentration in the water column. Within the sediment, however, such a correction is not possible.

The magnitude of optical cross-talk effects in conventional PO assemblies depends on a multitude of factors such as wall thickness and material, thickness of the support foil, content of scattering particles within the sensing layer and distribution of sediment oxygen concentration, to name only a few (Glud, 2008). It is beyond the scope of this study to determine the relative influence of all these factors and it is therefore not possible to precisely quantify the improvement

gained by using the HiPO.

**Spatial and temporal resolution of oxygen measurements -** The theoretically achievable spatial resolution of the HiPO system is limited by the optical performance of the setup and the blurring of the signal due to oxygen diffusion in the sensing chemistry (Kühl et al., 2007). The temporal resolution of all PO setups is regulated by the equilibration time of the sensing chemistry. In order to estimate the magnitude of both effects for the HiPO setup, a numerical diffusion model was set up, using finite element modeling as described in the methods section. This model allowed calculating the transient and steady-state oxygen fields within a cross section of the sensing layer, assuming a step change on the surface of the (polystyrene) sensing layer (Fig. 2.5A). Profiles of the response of the sensing layer (Fig. 2.5B) were obtained by averaging over all columns of the calculated oxygen field within the sensing layer of (Fig. 2.5A). This model can also be used to estimate the temporal response of the sensor after a change in oxygen concentration (Fig. 2.5B). If the sensor is initially oxygen-free and then the oxygen level is raised to 100% for half of the sensor surface, oxygen diffuses into the sensing chemistry changing the fluorescence properties in this area. After 1 s, the signal only reached 36% of the final concentration. A typical 90% response is reached between 5 and 10 s for a 20 µm thick sensing layer. After ∼20 s, steady-state is reached. The sharp boundary between the oxic and anoxic zone is then smeared and extended over about 100 µm (Fig. 2.5). The response of the sensing layer to a step change in concentration represents the highest gradient that can be resolved by the system. Thus, it provides the theoretical limit of resolution given by diffusion in the sensing layer. For all practical concerns, the difference between the 'real' oxygen concentration and the one measured by the PO setups will be smaller than in this extreme example.

Model runs assuming thinner sensing layers showed a linear relationship between layer thickness and spatial resolution (results not presented). A 2 µm thick layer therefore exhibits a resolution limit of about 10 µm. Since the change of layer thickness is essentially only affecting the scale of the model, this linearity is obvious. The resolution limit of planar optodes due to diffusion is therefore in the order of 5 times the thickness of the sensing layer, assuming polystyrene as matrix polymer. Thinner layers, however, demand for stronger excitation light sources and/or more sensitive cameras. Layers of 10-20 µm were found to be a good compromise for our setup. Depending on the brightness of the excitation light source, the imaged area, the sensitivity of the camera, the concentration of scattered particles and the choice of the fluorophore, thinner layers are possible (Kühl et al., 2007). Using polymers with a higher molecular diffusion coefficient for oxygen would result in faster responding optodes, but lower spatial resolution.

### 2.4.2. 2D light field measurements

The penetration of light into sediments is not uniform due to scattering and refraction at sediment grains, worm borrows, and gas bubbles, resulting in a patchy distribution of irradiance (Lassen et al., 1992b, Kühl et al., 1994). To quantify scalar irradiance within sediments, light intensity images were taken through the HiPO. Projections of a laser line from different angles were

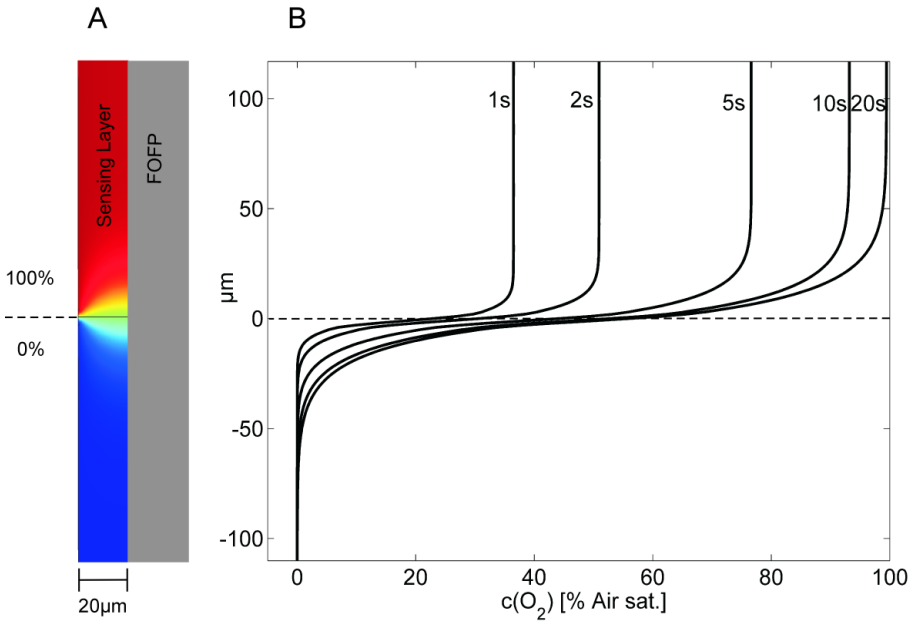


Figure 2.5.: (A) Modeled steady-state oxygen concentration within a cross section of a 20 µm thick sensing layer, exposed to a step change in oxygen concentration at $y$ =0 µm. The fiber optic face plate (FOFP) is impermeable for oxygen. See Fig. 2.4 for the color scale; values in percentage air saturation. (B) Modeled temporal and spatial response of the sensing layer to a step change in oxygen concentration. Initially, the foil was modeled to be completely anoxic. At t = 0 s, the upper half ($y > 0$ µm) was exposed to 100% air saturation.

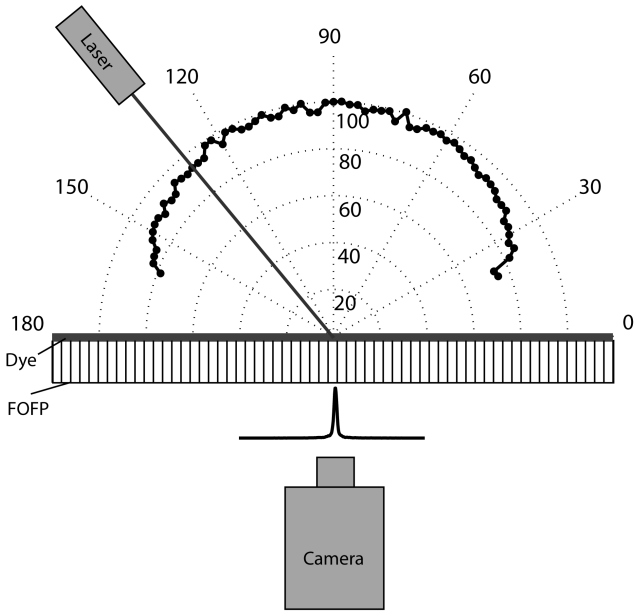


Figure 2.6.: Light acceptance angle of the FOFP with scattering sensing layer. A laser line was projected onto the surface under seawater at different angles and the captured light was imaged with a CCD camera. Measured peak areas are given, normalized to the 90° value.

performed to assess the acceptance angle of the HiPO (Fig. 2.6). Between 90° ± 30° incident light was transported equally well, while in the range of 40-60°, capture efficiency drops to 90%. Below 20°, a strong drop in light acceptance was observed (Fig. 2.6). This almost hemispherical acceptance characteristic of the HiPO allows using light intensity images to be used as a measure for scalar irradiances. It has to be noted, that the spatial heterogeneity of scalar irradiances close to walls (like the HiPO) is likely to be higher than in unconstrained sediments. Especially in the top layers of the sediment where heterogeneities are most pronounced (Lassen et al., 1992b), the HiPO tends to overestimate spatial variability. Assuming a 20 µm thick sensing layer and a light acceptance angle of 130°, a theoretical resolution of ∼120 µm can be estimated. This is in the same order of magnitude as the resolution of typical scalar irradiance microsensors (Lassen et al., 1992a, ca. 100 µm).

Light field images were measured in sandy sediments and compared to light profiles obtained with microsensors for scalar irradiance (Lassen et al., 1992a). The images exhibit a high spatial variability, both horizontally and vertically. Light profiles were extracted by averaging intensities over columns of a 100 µm wide stripe (Fig. 2.7). Profiles differ considerably from each other due to different scattering, resulting in hot spots of high light intensities in otherwise darker sediments. Highest light intensities are not always directly above the sediment surface and the light intensity does not decrease steadily below the surface. However, the overall light penetration depth (defined as the depth, where scalar irradiance drops below 1 µmol photons $m^{-2} s^{-1}$) is similar in all extracted profiles (Fig. 2.7).

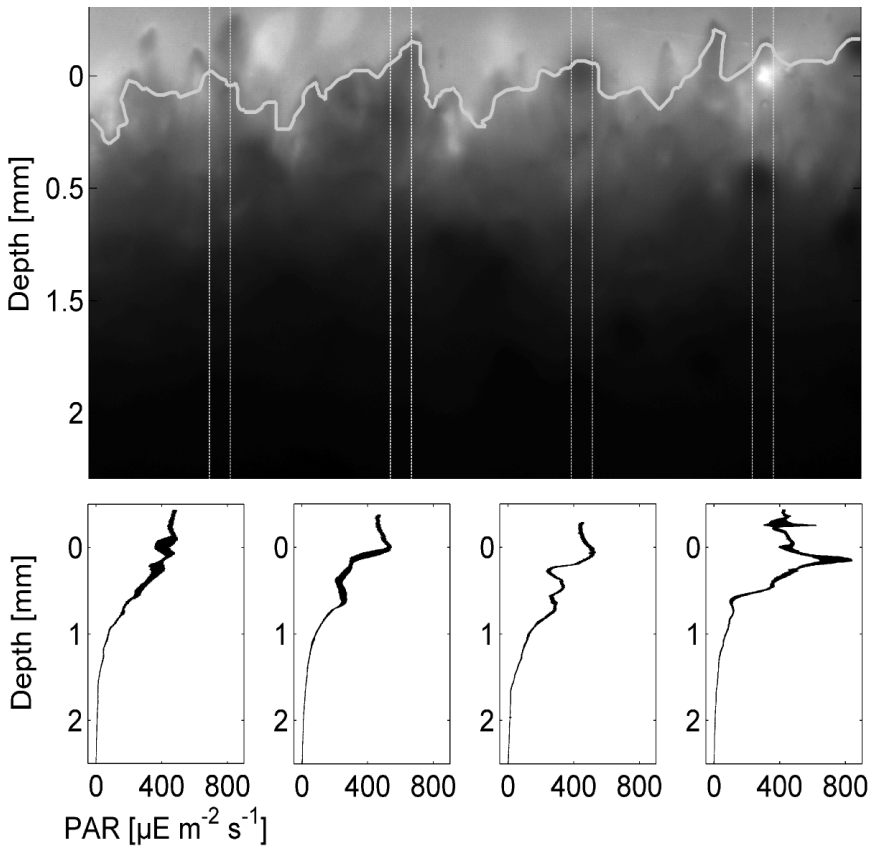


Figure 2.7.: Top: Light intensity image of a sandy sediment, taken through the HiPO. The sediment was illuminated from above with white light. Bottom: Four light profiles, each extracted from a 100 µm wide area of the image by averaging along the x-axis. The line width in horizontal direction indicates the standard deviation of the measured irradiance at each pixel.

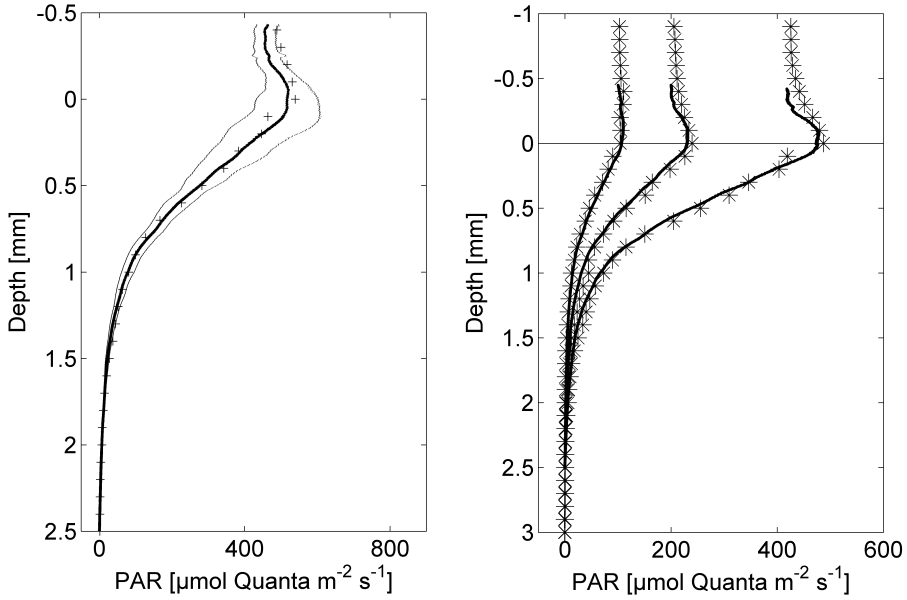


Figure 2.8.: Left panel: Mean light profile of photosynthetically active radiation (PAR), extracted from the light intensity image in Fig. 2.7 by averaging over all columns (thick line), standard deviation of the intensities (thin lines) and light profile, measured with a light microsensor (plus symbols). Right panel: Comparison of light profiles measured with a light microsensor and profiles obtained by averaging over all columns of an intensity image at 100, 200 and 410 µmol photons $m^{-2}\,s^{-1}$, respectively.

Mean profiles were extracted at three different incident irradiances by averaging over all columns of the intensity images and were compared with scalar irradiance microsensor measurements (Fig. 2.8). Strongest differences were observed above the sediment surface. Here, the HiPO provides up to 10% lower values than the microsensor. The reason might be that most of the light reflected at the sediment surface is traveling upwards. For spherical microsensors profiling from the top this is the preferred acceptance direction, while the HiPOs fibers are directed perpendicular. However, the microsensor readings are within the double standard deviation of the averaged columns' readings, indicating an overall agreement between both methods (Fig. 2.8, left). The better accordance of the two methods deeper within the sediment is related to the fact that the light field tends to approach isotropic radiance distribution with depth (Kühl et al., 1994). Comparisons at different light levels (Fig. 2.8, right) reveal the same profile pattern indicating that the HiPO can be calibrated against a scalar irradiance microsensor.

The most important difference between the two methods is the spectral response. The light microsensor can be used to assess spectral compositions of scalar irradiance or total photosynthetically active radiation (PAR) by using a spectrometer as detector (Kühl and Jørgensen, 1994). The spectral properties of the light field measurements with the HiPO are dependent on the spectral response of the CCD camera, the transmission characteristics of the FOFP with the

fluorophore coating and the emission filter for the oxygen sensing. The spectral response of the camera was nearly linear between 350 and 550 nm wavelength, therefore it is in principal suitable to measure PAR. However, the emission filter was a long pass filter with a cut-off wavelength of ∼580 nm, allowing only red light to pass through. If the spectral composition of the down-welling light does not change substantially within the sediment, the calibration against the PAR sensor in the overlying water is still valid for deeper layers. This assumption depends on the concentration and distribution of pigments within the sediment. It is known, that highly structured phototrophic communities absorb different wavelength at different depth (e.g. Ploug et al., 1993). This effect is less pronounced in sandy sediments due to the generally less structured community.

### 2.4.3. Oxygen dynamics in sandy sediments

Small-scale oxygen distributions and dynamics and their linkage to the light field have been studied extensively on microbial mats (e.g. Lassen et al., 1992b, Epping et al., 1999, Glud et al., 1999, Bachar et al., 2008), but less work has been done on sandy sediments without dense mat formation. Therefore, we applied the HiPO to phototrophic sandy sediments and measured oxygen production and respiration together with the light field as major driving force (Fig. 2.9). The sediment was inhabited (among others) by diatoms and cyanobacteria, exhibiting considerable photosynthesis during illumination.

**Light field within the sandy sediment -** The different incident light intensities, measured as down-welling irradiances above the sediment surface are indicated in Figs. 2.9 and 2.10 by (A), (B) and (C) (40, 100 and 280 µmol photons $m^{-2}$ $s^{-1}$, respectively). The light field within the sediment (Fig. 2.9, column 1) was highly inhomogeneous at sub-millimeter scale, most likely due to reflections and refractions by sediment grains. This effect was most pronounced close to the sediment surface (Kühl et al. 1994). Highest local light intensities were detected ∼100-200 µm below the sediment surface. Here, the scalar irradiance exceeded 200% of the surface down-welling irradiance at some spots. The average light penetration depth (defined as the depth, where scalar irradiance drops below 1 µmol photons $m^{-2}$ $s^{-1}$) was 5, 4.2 and 3.3 mm, at the three light conditions respectively (Fig. 2.10, Table 2.1). The three mean scalar irradiance profiles showed the same exponential decrease with depth (Table 2.1, $R_2 > 0.99$), leading to a mean vertical light attenuation coefficient $K$ of 0.85 $mm^{-1}$. Kühl et al. (1994) found a twice as high attenuation coefficient for wet quartz sand with particle sizes of 125-250 µm (1.65 $mm^{-1}$) and a four times higher attenuation coefficient for a coastal sediment with particle sizes of 63-250 µm. The lower light attenuation in our study can be explained by larger particles sizes of up to 450 µm and the low density of light absorbing photopigments (s. below).

**Oxygen concentration field -** The oxygen concentration field changed clearly within minutes upon changes in light conditions. However, transition times of more than 2 h after each change in illumination were needed to establish new steady-state situations. Similar transition times were found by Fenchel and Glud (2000) for a shallow-water sediment. At high incident light ($I_d(A)$), the first 5 mm of the sediment were oxygen super-saturated with concentrations up to

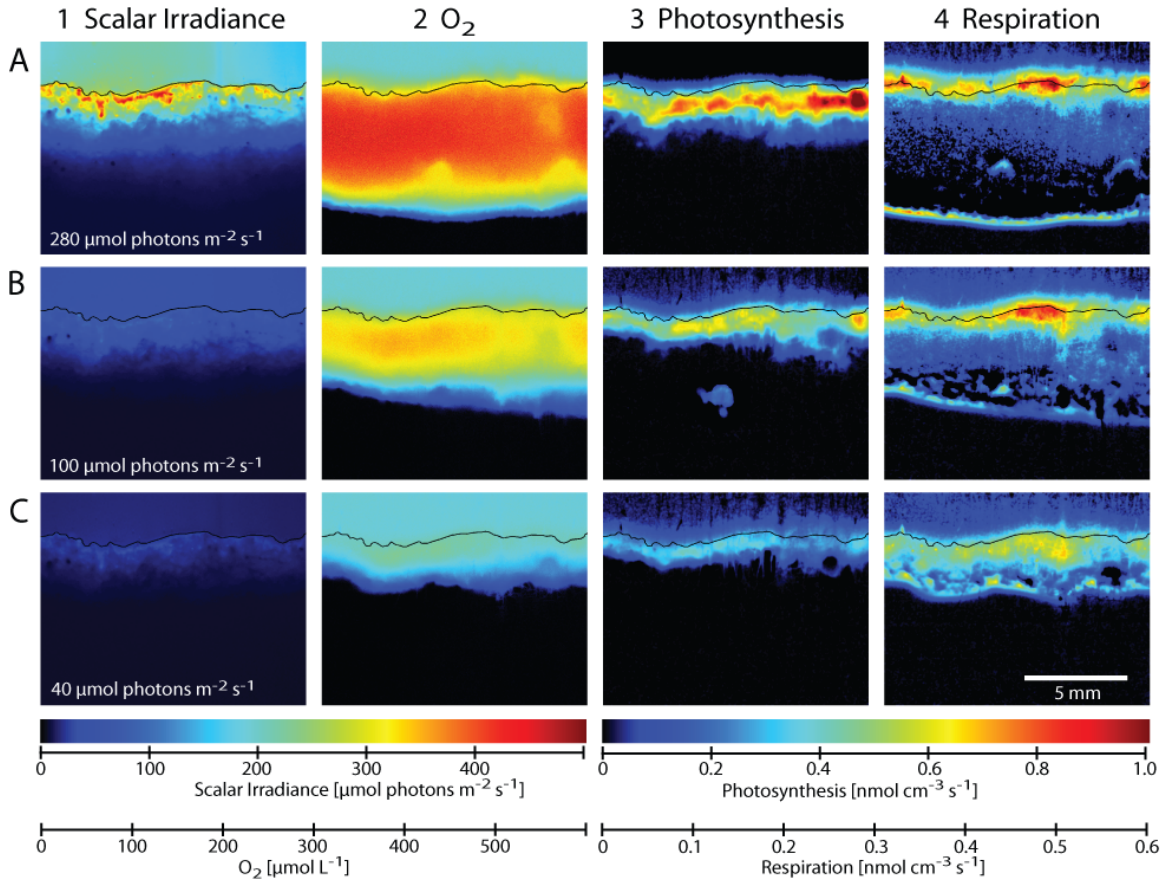


Figure 2.9.: Images of light (1), oxygen (2), photosynthesis (3) and respiration (3) at three different light conditions (A-C) in phototrophic sandy sediment after steady-state was reached. The black line indicates the sediment surface. Pixel size in theses images was 10.1 µm. The productive spot visible in the middle of the imaged area in B3 was related to a gas bubble formed as a result of the oxygen super-saturation during high light condition, supplying oxygen to the surrounding sediment.

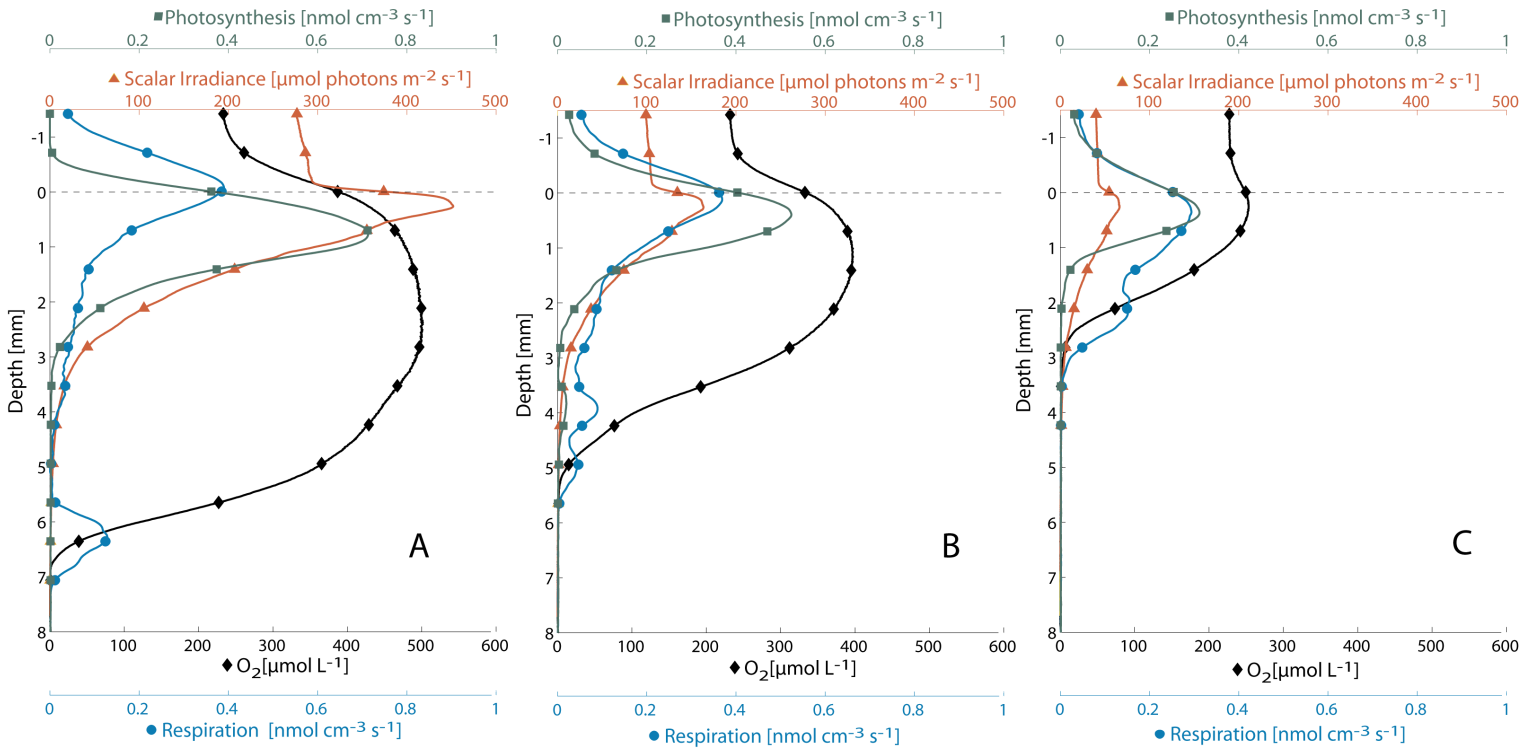


Figure 2.10.: Profiles of scalar irradiance, oxygen concentration, respiration rate and photosynthesis rate at three different steady-state situations (A, B, C) with different illuminations. The profiles were obtained by averaging over the columns of Fig.9, taking the position of the sediment surface into account. Symbols represent every 70th data point.

500 µmol $L^{-1}$; the mean oxygen penetration depth was about 6.8 mm and there was a net flux of oxygen (36 mmol $m^{-2}$ $d^{-1}$) into the overlying water (Fig. 2.10 and Table 2.1). The oxygen concentration distribution did not exhibit strong spatial heterogeneities on scales below 1 mm (Fig. 2.9, A2). After the light was switched off, oxygen concentrations immediately decreased, especially close to the sediment surface. However, the formation of three oxygen bubbles in the imaged area with diameters between 0.7 and 2 mm led to zones of supersaturation which persisted for more than 1h (data not shown). At $I_d(B)$, the mean oxygen penetration depth reduced to 5.2 mm (Fig. 2.10 B). There was a considerable difference in OPD within the averaged area, ranging from 3.9 to 5.6 mm (Fig. 2.9, B2). The oxic-anoxic interface was characterized by smaller gradients, also with strong horizontal differences; the super-saturated zone reduced to a mean of 3.5 mm sediment depth (Fig. 2.9) and showed stronger heterogeneities compared to those at high light intensities (Fig. 2.9, B2). At $I_d(C)$, still slight super-saturation occurred and photosynthesis exceeded respiration, leading to a net flux of 7 mmol $m^{-2}$ $d^{-1}$ $O_2$ out of the sediment (Table 2.1). The mean oxygen penetration depth reduced to 3.1 mm and the oxic-anoxic transition zone was even less straight compared to medium light conditions (Fig. 2.9, C2). During all three steady-state darkness situations between the illuminated periods, the mean oxygen penetration depth reduced to 1.7 mm (Table 2.1).

**Local net photosynthesis rates -** Photosynthesis (Fig. 2.9, column 3) was calculated from subsequent images immediately before and directly after the onset of illumination. This procedure results in estimations of local net photosynthesis rates. At $I_d(A)$, highest rates of net photosynthesis were observed on average 900 µm below the sediment surface (Fig. 2.10A) and appeared very patchy (Fig. 2.9, A3). The peak values of more than 1 nmol $O_2$ $cm^{-3}$ $s^{-1}$ were not located at the spots of highest light intensity within the sediment. Photo adaptation could explain this effect, as well as migration due to light stress (MacIntyre and Cullen, 1995, Underwood et al., 2005). The entire productive zone was about 3.5 mm thick and almost identical to the area, in which light intensities were $> 30$ µmol photons $m^{-2}$ $s^{-1}$ (Fig. 2.10A). At medium light conditions ($I_d(B)$), the overall thickness of the productive zone was only slightly reduced ($\sim$3 mm), but the peak values of photosynthesis diminished and the heterogeneity in production was less pronounced. Highest production was now close to areas with highest light intensities but the average position of peak photosynthesis was still below the position of peak scalar irradiance (Fig. 2.11B). At $I_d(C)$, the zone of primary production was limited to a thickness of 1 mm. A spatial coincidence of peak scalar irradiance and photosynthesis rates was found for this lowest incident irradiance (Figs. 2.9, C1 and 2.9, C3; Fig. 2.10C).

**Correlation of local net photosynthesis and light availability -** The relationship between local net photosynthesis and scalar irradiance at the respective positions within the sediment was used to construct curves of mean local photosynthesis vs. scalar irradiance (Fig. 2.11A). A comparable approach in 1D was taken by Dodds (1992) and Dodds et al. (1999). However, they used the light-dark shift method and reported local gross photosynthesis vs. irradiance curves for different depths intervals, while we provide curves of net photosynthesis vs. irradiance, averaged over all measurements at one incident irradiance. The curves in Fig. 2.10A

differ from conventional P-I curves since they do not represent the average response of the whole sediment community to changing incident light intensities but the mean local response to the resulting scalar irradiance within the sediment. All three curves show the same general pattern of increasing photosynthesis with increasing irradiance, until a maximum is reached (Fig. 2.10A). At higher irradiances, the photosynthetic activity decreases again, most likely due to photoinhibition (e.g. Serôdio et al., 2005, and references therein). Therefore, curves calculated for the three different $I_d$ exhibit maximum photosynthesis rates at different light intensities. While at $I_d(A)$, the highest photosynthetic rates were observed at around 300 µmol photons $m^{-2}$ $s^{-1}$, this value was reduced to 230 and 100 µmol photons $m^{-2}$ $s^{-1}$ for $I_d(B)$ and $I_d(C)$, respectively (Fig. 2.11A). Since the same scalar irradiance is found in different depths within the sediment at different incident light conditions, it is likely that the responses reflect a stratified community. Adaption to the incident irradiance on single-cell level even in time scales of minutes (Serôdio et al., 2005), as well as migratory behavior of algal cells (Barranguet et al., 1998, Saburova and Polikarpov, 2003) and cyanobacteria (Castenholz et al., 1991) are also likely.

**Photosynthetic efficiency -** The efficiency of light utilization by the phototrophic community changes with sediment depth as well as with incident light intensity (Fig. 2.11B). A general trend of increasing photosynthetic efficiency with depth can be seen. At $I_d(A)$, no maximum is reached while at $I_d(B)$ and $I_d(C)$ maximum values are located in 4.5 and 3.5 mm sediment depth, respectively. As a consequence of light adaptation, the maximum efficiency at the lowest incident irradiance (0.42 µmol photons $m^{-2}$ $s^{-1}$) is higher than at medium irradiance (0.32 µmol photons $m^{-2}$ $s^{-1}$). Lowest efficiencies are found for $I_d(A)$. The net photosynthetic efficiency depends on the prevalent respiration rate, the amount of photopigments present and on the efficiency light usage for photosynthesis (Lassen et al., 1992b). The latter is partly dependent on irradiance and decreases as the intensity exceeds the light saturation of the population. The differences of photosynthetic efficiencies between the three different incident light intensities can therefore be explained by photo-acclimation, changing the efficiency of single cells (Serôdio et al., 2005) and migration of phototrophic organisms (e.g. Perkins et al., 2001, Underwood et al., 2005), changing the pigment concentration in a given sediment horizon. Lassen et al. (1992b) found comparably shaped profiles of photosynthetic efficiency with depth and a comparable influence of different incident light intensities for microbial mats. However, their reported efficiencies exceed the values presented here by 2 - 3 orders of magnitude. The most likely reason is the much higher pigment density in microbial mats compared to the sandy sediment in our study. The low light attenuation coefficient of our sediment (s. above) supportes this assumption.

**Oxygen exchange rates and $O_2$ budget -** The distribution of oxygen exchange rates within the sediment exhibited two conspicuous zones of high consumption at all three light conditions (Fig. 2.9, column 4). One was located directly at the oxic-anoxic interface. It can be explained by chemical oxidation of reduced compounds that are formed during anaerobic metabolic activities, diffusing upwards (e.g. Canfield et al., 1993). Additionally, some microorganisms (e.g. some species of sulfate reducing bacteria) live preferentially in this transition zone and respire oxygen at high rates (Cypionka, 2000). This zone was most obvious at $I_d(A)$, where it was located deepest

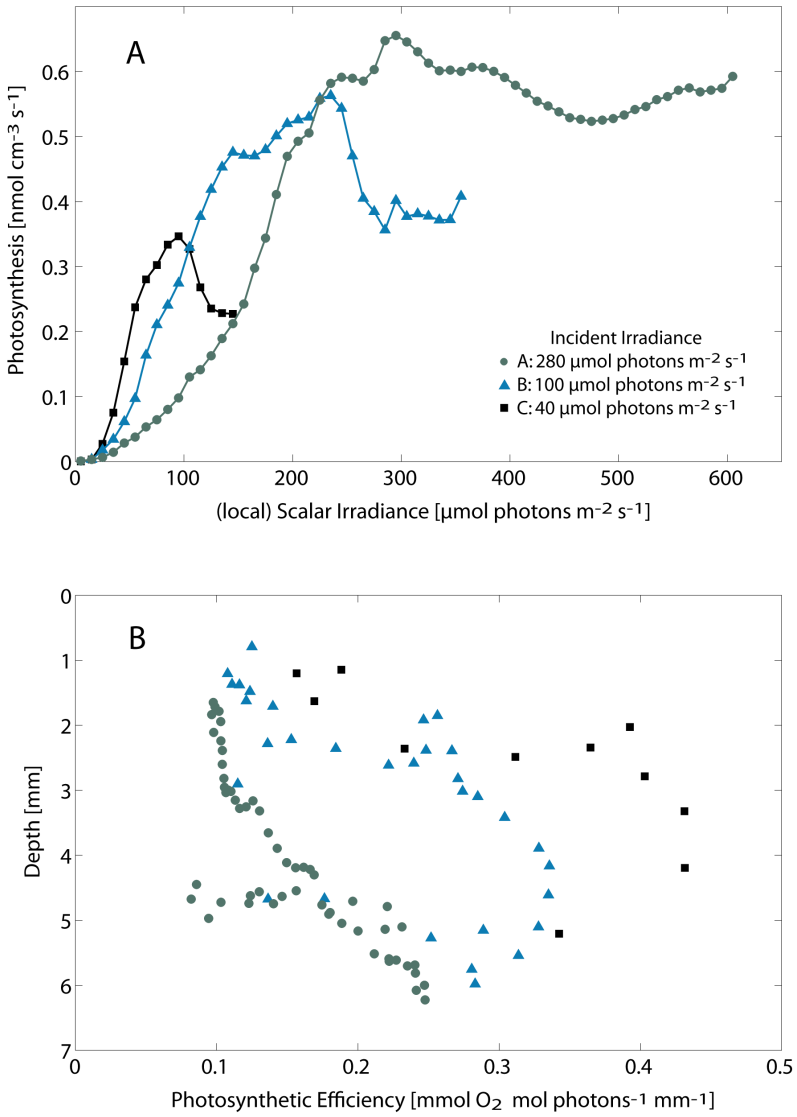


Figure 2.11.: (A) Average local photosynthesis plotted against average local scalar irradiance (Fig. 2.9, column 3&1) The three curves represent the three different illuminations (A, B, C) as in Figs. 2.9 and 2.10. (B) Photosynthetic efficiency at the three light conditions calculated as the local photosynthesis divided by the local scalar irradiance and plotted against sediment depth

within the sediment and had a thickness of <1 mm (Fig. 2.9, A4) . Here, reoxidation processes are likely to be more relevant than further upwards due to the higher relative importance of anaerobic processes deeper in the sediment. Such narrow zones of very high oxygen uptake directly at the oxic-anoxic interface have been reported before (e.g. Revsbech et al., 1986). The second zone of high oxygen uptake was located close to the sediment surface. Here, again, two mechanisms play a role; the density of respiring organisms and the accumulation of labile organic matter are likely to be highest close to the surface. Additionally, photoexsudates, excreted by phototrophic organisms, might have fueled oxic respiration (Bateson and Ward, 1988). Because of the net oxygen production some of the oxygen is also removed by diffusion into the well-mixed overlying water column. However, the modeling of diffusion did not account for the enhanced eddy diffusivity in the water column above the sediment surface. Thus, calculated rates of respiration above the surface should be taken with caution.

The integrated dark respiration rates in the order of $\sim$20 mmol m$^{-2}$ d$^{-1}$ (Table 2.1) are in the range of values found for coastal sandy sediments (Middelburg et al., 2005). The average $O_2$ consumption is stimulated to $\sim$50 mmol m$^{-2}$ d$^{-1}$ during illumination. Similar increases in light-respiration have previously been reported (e.g. Epping and Jørgensen, 1996, Fenchel and Glud, 2000). Integrated rates of oxygen consumption and production are used to compile oxygen budgets for the different light conditions. The resulting fluxes can be compared to flux estimates from average oxygen profiles to cross-check the plausibility of measurements and calculations. The diffusive oxygen flux across the sediment/water interface (DOE) under illuminated conditions is governed by the integrated rates of net photosynthesis ($J_P$, Eq. 2.3), comprising gross photosynthesis plus respiration. These two parameters should therefore match. However, $J_P$ shows a higher efflux of oxygen from the sediment than the average DOE at all three light conditions, while the differences decreased with decreasing irradiance (Table 2.1). These discrepancies between DOE and $J_P$ might indicate different respiration rates in the light and in the dark. The net photosynthesis rates ($J_P$) were obtained directly after the onset of illumination; they thus include a sediment respiration close to the dark respiration, while the DOE was determined 3 h after the onset of illumination and represent the higher light respiration, where photoexsudates and the increased area of the oxic zone resulted in enhanced oxygen uptake (Epping and Jørgensen, 1996). It is also likely, that the mean DOE was underestimated by the averaging procedure, used to obtain a single oxygen profile from an oxygen image, since small inaccuracies in the position of the sediment surface lead to a smeared gradient in the average profile. Additionally, the formation of gas bubbles may lead to underestimations of DOE (Epping and Jørgensen, 1996) and the PO might interfere with the DBL (Glud, 2008).

A light enhanced respiration, however, is not reflected in the integrated respiration rates ($J_R$, Eq. 2.3, Table 2.1). The assumption of the same molecular diffusion coefficient in the water column as in the sediment, rather than eddy diffusion, bias the respiration rates calculated for areas closely below the sediment surface. Also changes in respiration rates during the time step of 2 min, before the dark respiration image was taken, might have occurred. More sophisticated modeling of the diffusion step and additional light-dark shift measurements with microsensors

Table 2.1.: Down-welling irradiance $I_d$, vertical light attenuation coefficient $K$, oxygen penetration depth $z_{ox}$ and oxygen budget for sandy sediment at three different illuminations. Oxygen penetration depth, light attenuation coefficient and diffusive oxygen exchange ($DOE$) have been calculated from the mean oxygen profiles (Fig. 2.9). Integrated rates of respiration ($J_R$) and net photosynthesis ($J_P$) were calculated from data presented in Fig. 2.9, columns 3 and 4. A, B and C correspond to the respective panels in Figs. 2.9 and 2.10. Values in the last line were calculated from an oxygen image at steady-state situation during the dark (image not shown). Negative values imply fluxes out of the sediment.

| Panel | $I_d$ | $K$ | $z_{max}$ | $J_R$ | $J_P$ | DOE | $J_P + DOE$ |
|---|---|---|---|---|---|---|---|
| | µmol photons $m^{-2}$ $s^{-1}$ | $mm^{-1}$ | mm | mmol $m^{-2}$ $d^{-1}$ | | | |
| A | 280 | 0.85 | 6.8 | -47 | 89 | -36 | 53 |
| B | 100 | 0.86 | 5.2 | -53 | 54 | -29 | 25 |
| C | 40 | 0.84 | 3.1 | -49 | 24 | -7 | 17 |
| - | 0 | - | 1.7 | - | - | 22 | - |

could be performed to clarify these uncertainties.

## 2.5. Comments and Recommendations

The novel planar optode imaging setup provides spatially resolved insights into oxygen dynamics in phototrophic sediments and microbial mats at high spatial resolution together with local estimations of scalar irradiance. This facilitates studies concerning the functioning of phototrophic microbial communities in detail, together with the local light field as the most important driving force. The HiPO together with the proposed calculation scheme enables the determination of spatial correlations of photosynthesis and respiration rates with the scalar irradiance distribution. New insights into the coupling between autotrophic and heterotrophic communities and their spatial organization can be gained. It provides higher certainty for oxygen measurements at small scales and high gradients by the suppression of the optical cross-talk effect present for conventional POs. Since the sensing layer is coated directly onto a glass surface, there is no oxygen diffusion within the support foil or imaging window to be taken into account. To optimize the adhesion of the sensing layer to the glass surface, silanization of the FOFP prior to coating could be performed (Kühl et al., 2007). The overall mechanical complexity of the new setup is only slightly increased compared to conventional POs and the optical system, electronics and software are identical. Therefore, the implementation of the new method is straightforward. The present FOFP setup provides suitable scalar irradiance measurements for the investigated sediment, however, the accuracy and applicability can be improved by using different coatings and filter setups. A white scattering material as used for scalar irradiance microsensors (Lassen

et al., 1992a) instead of the red sensing layer would allow to image the spectral composition of the light field, using different filter sets or hyperspectral imaging. Thus, wavelength dependent light attenuation coefficients could be calculated. Such adaptations would however limit the combined oxygen-irradiance measurements. Rotating filters in front of the CCD camera and a mosaic-like structure of oxygen sensing dye and white scattering layer would allow performing both measurements, but would increase the overall measurement time and decrease the spatial resolution.

The principle of the HiPO can also be used together with *in situ* modules (Glud et al., 2001); the FOFP would then have to be inserted into the periscope of the module. This would enable studying oxygen dynamics in benthic phototrophic communities in sediments or microbial mats together with the changing light conditions due to diurnal cycles, cloud coverage and sediment rearrangements by infauna.

A general aspect of all types of PO measurements which has to be considered is the fact that they act as an impermeable boundary within the sediment, disturbing the original oxygen and light distribution. Especially strong heterogeneities within the sediment are influenced and small features of elevated or reduced oxygen concentration are magnified by this effect. Furthermore, it should be noted that the diffusive boundary layer (DBL) can be widened by the presence of the optode (Glud, 2008). To broaden the applicability of our method, the use of fluorophores for other parameters is possible. To date, sensing chemistries for pH (Stahl et al., 2006), $pCO_2$ (Zhu et al., 2006), $NH_4^+$ (Strömberg and Hulth, 2005) and temperature (Borisov et al., 2006) are available which could be easily combined with the HiPO.

**Acknowledgements -** We are grateful for assistance with the calculations by Dieter Wolf-Gladrow, helpful discussions with Arzhang Kalili and valuable comments from Rita Dunker. Two anonymous reviewers helped to improve an earlier version of the manuscript. This research was supported by the Max Planck Society.

# References


Bachar, A., Polerecky, L., Fischer, J. P., Vamvakopoulos, K., de Beer, D., Jonkers, H. M., 2008. Two-dimensional mapping of photopigment distribution and activity of Chloroflexus-like bacteria in a hypersaline microbial mat. FEMS Microbiol. Ecol. 65 (3), 434–448.

Barranguet, C., Kromkamp, J., Peene, J., 1998. Factors controlling primary production and photosynthetic characteristics of intertidal microphytobenthos. Mar. Ecol. Prog. Ser. 173, 117–126.

Bateson, M. M., Ward, D. M., 1988. Photoexcretion and fate of glycolate in a hot spring cyanobacterial mat. Appl. Environ. Microbio. 54 (7), 1738–1743.

Behrens, J., Stahl, H., Steffensen, J., Glud, R., 2007. Oxygen dynamics around buried lesser sandeels ammodytes tobianus (Linnaeus 1785): mode of ventilation and oxygen requirements. J. Exp. Biol. 210 (6), 1006.

Berner, R., 1980. Early Diagenesis: A Theoretical Approach, 1st Edition. Princeton Series in Geochemistry. Princeton University Press.

Borisov, S., Vasylevska, A., Krause, C., Wolfbeis, O., 2006. Composite luminescent material for dual sensing of oxygen and temperature. Adv. Funct. Mat. 16 (12), 1536–1542.

Boudreau, B. P., 1997. Diagenetic models and their implementation: modelling transport and reactions in aquatic sediments. Springer, Berlin, Heidelberg.

Cai, L. D., 1988. Some notes on repeated averaging smoothing. In: Pattern recognition, 4th Int. Conf. Proc. Vol. 301. pp. 597–605.

Canfield, D. E., Jørgensen, B. B., Fossing, H., Glud, R., Gundersen, J., Ramsing, N. B., Thamdrup, B., Hansen, J. W., Nielsen, L. P., Hall, P. O. J., 1993. Pathways of organic carbon oxidation in three continental margin sediments. Mar. Geol. 113 (1-2), 27–40.

Castenholz, R. W., Jørgensen, B. B., D'Amelio, E., Bauld, J., 1991. Photosynthetic and behavioral versatility of the cyanobacterium Oscillatoira boryana in a sulfide-rich microbial mat. FEMS Microbiol. Lett. 86 (1), 43–58.

Crank, J., 1979. The Mathematics of Diffusion, 1st Edition. Oxford University Press.

Cypionka, H., 2000. Oxygen respiration by desulfovibrio species. Ann. Rev. Microbio. 54 (1), 827–848.

Dodds, W. K., 1992. A modified fiber-optic light microprobe to measure spherically integrated photosynthetic photon flux density: characterization of periphyton photosynthesis-irradiance patterns. Limnol. Oceanogr., 871–878.

Dodds, W. K., Biggs, B. J. F., Lowe, R. L., 1999. Photosynthesis-irradiance patterns in benthic microalgae: variations as a function of assemblage thickness and community structure. J. Phycol. 35 (1), 42–53.

Epping, E., Jørgensen, B., 1996. Light-enhanced oxygen respiration in benthic phototrophic communities. Mar. Ecol. Prog. Ser. 139 (1), 193–203.

Epping, E. H. G., Khalili, A., Thar, R., 1999. Photosynthesis and the dynamics of oxygen consumption in a microbial mat as calculated from transient oxygen microprofiles. Limnol. & Oceanog. 44 (8), 1936–1948.

Fenchel, T., Glud, R. N., 2000. Benthic primary production and $O_2 - CO_2$ dynamics in a shallow-water sediment: spatial and temporal heterogeneity. Ophelia 53 (3), 159–172.

Franke, U., 2005. Applications of planar oxygen optodes in biological aquatic systems. Phd thesis, University Bremen.

Franke, U., Polerecky, L., Precht, E., Huettel, M., 2006. Wave tank study of particulate organic matter degradation in permeable sediments. Limnol. Oceanogr. 51 (2), 1084–1096.

Frederiksen, M., Glud, R., 2006. Oxygen dynamics in the rhizosphere of zostera marina: A two-dimensional planar optode study. Limnol. Oceanogr. 51 (2), 1072–1083.

Glud, R., Kühl, M., Kohls, O., Ramsing, N., 1999. Heterogeneity of oxygen production and consumption in a photosynthetic microbial mat as studied by planar optodes. J. Phycol. 35 (2), 270–279.

Glud, R., Ramsing, N., Gundersen, J., Klimant, I., 1996. Planar optrodes: a new tool for fine scale measurements of two-dimensional $O_2$ distribution in benthic communities. Mar. Ecol. Prog. Ser 140 (1-3), 217–226.

Glud, R., Wenzhöfer, F., Tengberg, A., Middelboe, M., Oguri, K., Kitazato, H., 2005. Distribution of oxygen in surface sediments from central Sagami Bay, Japan: In situ measurements by microelectrodes and planar optodes. Deep-Sea Res. Part I 52 (10), 1974–1987.

Glud, R. N., 2008. Oxygen dynamics of marine sediments. Mar. Biol. Res. 4 (4), 243 – 289.

Glud, R. N., Tengberg, A., Kühl, M., Hall, P. O. J., Klimant, I., Holst, G., 2001. An in situ instrument for planar $O_2$ optode measurements at benthic interfaces. Limnol. Oceanogr. 46 (8), 2073–2080.

Hargrave, B. T., 1972. Aerobic decomposition of sediment and detritus as a function of particle surface area and organic content. Limnol. Oceanogr. 17 (4), 583–596.

Holst, G., Franke, U., Grunwald, B., 2001. Transparent oxygen optodes in environmental applications at fine scale as measured by luminescence lifetime imaging. Proc. SPIE 4576, 138–148.

Holst, G., Grunwald, B., 2001. Luminescence lifetime imaging with transparent oxygen optodes. Sens. Actu. B 74 (1-3), 78–90.

Holst, G., Kohls, O., Klimant, I., König, B., Kühl, M., Richter, T., 1998. A modular luminescence lifetime imaging system for mapping oxygen distribution in biological samples. Sens. Actu. B 51, 163–170.

Jensen, S.T., K. M. G. R. J. B. P. A., 2005. Oxic microzones and radial oxygen loss from roots of Zostera marina. Mar. Ecol. Prog. Ser. 293, 49–58.

Jørgensen, B., des Marais, D., 1986. A simple fiber-optic microprobe for high resolution light measurements: Application in marine sediment. Limnol. Oceanogr. 31 (6), 1376–1383.

Jørgensen, B. B., Revsbech, N. P., 1985. Diffusive boundary layers and the oxygen uptake of sediments and detritus. Limnol. Oceanogr. 30 (1), 111–122.

Koenderink, J., 1984. The structure of images. Biol. Cybern. 50 (5), 363–370.

König, B., Kohls, O., Holst, G., Glud, R., Kühl, M., 2005. Fabrication and test of sol-gel based planar oxygen optodes for use in aquatic sediments. Mar. Chem. 97, 262–276.

Kühl, M., Holst, G., Larkum, A. W. D., Ralph, P., 2008. Imaging of oxygen dynamics within the endolithic algal community of the massive coral Porites Lobata. J. Phycol. 44 (3), 541–550.

Kühl, M., Jørgensen, B. B., 1992. Spectral light measurements in microbenthic communities with a fiber-optic microprobe coupled to a sensitive diode array detector system. Limnol. Oceanogr. 37, 1813 – 1823.

Kühl, M., Jørgensen, B. B., 1994. The light field of microbenthic communities: Radiance distribution and microscale optics of sandy coastal sediments. Limnol. Oceanogr. 39 (6), 1368–1398.

Kühl, M., Lassen, C., Jørgensen, B., 1994. Light penetration and light intensity in sandy marine sediments measured with irradiance and scalar irradiance fiber-optic microprobes. Mar. Ecol. Prog. Ser. 105, 139–148.

Kühl, M., Polerecky, L., 2008. Functional and structural imaging of phototrophic microbial communities and symbioses. Aquat. Microb. Ecolo. 53 (1), 99–118.

Kühl, M., Rickelt, L., Thar, R., 2007. Combined imaging of bacteria and oxygen in biofilms. Appl. Environ. Micorbiol. 73 (19), 6289–6295.

Lassen, C., Ploug, H., Jørgensen, B. B., 1992a. A fibre-optic scalar irradiance microsensor: application for spectral light measurements in sediments. FEMS Microbiol. Ecol. 86 (3), 247–254.

Lassen, C., Ploug, H., Jørgensen, B. B., 1992b. Microalgal photosynthesis and spectral scalar irradiance in coastal marine sediments of Limfjorden, Denmark. Limnol. & Oceanog. 37 (4), 760–772.

MacIntyre, H., Cullen, J., 1995. Fine-scale vertical resolution of chlorophyll and photosynthetic parameters in shallow-water benthos. Mar. Ecol. Prog. Ser. 122 (1), 227–237.

Middelburg, J. J., Duarte, C. M., Gattuso, J. P., 2005. Respiration in coastal benthic communities. Respiration in aquatic ecosystems 1 (9), 206–225.

Oguri, K., Kitazato, H., Glud, R. N., 2006. Platinum octaetylporphyrin based planar optodes combined with an UV-LED excitation light source: An ideal tool for high-resolution $O_2$ imaging in $O_2$ depleted environments. Mar. Chem. 100 (1-2), 95–107.

Pamatmat, M. M., 1971. Oxygen consumption by the seabed. iv. shipboard and laboratory experiments. Limnol. Oceanogr. 16 (3), 536–550.

Perkins, R., Underwood, G., Brotas, V., Snow, G., Jesus, B., Ribeiro, L., 2001. Responses of microphytobenthos to light: primary production and carbohydrate allocation over an emersion period. Mar. Ecol. Prog. Ser. 223, 101–112.

Ploug, H., Lassen, C., Jørgensen, B. B., 1993. Action spectra of microalgal photosynthesis and depth distribution of spectral scalar irradiance in a coastal marine sediment of Limfjorden, Denmark. FEMS Microbiol. Ecol. 102, 261 – 270.

Poulsen, L., Ogilby, P. R., 2000. Oxygen diffusion in glassy polymer films: Effects of other gases and changes in pressure. J. Phys. Chem. A 104 (12), 2573–2580.

Precht, E., Franke, U., Polerecky, L., Huettel, M., 2004. Oxygen dynamics in permeable sediments with wave-driven pore water exchange. Limnol. Oceanogr. 49 (3), 693–705.

Revsbech, N., Jørgensen, B., Brix, O., 1981. Primary production of microalgae in sediments measured by oxygen microprofile, $H^14CO_3$-fixation, and oxygen exchange methods. Limnol. and Oceanogr. 26 (4), 717–730.

Revsbech, N. P., Jørgensen, B. B., 1983. Photosynthesis of benthic microflora measured with high spatial resolution by the oxygen microprofile method: capabilities and limitations of the method. Limnol. Oceanogr. 28 (4), 749–756.

Revsbech, N. P., Madsen, B., Jørgensen, B. B., 1986. Oxygen production and consumption in sediments determined at high spatial resolution by computer simulation of oxygen microelectrode data. Limnol. Oceanogr. 31 (2), 293–304.

Saburova, Maria, A., Polikarpov, Igor, G., 2003. Diatom activity within soft sediments: behavioural and physiological processes. Mar. Eco. Prog. Ser. 251, 115–126.

Serôdio, J., Vieira, S., Cruz, S., Barroso, F., 2005. Short-term variability in the photosynthetic activity of microphytobenthos as detected by measuring rapid light curves using variable fluorescence. Mar. Biol. 146 (5), 903–914.

Stahl, H., Glud, A., Schroder, C. R., Klimant, I., Tengberg, A., Glud, R. N., 2006. Time-resolved ph imaging in marine sediments with a luminescent planar optode. Limnol. Oceanogr. Meth. 4 (51), 336–345.

Stockdale, A., Davison, W., Zhang, H., 2009. Micro-scale biogeochemical heterogeneity in sediments: A review of available technology and observed evidence. Earth-Sci. Rev. 92 (1), 81–97.

Strömberg, N., Hulth, S., 2005. Assessing an imaging ammonium sensor using time correlated pixel-by-pixel calibration. Anal. Chim. Acta 550 (1-2), 61–68.

Underwood, G. J. C., Perkins, R. G., Consalvey, M. C., Hanlon, A. R. M., Oxborough, K., Baker, N. R., Paterson, D. M., 2005. Patterns in microphytobenthic primary productivity: species-specific variation in migratory rhythms and photosynthetic efficiency in mixed-species biofilms. Limnol. Oceanogr. 50 (3), 755–767.

Wenzhöfer, F., Glud, R., 2004. Small-scale spatial and temporal variability in benthic $o_2$ dynamics of coastal sediments: Effects of fauna activity. Limnol. Oceanogr. 49 (5), 1471–1481.

Zhou, Z., Shinar, R., Allison, A. J., Shinar, J., 2007. Enhanced photoluminescence of oxygen sensing films through doping with high dielectric constant particles. Adv. Funct. Mat. 17 (17), 3530–3537.

Zhu, Q. Z., Aller, R. C., Fan, Y. Z., 2006. A new ratiometric, planar fluorosensor for measuring high resolution, two-dimensional $pCO_2$ distributions in marine sediments. Mar. Chem. 101 (1-2), 40–53.

# Chapter 3.

# Oxygen dynamics in the Kattegat

---

Jan P. Fischer[1], Hans Røy[2], Felix Janssen[1], Christoph Waldmann[3], Frank Wenzhöfer[1]

In preparation for Limnology and Oceanography

[1]Max Planck Institute for Marine Microbiology, Bremen, Germany
[2]Center for Geomicrobiology, University of Aarhus, Denmark
[3]MARUM - Center for Marine Environmental Sciences, University of Bremen, Germany

## 3.1. Abstract

Sediment oxygen distributions and dynamics were measured *in situ* in the western part of the Kattegat on different spatial scales, using the benthic crawler C-MOVE as instrument carrier. The crawler was equipped with a transecting microelectrode profiler, a planar optode module, a benthic chamber and a surface topography scanner. Additional measurements with the eddy correlation technique completed the data set. Planar optode and benthic chamber were provided with artificial illumination to evaluate benthic photosynthesis. Macrozoobenthos and macrophytes apparently played a dominant role in the oxygen dynamics of the study side, whereas microphytobenthos was of minor importance at the stations during our sampling period. A high degree of both lateral and temporal variability in oxygen dynamics was found. The oxygen penetration depth showed no clear correlation to light availability and the system had a slow response upon changes in light conditions. Together with the observation of rapidly changing bottom water concentrations, the oxygen concentration distribution within the sediment is concluded to rarely reach steady state conditions.

## 3.2. Introduction

Coastal oceans play an important role in the benthic carbon cycle. Although they comprise only a small area ( 7% of the global ocean), they account for half of the marine benthic carbon oxidation (Glud, 2008). However, most *in situ* studies on benthic mineralization focus on either deep-sea sediments (e.g. Smith, 1978, Reimers, 1987, Wenzhöfer and Glud, 2002, Glud et al., 2005) or on easily accessible sites near the beach (e.g. Migné et al., 2004, de Beer et al., 2005, Kim and Kim, 2007) The few studies on subtidal sediments focused mostly on very shallow sites with water depths <5 m (e.g. Sundbäck and Miles, 2000, Wenzhöfer and Glud, 2004, Cook et al., 2007). Beside the importance of carbon mineralization these studies also indicate that benthic primary production (BPP) plays a major role in intertidal and shallow subtidal settings. Here, BPP often reaches or even exceeds pelagic primary production (MacIntyre et al., 1996, Underwood and Kromkamp, 1999). Up to now, the contribution of benthic communities to the production of the global coastal ocean is highly unconstrained, but it was estimated by Gattuso et al. (2006) that up to 33% of the global shelf sediment receives enough light to sustain net autotrophic conditions. Sediment oxygen dynamic is a relatively easily accessible parameter that can serve as a proxy for benthic primary production and overall organic matter degradation. Consequently, it has attracted a lot of interest, together with its controlling factors (e.g. Glud, 2008). The uptake of oxygen by marine sediments is mainly regulated by the net decomposition of organic matter (Graf et al., 1982, Thamdrup and Canfield, 2000). Although, most of the organic matter in coastal sediments is oxidized anaerobically (Jørgensen, 1978, Canfield et al., 1993), oxygen is by far the most important terminal electron acceptor. It is reduced either directly by aerobic respiration or indirectly upon the (biologically mediated or purely chemical) reoxidation of reduced products of anaerobic metabolism ($NH_4^+$, $Mn^{2+}$, $Fe^{2+}$, $H_2S$ etc.). The relative partition-

ing between the different remineralization pathways is largely shaped by local oxygen availability (Canfield, 1994). An increasing number of studies report high spatial variability of benthic biogeochemical processes in general (Stockdale et al., 2009) and oxygen penetration depth and fluxes specifically (Guarini et al., 1998, Grenz et al., 2003). Additionally, high temporal variability on different scales was reported (Fenchel and Glud, 2000, Wenzhöfer and Glud, 2004). However, there is a fundamental lack of knowledge about the relevant scales of heterogeneity and temporal variability (Middelburg et al., 2005), while this knowledge is a prerequisite for the comparison of different sites and all scaling-up endeavors. Different methodologies are commonly used to determine sediment oxygen dynamics. Core- or chamber incubations can be used as a measure of total areal oxygen exchange (TOE), including fauna-mediated respiration and processes in the overlying water column. However, this approach does not provide information about the vertical organization of aerobic respiration rates, nor does it resolve lateral variability. Oxygen microelectrode profiles (Revsbech et al., 1980) provide information about the vertical structure and have become a well adopted tool in marine sciences (Smith, 1978, Reimers et al., 1986). Diffusive oxygen exchange (DOE) can be calculated from the oxygen gradient across the sediment / water interface (Jørgensen and Revsbech, 1985). To obtain information about lateral variability, it is necessary to measure many profiles at different spots, which can either be accomplished by using a transecting profiler (Gundersen and Jorgensen, 1990, Røy et al., 2002, Glud et al., 2009) or by replicate deployments. Since a single profile requires at least between 15 - 30 min (depending also on the depth resolution), this approach cannot provide oxygen profiles along transects in short time. Planar optodes (PO) resolve this shortcoming. This technology enables two-dimensional oxygen imaging of cross-sections of sediments, either in the laboratory or *in situ*. Several studies have taken advantage of *in situ* 2D-oxygen imaging, often showing high spatial variability on small scales (Glud et al., 2001, Wenzhöfer and Glud, 2004, Glud et al., 2005). All stated methods act on different length scales: While microelectrodes provide information about single spots and planar optodes cover a cross-section of several centimeters, benthic chambers integrate over an area, typically smaller than 1 $m^2$. However, they are all invasive to different degrees as they have to penetrate the sediment. The eddy correlation technique, in contrast, averages fluxes over much larger areas (10-50 $m^2$) in a non-invasive way (Berg et al., 2003). In this study, we used a multi-scale *in situ* approach, employing transecting microelectrode profiling, planar optode imaging, benthic chamber incubations and eddy correlation measurements, to investigate lateral and short-term temporal variability in benthic oxygen dynamics as well as averaged fluxes in a subtidal marine sediment. To further tackle the role of the microphytobenthos for oxygen dynamics in these sediments, potential benthic photosynthesis activities were estimated by means of *in situ* experiments using an artificial light source. Short-term sediment transport was monitored with a surface topography scanner and visual impressions from video streamings helped estimating the importance of macrofaunal activity and the prevalence of macrophytes. Data are discussed in terms of spatial variability and the relative contribution fauna, macrophytes and microphytobenthos to the sediment oxygen dynamics.

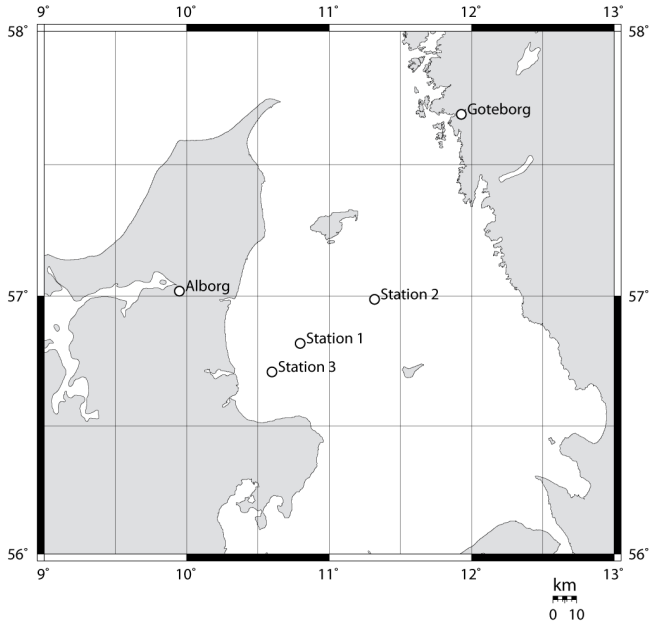


Figure 3.1.: Sample site with sampling stations (northern Kattegat)

## 3.3. Methods

### 3.3.1. Study site

The studies were conducted from the research vessel 'F/S Heincke' between 04 July and 13 July 2006 in the western Kattegat, a 100-150 km wide and on average 23 m deep channel that forms the major hydrographic transition zone between the North Sea and the Baltic Sea (Fig. 3.1) (Floderus and Pihl, 1990). The work was grouped around 3 main stations, while most of our work focused on station 3. The crawler MOVE was deployed once at station 1 and 2 (D1 and D2) and three times at station 3 (D3a-D3c; Table 3.1). The maximum distance between deployments at station 3 was 1.6 km. In addition to the instruments carried by MOVE, the oxygen flux was also measured by Eddy Correlation at D3c. By monitoring the video stream of MOVE's pan-tilt camera in real time, we identified spots, where we could use all our instruments without interference by macro algae, rocks etc. After a set of measurements was finished, MOVE was driven to the next sampling position, typically some meters away. The water depth in our study area was between 10 and 15 m and the bottom water temperature varied from 11 to 17°C (Table 1). The sediment was dominated by fine sand with a median grain size of 125 µm and an average porosity of 0.36.

### 3.3.2. C-MOVE

The benthic crawler C-MOVE (Marum, Bremen) is an underwater platform capable to carry different instruments with the possibility to get real-time access to the instruments from the

Table 3.1.: Overview of the three stations and five MOVE deployments. Bottom water oxygen, salinities and temperatures are average values. The maximum scalar irradiance gives the highest value reached during the deployment close to seafloor, while the mean irradiance represents the daily average. Instrument abbreviations: Profiler (Pr); benthic chamber (Ch); planar optode (PO); topography scanner (TS); eddy correlation (EC).

| Stat. | Depl. | Position | | Dist. D3c | z | BW $O_2$ | Sal. | Temp. | Irradiance max | Irradiance mean | Instruments | | | | |
|---|---|---|---|---|---|---|---|---|---|---|---|---|---|---|---|
| | | Lat | Lon | m | m | µmol $L^{-1}$ | ‰ | °C | µmolphot $m^{-2}$ $s^{-1}$ | | Pr | Ch | PO | TS | EC |
| 1 | D1 | 56°49.147′N | 10°47.828′E | 17250 | 14.3 | 313 | 27.6 | 11.2 | 50 | 13 | x | x | | x | |
| 2 | D2 | 56°59.286′N | 11°19.190′E | 50790 | 11.3 | 319 | 22.8 | 16.7 | 19 | 10 | x | x | | | |
| 3 | D3a | 56°43.118′N | 10°37.202′E | 1652 | 12.2 | 301 | 28.0 | 11.5 | 41 | 10 | x | x | x | | |
| 3 | D3b | 56°42.538′N | 10°36.032′E | 54 | 10.2 | 302 | 27.4 | 11.5 | 58 | 14 | | x | x | x | |
| 3 | D3c | 56°42.510′N | 10°36.020′E | 0 | 10.3 | 295 | 27.9 | 11.5 | 39 | 5 | x | x | x | x | x |

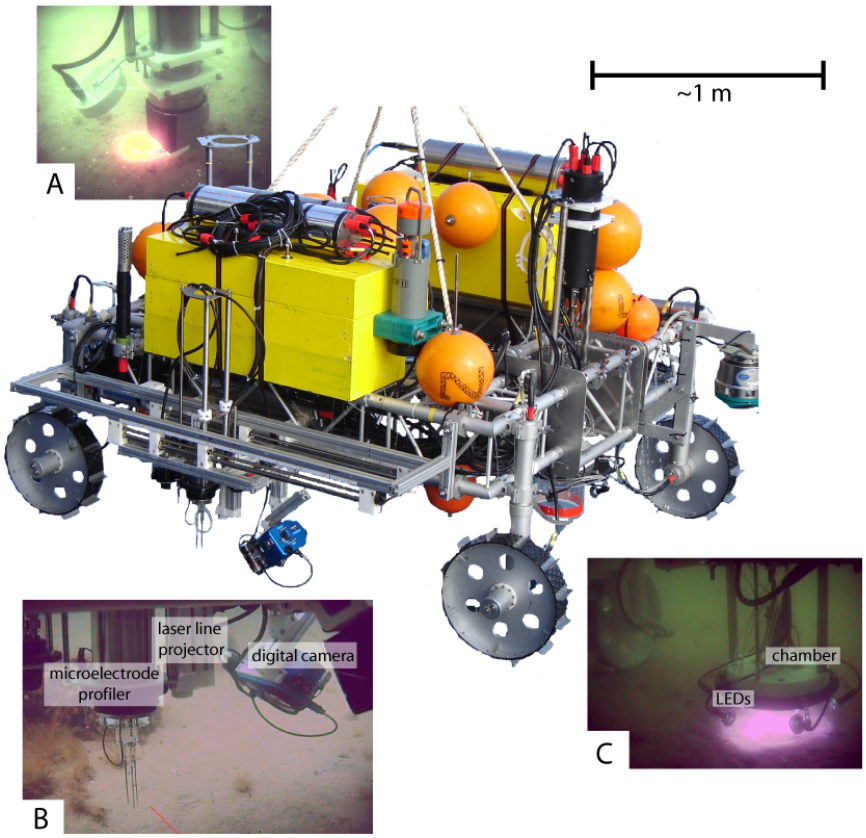


Figure 3.2.: The crawler C-MOVE and the scientific payload. A: Planar optode periscope with optional LED illumination. B: Surface topography scanner, consisting of laser line projector and digital camera, together with the microelectrode profiler for oxygen profiling (laser line on the seafloor highlighted). C: Benthic chamber with optional LED illumination

ship. It is based on the idea of a moving lander, a (possibly autonomous) vehicle, equipped with different sensors and measuring systems that is able to transit on the seafloor (Smith et al., 1997). The operating range of C-MOVE is in the order of 1 km at a speed of up to 10 cm $s^{-1}$ (Fig. 3.2). A pan-tilt camera and LED lights enabled visual inspection of the seafloor and the attached instruments. Navigation was carried out by doppler velocity log and path integration. The use of standardized aluminum profiles for the $2 \times 2\,m^2$ frame makes C-MOVE highly flexible concerning the integration of scientific payload with a submerged weight up to 200 kg. To recover C-MOVE, weights are being released acoustically and it floats to the surface. During our study, all instruments, except for the RCM11 CTD, were connected to the on-board computer of C-MOVE via TCP/IP and a fiber optic cable connection to a surface buoy and subsequent wireless LAN transmission to the ship. This enabled real time access to data and changes in measuring programs of the different instruments according to already obtained results.

### 3.3.3. Transecting Micro Profiler

The microelectrode profiler represents a miniaturized version of the instrument described in Gundersen and Jorgensen (1990) and held 3-4 electrodes (Fig. 3.2B). This compact design allowed us to mount the profiler on the laterally movable sledge of the surface topography scanner (s. below) for transecting measurements. We used 3 clark-type oxygen microelectrodes with internal reference and guard cathode (Revsbech, 1989). A 4 mm diameter spherical quantum irradiance sensor (US-SQS/L and LI 250A, Walz GmbH) was used to assess the light field close to the sediment surface and close to the position of the oxygen electrodes in order to account for the effect of shading by the instruments. Irradiance data at the seafloor were correlated to data collected with the ship's atmospheric downwelling radiance sensor. The submerged sensor operated 10 cm above the oxygen sensor tips to prevent it from penetrating the sediment. The 3 oxygen sensors and the irradiance sensor were attached to the electronics cylinder of the microelectrode profiler in a distance of 18 mm. Oxygen electrodes were calibrated *in situ* using the bottom water oxygen concentration from the RCM11 Aanderaa optical oxygen sensor (s. below) and the zero value, reached within the anoxic part of the sediment. Profiling was done in 0.1 mm steps. Oxygen microelectrode profiling took place at all stations and during all C-MOVE deployments, denoted by D1-D3c (Table 1). To gain information on spatial as well as temporal variability, the movable sledge was programmed to re-visit a number of positions during deployments D1-D3a. During deployment D3a, the profiler, equipped with 3 oxygen electrodes, was moved to 3 positions with 100 mm spacing by means of the scanner sledge. Therefore, a total number of 9 positions were measured repeatedly (3 sensors $\times$ 3 positions). Each position was visited 6-times; the duration of the whole measurement was 17.5 h covering a light range from darkness to 40 µmol photons $m^{-2}$ $s^{-1}$. During D3c, single profiles (3 sensors) at 7 different positions were measured resulting in a total number of 21 oxygen microprofiles along a 64 m transect. Oxygen fluxes were calculated from microprofiles within the diffusive boundary layer (DBL) (Jørgensen and Revsbech, 1985, Gundersen and Jorgensen, 1990) using Fick's first law of diffusion as the product of the oxygen gradient within the DBL times the molecular oxygen diffusion coefficient of seawater at the respective temperature, salinity and depth (Li and Gregory, 1974, Schulz and Zabel, 2000). The thickness of the DBL was estimated from the profiles as described in Jørgensen and Revsbech (1985). The oxygen penetration depth (OPD) was calculated as the distance between the lower boundary of the DBL (=sediment surface) and the depth where the oxygen profile reached zero.

### 3.3.4. Benthic Chamber

Total diffusive oxygen uptake (TOU) was measured by a transparent benthic chamber, enclosing sediment with supernatant water (e.g. Wenzhöfer and Glud, 2004). The cylindrical chamber had a diameter of 38 cm with ~15 cm overlying water and consisted of transparent polycarbonate. The whole chamber was lowered into the sediment by a spindle-driven elevator system and the exact height of the enclosed overlying water was determined by a scale on the outside of the

chamber that was visible trough the pan-tilt camera of C-MOVE. Two clark-type oxygen electrodes mounted inside the lid of the chamber measured the oxygen concentration in the chamber water. The chamber was stirred constantly by a motorized stirrer bar with an appropriate speed to ensure a well mixed water body without creating a strong pressure gradient across the sediment surface (Janssen et al., 2005). To assess the influence of the light conditions on oxygen fluxes *in situ*, artificial illumination of the sediment within the chamber was carried out. Six self-made LED spotlights, surrounded the chamber and facilitated the application of 4 different light intensities by changing the LED current (∼10, ∼50, ∼100, ∼200 µmol photons $m^{-2}$ $s^{-1}$). Each spotlight consisted of 20 single LEDs with a color temperature of 2850 K in a MR16 housing (Conrad Electronic) (Fig. 3.2C). The incubation chamber was used at all 3 stations and deployments (D1-D3a and D3c; Table 3.1). During D1 to D3a, the chamber measured at one position during the night over a period of 11 h, 7 h and 17 h, respectively. During each of these measurements, the artificial illumination was increased in 4 steps with durations of 1 h to investigate the response of benthic photosynthesis to increasing light intensity. During D3c, the chamber was placed at 4 different positions for 2 h each at highest light intensity to compare benthic photosynthesis at the same illumination.

### 3.3.5. Planar Optode (PO)

To investigate the small-scale variability on centimeter scale, planar optode images of the oxygen concentration were taken across the sediment-water interface. The basic optical, mechanical and electronically setup of the PO module is described in detail in Glud et al. (2005). The PO consists of a vertical titanium cylinder with a sensitive, fast gateable 12 bit digital camera (SensiMod, PCO imaging). The window of a periscope head at the lower end of the cylinder carries the oxygen sensitive foil. This periscope could be moved into the sediment with an elevator system (Fig. 3.2A). The foil contains an oxygen sensitive dye, exhibiting different fluorescence intensities and lifetimes at different oxygen concentrations. It is being illuminated by blue LEDs (4× LUXEON Star Royal Blue 5 W LXHL-MRRC, $\lambda_{max}$ =455 nm, Lumiled) and the resulting fluorescence can be imaged by the camera through a long pass filter (Kodak red wratten gelatine filter Nr. 29 ('deep-red'), Kodak, Inc., cut-off wavelength 610 nm) which filters the excitation light from the fluorescence signal. We analyzed the fluorescence lifetime as described in Holst et al. (1998). The PO sensor is based on a 125 µm thick PET foil (Goodfellow Inc.), coated with a 20 µm thick oxygen sensing layer that consisted of platinum(II) mesotetra (pentafluorophenyl) porphyrin (Frontier Scientific, Inc.), dissolved together with polystyrene in chloroform (Precht et al., 2004). To increase the amount of excitation light within the sensing layer, titanium dioxide particles ($TiO_2$ , 5 µm, Aldrich) were added (König et al., 2005). Since the excitation light might have an influence on the oxygen concentration field by stimulating photosynthesis, a 20 µm thick layer of black silicone optically insulated the PO. The total imaged area was 73.1 × 58.4 $mm^2$ with a resolution of 57 µm $pixel^{-1}$. For the analysis of the PO data, vertical profiles were extracted from the oxygen images by averaging over 5 columns (=286 µm), spaced 1 mm apart. The sediment

surface and oxygen penetration depth was determined as described for the microprofiler. Oxygen fluxes were not calculated from the PO images, since the optode periscope might compromise the sediment water interface (Glud et al., 1996). To stimulate benthic photosynthesis, the sediment area in front of the PO was artificially illuminated. A flashlight, consisting of 8 high-power LEDs (LUXEON Star Warm White, 1 W, LXHL-MWGC, Lumiled) with collimating optics in a self-made underwater housing was mounted above the inverted periscope and allowed to create an irradiance of ∼200 µmol photons $m^{-2}$ $s^{-1}$ (Fig. 3.2A). The planar optode module was utilized during D3a-D3c. During D3a and D3b, time series of oxygen images were taken over a time period of 15 h and 11.3 h, respectively. Here, 5 consecutive oxygen images were recorded every 15 min. While the measurements at D3a were carried out at night, natural scalar irradiance during D3b changed from a maximum value of 60 µmol photons $m^{-2}$ $s^{-1}$ to darkness at the end of the measurement. During D3c, measurements were performed at 4 different positions, spaced several meters apart. During two of these measurements, artificial illumination of the sediment in front of the PO was applied for 2h to stimulate benthic primary production.

### 3.3.6. Surface topograpy scanner

Millimeter scale topography was measured by laser scanning acording to Røy et al. (2005). A laser sheet (10 mW, 670 nm line-generating diode laser) was projected vertically onto the seafloor where it resulted in a less than 1 mm wide straight laser line of ∼400 mm length. A digital still camera (Nikon CoolPix 990) in an underwater housing (UK Germany) was equipped with a 670 × 40 nm band pass filter to reduce the background illumination due to ambient light. Images of the laser line were taken at a spacing of 5 mm along a 700 mm long stretch, covered by a horizontal linear drive, moving both laser projector and camera (Fig. 3.2B). In the obtained digital images, taken from an angle of 45° relative to the laser sheet, seafloor elevations were represented by upward shifts in the position of the laser line. The substantial perspective distortion of the images that result from the inclined camera position was removed by rectifying the images using the 'spherize' and 'perspective' filter tools of the software Photoshop (Adobe Systems Inc.). The best settings of these tools were determined beforehand by processing calibration-images taken of a regular 5 × 5 $mm^2$ grid that was positioned exactly in the plane of the laser sheet. The detection of the laser line center in the respective pixel columns of the rectified images takes place automatically as described in Røy et al. (2005) using a Matlab (MathWorks, Inc.) routine. After conversion of the laser-line position in each of the pictures into mm-coordinates, the resulting elevation-profiles are assembled to a 3D set of coordinates describing the sediment surface topography on a regular grid.

### 3.3.7. Eddy correlation

Eddy correlation relies on measuring turbulent fluctuations in the vertical velocity and the corresponding $O_2$ concentration simultaneously and at the same point above the sediment surface. The measurements are done with an adequate temporal resolution to capture these fluctuations

and for a period long enough to obtain a statistically sound representation of their variations. The vertical flux of $O_2$ can then be calculated by keeping track of the discrepancy between upward and downward flux. The plane of measurement is a horizontal plane that passes trough the measuring point of the instrument (Berg et al., 2007), in our case 35 cm above the seafloor. The sensor package used was, in principle, identical to the system described by Berg et al. (2003). The instrument, however, was fully autonomous with on board data storage and power supply. The instrument was programmed to collect 20 minutes long data series of oxygen and velocity at 25 Hz. After each 20 minutes data set the instrument actively turned into the current based on the average current direction in the preceding 20 minutes and a new 20 minutes series immediately initiated. Downwelling irradiance was measured concurrently with $O_2$ and velocity at 25 Hz via a biospherical cosine collector sensor mounted on the instrument 50 cm above seafloor. Slow varying changes in the $O_2$ concentration were recorded at 0.1 Hz by an Aanderaa optical oxygen sensor mounted down-stream from the main oxygen sensor. The raw $O_2$ data were calibrated from the zero signal in deoxygenated seawater on board and the *in situ* response together with the *in situ* oxygen concentration measured by the Aanderaa sensor. The average vertical velocity was corrected to zero by subtracting the average of the entire 20 minutes data set from each individual vertical velocity of that set. The flux was calculated simply by summing up the product of vertical velocity and $O_2$ concentration. The areal coverage depends on the flow regime and is typically 10-50 $m^2$ in upstream direction (Berg et al., 2007).

### 3.3.8. RCM11

Time series of conductivity, temperature, depth, turbidity, current velocity and bottom water oxygen concentration were recorded with the RCM11 Doppler Current Meter (Aanderaa Inc.) with a temporal resolution of 1 min.

### 3.3.9. Sediment characteristics

Cores for determination of chlorophyll distribution, sediment porosities and permeabilities was retrieved by a multi-corer with 30 mm diameter cores at all stations (Barnett et al., 1984). Depth resolved measurements of chlorophyll concentrations of the upper sediment layer were performed in 1 cm intervals. Cores were sliced on board and the sediment was stored frozen until analysis. After freeze-drying the sediment and extracting the pigments with 7.5 ml acetone (90%) per gram sediment, absorption at three different wavelengths was determined before and after acidification with 10% HCl (Lorenzen, 1967).

## 3.4. Results

A detailed multi-analytical investigation on the spatio-temporal variability of oxygen penetration depth and fluxes across the sediment water interface was carried out at station 3. Here, the 4 different methods (microelectrode profiling, PO imaging, chamber incubations and eddy correla-

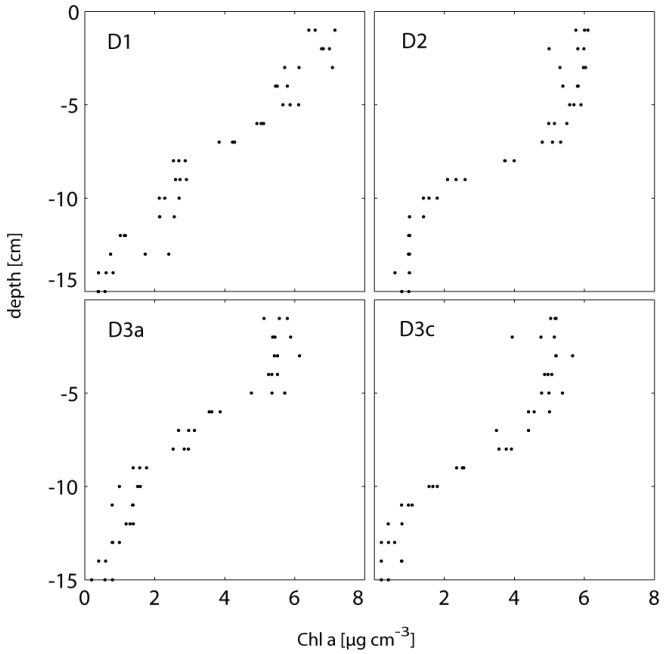


Figure 3.3.: Chlorophyll $\alpha$ concentrations in 4 different multi cores taken during deployments D1-D3c. At each depth interval (1 cm) 3 parallels have been measured.

tion) were used concurrently. Together with measurements from station 1 and 2 these data were used to assess the regional variability in oxygen penetration depth and diffusive oxygen uptake (Fig. 3.1).

### 3.4.1. Sediment characteristics

The chlorophyll concentration at all stations was constant within the first 5 cm of the sediment ($\sim$5-6 µg cm$^{-3}$) and declined strongly below this layer, reaching zero at $\sim$15 cm sediment depth (Fig. 3.3). Incident irradiance at the seafloor during our study did not only vary in diurnal cycles but changed also strongly within minutes due to shading by clouds (data not shown). The average daily (24 h) irradiance at the seafloor during our studies was $\sim$10 µmol photons m$^{-2}$ s$^{-1}$, while the maximum light intensity was $\sim$60 µmol photons m$^{-2}$ s$^{-1}$ (Table 3.1). The bottom water oxygen concentration also varied considerably. At site D3c, it stayed virtually constant at 300 µmol L$^{-1}$ over the first 11.5 h of the deployment, followed by a rapid decrease to 270 µmol L$^{-1}$ within about 1 h. At the same time, the temperature dropped from 11.6°C to 11.2°C. The absolute current speed oscillated between 2 and 10 cm s$^{-1}$, with a period of $\sim$6 h. Sites 1 and 2 showed comparable dynamics in bottom water oxygen concentration. At site 2, the variation in temperature was most pronounced with changes of up to 3°C in less than 1h (data of temperature, current speed and BW $O_2$ not shown). The sediment topography at our measuring positions was relatively flat with typical maximum elevations of $\pm$ 20 mm within the scanner area of 400 $\times$ 700 mm$^2$ (Fig.

Table 3.2.: Average oxygen penetration depth (OPD) in all planar optode images and microprofiles, diffusive oxygen exchange (DOE, microprofiles), total oxygen exchange (TOE) as measured by chamber incubations in the dark and oxygen uptake as measured by eddy correlation in the dark.

| MOVE depl. | mean Profiler | median Profiler | mean PO | median PO | mean DOE Profiler | TOE Chamber | TOE Eddy |
|---|---|---|---|---|---|---|---|
| | OPD [mm] | | | | $mmol\,m^{-2}\,d^{-1}$ | | |
| all | 4.6 ± 3.2 (n=102) | 3.2 | 4.3 ± 0.7[1] | 4.3[1] | -12.5 ± 6.7 (n=72) | - | - |
| D1 | 7.9 ± 4.2 (n=17) | 6.6 | - | - | -17.5 ± 4.2 (n=5) | -23.3 | - |
| D2 | 6.1 ± 4.2 (n=18) | 4.4 | - | - | -11.7 ± 5.3 (n=7) | -7.0 | - |
| D3a | 3.4 ± 1.4 (n=32) | 2.9 | 4.4 ± 0.5 | 4.5 | -13.0 ± 6.8 (n=28) | -22.1 | - |
| D3b | 3.7 ± 1.4 (n=18) | 3.1 | 4.0 ± 0.5 | 4.0 | -8.7 ± 8.3 (n=17) | - | - |
| D3c | 3.6 ± 2.6 (n=17) | 2.8 | 4.6 ± 0.9 | 4.1 | -11.7 ± 3.7 (n=15) | - | -56.1 |

[1] values calculated from D3a-D3c

3.9). Visual observations at station 1 showed a higher coverage by macrophytes and a generally more structured sediment surface, comprising small rocks which were not observed at station 2 and 3.

### 3.4.2. Oxygen penetration depth

The oxygen penetration depth (OPD) as derived from in total 102 microelectrode profiles at all sites was highly variable ranging from 2 to 19 mm with a median value of 3.2 mm (Table 3.1). Even on the smallest distances, as few as 18 mm apart from each other, oxygen profiles often exhibited strong heterogeneities in OPD (Fig. 3.4). Many profiles (14 %) appeared visually disturbed, probably by bioturbation and bioirrigation activity. They do not show the typical, steadily decreasing profile of respiring sediment communities. Instead, they exhibit locally strongly enhanced or decreased concentrations (e.g. Fig 3.4A, D2). The highest average OPD was measured at station 1 positioned in the middle of stations 2 and 3, (distance to stations 2 and 3: 30 and 20 km, respectively), with a median of 6.6 mm. Here, the variability was also highest (Fig. 3.5) with 60% of all profiles appearing to be influenced by faunal activity. A lower OPD with a median of 4.4 mm and reduced variability was determined for station 2. However, a 1-way ANOVA showed no significance for the difference in OPD between station 1 and 2. At station 2, 13% of the profiles appeared to be influenced by benthic fauna activity. All three deployments at station 3 (D3a-D3c) exhibited very similar microsensor OPDs with a median of ∼3 mm. The average OPD was statistically different to station 1 but not to station 2. The fraction of fauna-influenced profiles was lowest at station 3 (8%). Planar optode derived OPDs for D3a-D3c showed consistently a lower variability in OPD then microsensor profiles (Fig. 3.5, Table 3.2).

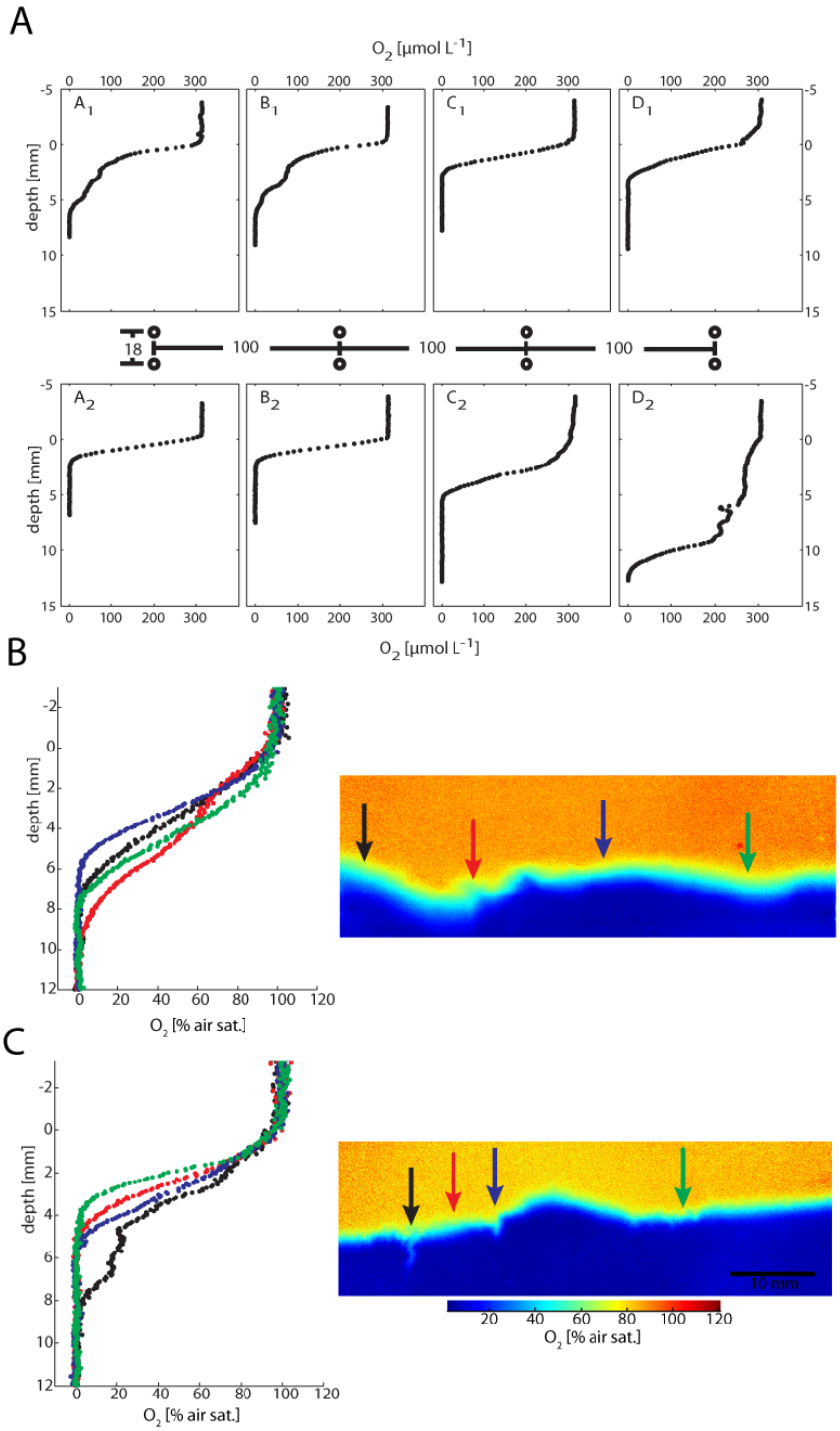


Figure 3.4.: (A) Oxygen microprofiles at 8 different positions. The circles between the panels depict the positions of profiles relative to each other (distances in millimeters) (B) Oxygen profiles (left) extracted from planar optode images (right). Arrows depict the position of the profiles; the color of the arrows identifies the different profiles. The oxygen penetration depth (OPD) differs due to sediment topography. (C) Differing OPD in PO image due to fauna activity

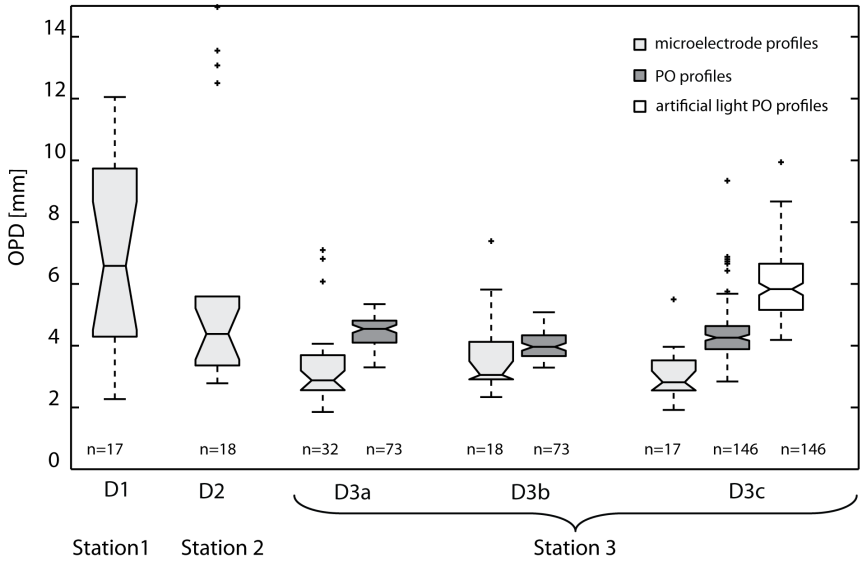


Figure 3.5.: Box plot of oxygen penetration depth (OPD) distribution in microelectrode profiles and profiles, extracted from planar optode measurements during all 5 deployments of MOVE (D1-D5) at all 3 Stations. Data for the rightmost box originate from PO images with artificial illumination for more than 1h before the measurement (s. text). The middle line in each box represents the median; the extension of the box gives the upper and lower quartile, respectively. Crosses depict outliers (values >1.5x upper quartile or <1.5x lower quartile); whiskers extend to the most extreme data points, which are not outliers. The notches of the boxes give the 5% significance level for the median of the OPDs. Values above 15 mm OPD have been omitted.

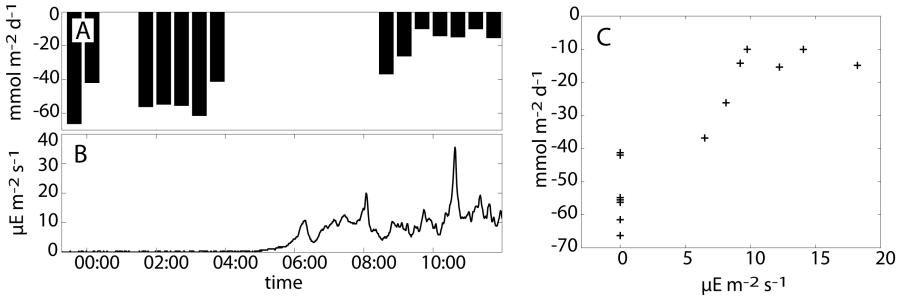


Figure 3.6.: Oxygen fluxes measured with the eddy correlation method over a period of 12h (A) and irradiance at the sediment surface (B). Right: scatter plot of irradiance versus oxygen flux (C).

### 3.4.3. Oxygen fluxes

Diffusive oxygen exchange between water column and sediment (DOE) varied between -32.2 and 4.0 mmol $m^{-2}$ $d^{-1}$ with a mean of $-12.5$ mmol $m^{-2}$ $d^{-1}$ for all deployments (Table 3.2); negative values imply fluxes from the overlying water to the sediment. The highest mean DOE was measured at D1 ($-17.5$ mmol $m^{-2}$ $d^{-1}$). A 1-way ANOVA revealed that only D1 differed significantly from the other deployments. At deployments D2 - D3c, the average DOE was lower than at station 1 (-11 mmol m-2 d-1). A total number of 5 profiles (4% of all profiles) during D3b showed fluxes from the sediment to the water column, indicating net autotrophic conditions. Total oxygen exchange (TOE) determined with the eddy correlation method at D3c were considerably higher than DOE values for this site, ranging between -68 and $-10$ mmol $m^{-2}$ $d^{-1}$ and were dependent on the incident irradiance (Fig. 3.6A and B). Overall TOE was higher than DOE at all deployments, except D2 (Table 3.2); here TOE was 40% lower than the DOE. For the other deployments D1 and D3a, total exchange rates were 25 and 41% higher, respectively.

### 3.4.4. Potential benthic photosynthesis

Strong artificial illumination of sediment in front of the planar optode at D3c stimulated benthic photosynthesis and led to zones of slight oxygen supersaturation within the top millimeters of the sediment (Fig. 3.7). However, these areas of net photosynthesis exhibited a high horizontal heterogeneity resulting in a rather patchy distribution within the investigated sediment horizon. Eddy correlation fluxes also exhibited a strong light dependency, with decreasing fluxes to the sediment at increasing incident irradiances (Fig. 3.6 A,B). *in situ* experiments with the artificially illuminated chamber showed a trend of decreasing TOE with increasing light intensity (Table 3.3), yet the result was not as clear as with the eddy correlation measurements using the natural light conditions. At D1 and D2, for example, the TOE was initially increased when the light was switched from darkness to 10 µmol photons $m^{-2}$ $s^{-1}$ (Table 3.3). Lowest oxygen uptake rates were observed at light intensities of 100 and 200 µmol photons $m^{-2}$ $s^{-1}$, respectively. At station

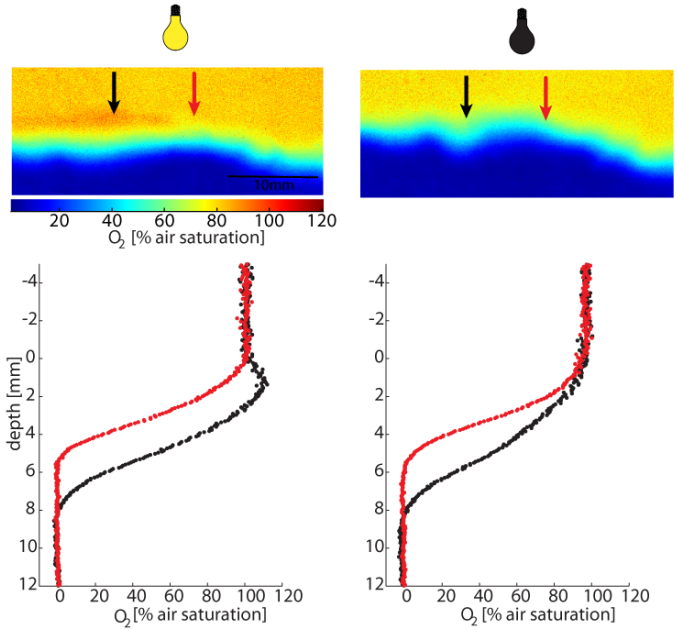


Figure 3.7.: Planar optode images (top) and profiles extracted at the positions given by the arrows (bottom) at two different light conditions. In the left panel, the sediment in front of the optode was illuminated artificially. The right panel shows the situation 1h after the light was switched of.

D3c, the chamber was deployed at 4 different positions, spaced several meters apart, for 2 h each, at highest illumination. Here, TOE varied strongly between a net oxygen uptake of the sediment of $-26\,\mathrm{mmol\,m^{-2}\,d^{-1}}$ and a net oxygen release of $84\,\mathrm{mmol\,m^{-2}\,d^{-1}}$ (Table 3.3).

### 3.4.5. Temporal variability

A high degree of temporal variability was detected in the microprofile measurements. At deployment D3a time series of microprofiles for a total number of 9 positions were measured, where each position was visited 6 times (Fig. 3.8). In the most extreme case, the OPD changed from 3.6 mm to 10.1 mm within 2 h. Another 3.5 h later, the same position showed an OPD of 3.9 mm (Fig. 3.8).

At deployment D3b, the PO was left in the sediment for a prolonged period of 11.5 h without artificial illumination and oxygen images were obtained every 15 min. After insertion of the PO module into the sediment, the oxygen distribution appeared to be initially strongly disturbed. The whole imaged area was oxic and the system needed more than 1.5 h until a steady-state situation was reached. After this period, OPD varied from a minimum average of 3.9 mm to a maximum average of 4.6 mm (data not shown). However, there was no clear trend and no correlation to irradiance or daytime and the changes were statistically not significant, given the technical variance of the method. The sediment surface, however, was clearly moved on a

Table 3.3.: Total oxygen exchange (TOE) at D1-D3a during 5 different (artificial) light conditions. Each light condition lasted for 1h. After the most intense illumination, another period in the darkness was measured. At D3c, four measurements were carried out at different positions and highest light intensity. Negative values indicate oxygen fluxes into the sediment.

| | Irradiance [µmol photons $m^{-2}$ $s^{-1}$] | | | | | |
|---|---|---|---|---|---|---|
| | 0 | 10 | 50 | 100 | 200 | 0 |
| | TOE [mmol $m^{-2}$ $d^{-1}$] | | | | | |
| D1 | -20 | -31 | -17 | -11 | -12 | -25 |
| D2 | -9 | -16 | -10 | -8 | -6 | - |
| D3a | -22 | -16 | -17 | -13 | -14 | -23 |
| D3c | - | - | - | - | 84 | - |
| D3c | - | - | - | - | 18 | - |
| D3c | - | - | - | - | -3 | - |
| D3c | - | - | - | - | -26 | - |

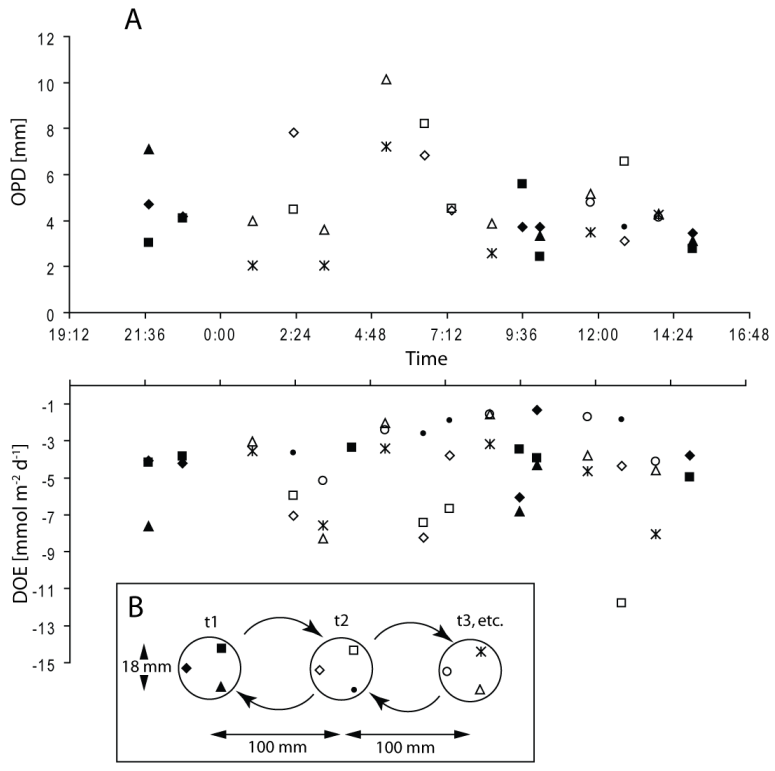


Figure 3.8.: (A) Changes in oxygen penetration depth (OPD) and diffusive oxygen exchange (DOE) at 9 different positions (denoted by the different symbols) over time. (B) Measuring procedure. The 9 positions result from a measurement, where the transecting profiler was programmed to re-visit 3 positions (t1, t2, ...). At each of these positions, profiles were measured with 3 sensors.

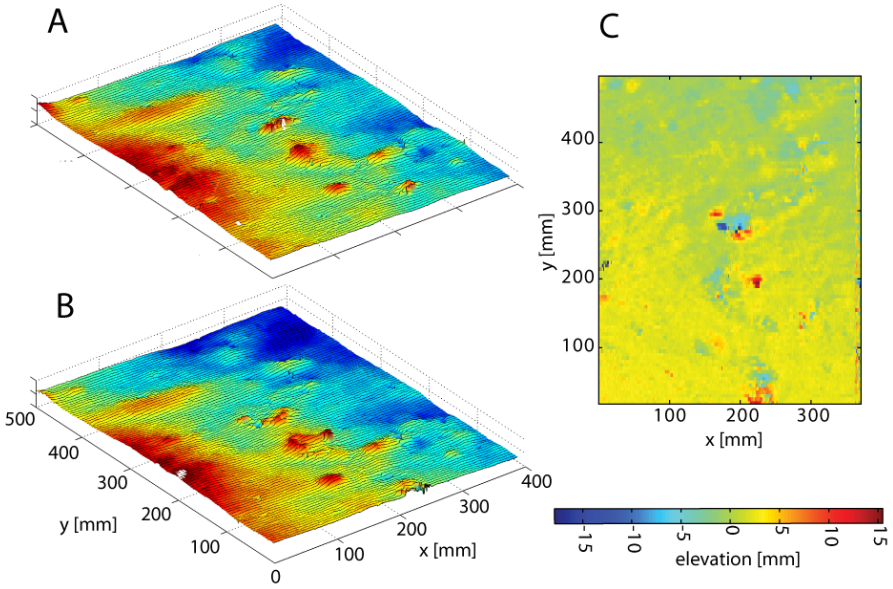


Figure 3.9.: Example of surface topography at station D3b (A) and a second measurement 3 h later (B). The difference between the two topographies is shown in panel C.

small (sub-millimeter) scale from image to image. These changes, most likely caused by faunal activity, were usually confined to small areas and happened unsteadily. During the last third of the measurement, one periodically oxygenated worm burrow appeared. Benthic photosynthesis in front of the PO was stimulated by artificial illumination. However, even 1 h after the light was switched off, the oxygen penetration depth in profiles extracted from the zones of high production had not changed as indicated by a two-tailed t-test ($p>0.05$) of all profiles extracted from two PO images, one taken immediately before and one 1 h after the light was switched off (Fig. 3.7). Net sediment transport on the time scale of hours was very limited. During deployment D3b and D3c, surface topographies were measured at the same position with several hours time in between. Most of the changes in sediment topography were related to faunal activity like sliding mussels (Fig. 3.9).

## 3.5. Discussion

### 3.5.1. Carbon mineralization and benthic primary production

Shelf sediments are characterized by an active benthic compartment that remineralizes the settled organic matter and releases most of the nutrients back into the water column (Middelburg et al., 2005). Often, pronounced benthic primary production can be found. The average diffusive oxygen flux to the sediment during our study in the order of 13 $\mathrm{mmol\,m^{-2}\,d^{-1}}$ indicates a net heterotrophic system. The flux is in the lower range of previous measurements in coastal

sediments in comparable water depths, ranging from below 1 to several 100 mmol $m^{-2}$ $d^{-1}$ (Middelburg et al., 2005, and references therein). Dark core incubations with sediment from the NE Kattegat resulted in similar total oxygen uptake rates (15 mmol $m^{-2}$ $d^{-1}$) (Sundbäck et al., 1991). A total annual carbon mineralization rate of 40 - 130 gC $m^{-2}$ $yr^{-1}$ can be estimated for our study site, assuming a respiratory quotient of 1.3 mol $O_2$ $mol^{-1}$ $C_{org}$, if the measured total oxygen exchange rates from chamber measurements between -7 and 23 mmol $m^{-2}$ $d^{-1}$ would be representative throughout the whole year. An empirical relationship between water depth and benthic respiration in coastal sediments derived by Middelburg et al. (2005) yields values around 130 gC $m^{-2}$ $yr^{-1}$ for the depths of our study sites and is thus in good accordance.

The high seasonal dynamic in temperature and input of organic matter of coastal benthic ecosystems in temperate regions generally leads to high rates of benthic mineralization during the summer and lower rates in winter (Thamdrup et al., 1994). Our study was conducted during the summer; therefore the estimate for the annual respiration rate can be seen as an upper boundary. However, periodic events like algal blooms can have profound impact on benthic mineralization rates. Hansen and Blackburn (1992) found an immediate increase in benthic oxygen uptake of 39% after the addition of phytoplankton to coastal sediment from similar water depth. They estimated a half-life time of 2-3 weeks for the material, highlighting the rapid cycling. Faunal activity and grazing pressure on microphytobenthos also vary strongly throughout the year (Miller et al., 1996). For a complete overview of the benthic mineralization in this region, measurements at different times of the year are thus desirable.

Benthic photosynthesis has a profound impact for the functioning of shelf sediments by affecting the exchange of oxygen and nutrients across the sediment water interface and providing a food source for heterotrophic organisms (MacIntyre et al., 1996). The eddy correlation measurements provide clear evidence for BPP during our study (Fig. 3.6). However, even at the highest incident irradiances, the rate of gross photosynthesis did not balance sediment respiration. Gattuso et al. (2006) reported necessary light intensities to reach the compensation points for seagrass- and macroalgae beds of ∼30 and ∼20 µmol photons $m^{-2}$ $s^{-1}$, respectively, but only ∼3 µmol photons $m^{-2}$ $s^{-1}$ for microphytobenthos. Therefore, the light availability at the seafloor during our study with peak values of up to 60 µmol photons $m^{-2}$ $s^{-1}$ and average daily values of around 10 µmol photons $m^{-2}$ $s^{-1}$ (Table 3.2) would be sufficient for net autotrophic conditions and thus the microphytobenthos was not light limited. High grazing pressure could be a reason that the microphytobenthos did not exploit the available light (Evrard, 2007). In a laboratory study with sediment from the SE Kattegat, Sundbäck et al. (1991) also report net heterotrophic conditions at a daily average photon flux density of 13 µmol photons $m^{-2}$ $s^{-1}$. During the illumination (20 µmol photons $m^{-2}$ $s^{-1}$), however, they observed a net efflux of oxygen to the water column, in the order of 6 mmol $m^{-2}$ $d^{-1}$, in contrast to our findings. The exclusion of macrofauna in their experiments is a likely reason for this difference.

The incident irradiance did not induce increased OPDs in both microprofiles and PO images (Fig. 3.10B). The assumption that higher light intensities would generally lead to higher oxygen penetration depth due to benthic photosynthesis (Epping and Jørgensen, 1996) did therefore not

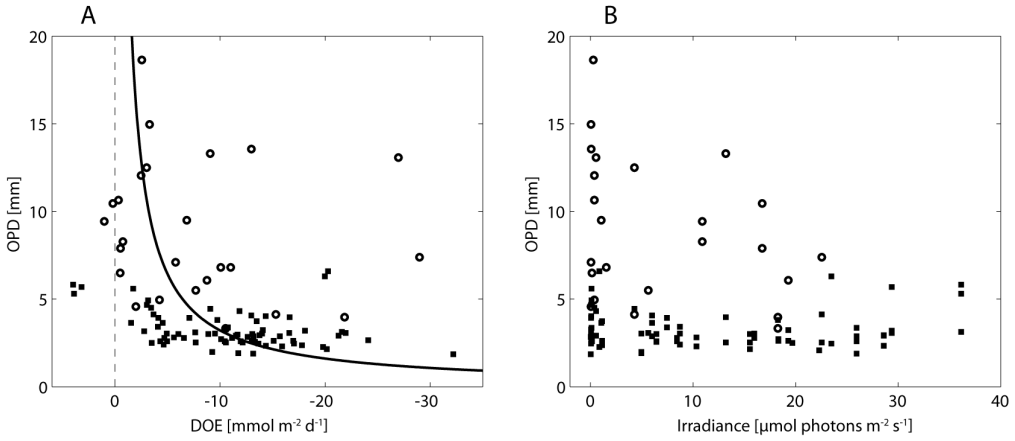


Figure 3.10.: Evaluation of all oxygen profiles from station 1-3. (A) Diffusive oxygen exchange (DOE) vs. oxygen penetration depth (OPD). Circles represent profiles that where clearly influenced by fauna (see text). The solid line represent the empirical relationship found by Cai and Sayles (1995). (B): Average Irradiance at the seafloor in the 30min before the profile was started, plotted against the OPD.

hold true in our study. Although a large number of microprofiles were measured during daytime, only 5 profiles exhibited signs of flux from the sediment to the water column. However, longer uninterrupted strong artificial illumination (∼3× the measured max. natural irradiance) in front of the PO caused an increase in OPD and patches with slight super-saturation (Figs. 3.5 and 3.7) and the artificial illumination in chamber experiments also resulted in reduced sediment oxygen uptake. Since planar optode measurements do not include the effect of macrophytes and the chamber was also not positioned above apparent patches of macrophytes, it can be concluded that a benthic microbial phototrophic community was present. This finding is backed by chlorophyll concentration profiles in the sediment (Fig. 3.3). The influence of this community on oxygen penetration depth at typical ambient light conditions is limited or it is obscured by fauna activity.

The eddy correlation method includes the effect of macrophytes since it averages over much larger areas (Berg et al., 2007). The average eddy correlation fluxes in the darkness of -54 $\mathrm{mmol\,m^{-2}\,d^{-1}}$ reduced with increasing incident irradiance to $-13\,\mathrm{mmol\,m^{-2}\,d^{-1}}$ (Fig. 3.6C). Most of this reduction in sediment oxygen uptake during the day can thus be attributed to macrophytes. No further reduced eddy correlation fluxes at irradiances above 10 $\mathrm{\mu mol\,photons\,m^{-2}\,s^{-1}}$ were found (Fig. 3.6C). The light saturation of the phototrophic community was reached or enhanced respiration of the sediment was induced, e.g. due to light-stimulated fauna activity (Wenzhöfer and Glud, 2004) or light enhanced microbial respiration (Epping and Jørgensen, 1996). It is well known for intertidal sediments that a large proportion of the carbon fixed by microphytobenthos is excreted as extracellular polymeric substances (EPS) (e.g. Middleburg

et al., 2000, De Brouwer and Stal, 2001). This easily degradable pool of organic carbon is quickly oxidized by bacteria and deposit feeders (Middleburg et al. 2000) and can therefore lead to substantially enhanced respiration rates in the light. Recently, Evrard et al. (2008) reported that the proportion of assimilated carbon by microphytobenthos that is excreted as EPS can exceed 50% in shallow subtidal sediments.

### 3.5.2. Spatial and temporal variability

Entirely uniform habitats or organism distributions are rare in nature and heterogeneities may have important impact on the functioning of marine benthic ecosystems (Ellingsen et al., 2007). Differences in average oxygen dynamics were found on the scale of several 10 kilometers during our study between station 1 and 3, while no significant differences in average OPD and DOE were found for the three deployments at station 3 (D3a-D3c), spaced at maximum 1.7 km apart (Fig 3.5, Table 3.2). This indicates a low heterogeneity for the scale of hundreds of meters. However, 4 chamber incubations at D3c at constant illumination, spaced several meters apart, yielded very different TOE values (Table 3.3), suggesting that patches with typical sizes of meters existed. The variability in OPD was generally less pronounced in profiles extracted from PO images compared to microsensor profiles (Table 3.2, Fig. 3.5). The microsensor measurements at each C-MOVE deployment were carried out at distances of 18 mm to several meters, while all extracted PO profiles originate from a cross-section of 73 mm sediment. The lower variability in OPD in PO images is concluded to be an effect of the different scales involved: Variability on the scale of millimeters to few centimeters was therefore less pronounced then variability on scales of several centimeters to meters. The same conclusions can be drawn from experiments with stimulated BPP by artificial illumination in front of the PO. The size of supersaturated patches below the sediment surface was in the order of centimeters, heterogeneities in production on smaller spatial scales were not detected. A likely reason for these patches is an inhomogeneous lateral distribution of MPB. Patchy distributions of MPB down to centimeter-scale have previously been reported (e.g. Jesus et al., 2005, Morris, 2005). They can be caused by responses to environmental variables (Christie et al., 2000) and macrofaunal activity (e.g. grazing) (Cartaxana et al., 2006). Recently, Dyson et al. (2007) reported that heterogeneities in nutrient concentration within sediments caused by the decomposition of organic matter led to heterogeneities in MPB distribution. All these studies were carried out on intertidal, mostly muddy sediments, but it is likely that the stated mechanisms are also existent in subtidal systems.

The insertion of the PO periscope disturbed the oxygen distribution within the sediment. Oxygenated bottom water was dragged down in former anoxic regions and it lasted for more than 1 h to re-establish close to steady state conditions. This slow response of the sediment can be a consequence of relatively low microbial respiration rates. The same effect was observed after changes in light conditions in front of the PO. Although the phototrophic community reacts instantaneously, the oxygen penetration depth remained unchanged for at least 1 h (Fig. 3.7). Given the high fluctuations in the light field due to shading by clouds, the frequent changes

in bottom water oxygen concentration and the actively burrowing and pumping infauna, this slow response will result in non-steady state oxygen distribution for most of the time. As a consequence, benthic microorganisms and meiofauna are faced with constantly changing ambient oxygen concentrations. Depth resolved respiration rates calculated from microsensors profiles (Berg et al., 1998) should be taken with caution in these sediments, since they rely on the steady-state assumption.

The distribution of chlorophyll within sediments can be used to quantify sediment mixing, since the chlorophyll turnover in coastal sandy sediments is high (Hansen and Blackburn, 1992) and light only penetrates the first millimeters (Kühl and Jørgensen, 1994). Therefore, chlorophyll that is found in deeper layers was most likely transported downwards. The virtually constant chlorophyll content in the top 5 cm of the sediment (Fig. 3.3) thus indicates a strong physical mixing of this sediment horizon. Bioturbation can explain part of this mixing (Rusch et al., 2000). The high degree of homogenization and accord between the different cores makes it plausible that re-suspension events also play an important role. However, the sediment morphology did not change strongly during several hours between consecutive topography scans (Fig. 3.9), although the prevalent current speeds were in a typical range for this region (Floderus, 1988). Thus, the mixing seems not to happen constantly but episodic. The most important factors for strong resuspension events in the Kattegat are wind-induced wave action and trawling (Floderus and Pihl, 1990) and therefore, the observed mixing most likely occurs periodically during such events. The effect of sudden, intense sediment rearrangements on the functioning of the benthos in the Kattegat remains to be studied.

### 3.5.3. Importance of fauna

The high average OPD and the variances between the microprofiles of station 1 can be explained to a large extend by fauna activity, given the high proportion of fauna-influenced microprofiles. Generally, increased oxygen uptake leads to decreased OPDs (Glud, 2008). While this holds true for single profiles (Fig. 3.10), averages for all profiles of one station show the highest average OPD to be correlated to the highest average DOE at station 1 (Table 3.2). Jørgensen et al. (2005) report a 2-fold increase in oxygen flux in sediments with higher abundance of polychaetes. They conclude that the increased DOE might be a consequence of fauna activity. This effect can be partitioned into direct faunal respiration and faunal stimulated bacterial activities due to irrigation of otherwise anoxic sediment layers (Aller and Aller, 1998). Wenzhöfer and Glud (2004) found the latter process to be clearly dominant in very shallow, coastal sediment. They report a fauna mediated portion of the total sediment oxygen uptake of 50-70%. In our study, the difference of total oxygen exchange (TOE) and diffusive oxygen exchange (DOE) yields a slightly lower contribution of 30-40% of faunal respiration to the total sediment oxygen uptake.

Strong heterogeneity down to centimeter scale could be detected, comparing single microsensor profiles, with differences in OPD of up to 300% within 18 mm (Fig. 3.4A). Many of these heterogeneities can be explained by burrowing fauna. Additional evidence for this effect is

also seen in the planar optode images where worm borrows could be identified (Fig.3.4C). This active reworking of the top sediment layer has a profound impact on the biogeochemistry of the sediments, since it increases the exchange of both solutes and solid particles. Berg et al. (2001) calculated that the effect of fauna on solute transport can be as important as molecular diffusion for sandy coastal sediments. The large impact of fauna on the average OPD during our study suggests an even larger influence (Fig. 3.10), at least at station 1, were 60% of the microprofiles appeared to be disturbed by fauna.

Most changes in sediment morphology, as measured with the topography scanner, originated from crawling fauna (Fig. 3.9). This interpretation is backed by the PO time series. Here, the sediment surface was clearly moved on a small (sub-millimeter) scale from image to image. These changes were confined to small areas and happened unsteadily. The high temporal variability in oxygen profiles at the same position is another indicator for intense bioturbation/bioirrigation since no correlation of OPD to other factors like daytime or light was observed (Fig. 3.8 and 3.10B). Macrofauna was thus the most important factor for the depth of the oxic/anoxic interface and for the total volume of oxygenated sediment.

### 3.5.4. Topography effects

Seafloor topography, whether resulting from physical (e.g. current) or biological (e.g. bioturbation) processes, may stimulate exchange rates between sediments and water column (Forster et al., 1996, Røy et al., 2002). Topography can also enhance the OPD on small scales since an uneven sediment surface is consequently penetrated by microsensors at different angles (Fig. 3.4B). This effect most likely did not increase the average measured OPD for more than 5-10%, given the relatively moderate surface roughness found at our study sites (Røy et al., 2005). A much stronger effect of sediment topography on oxygen penetration depth can occur, if advective flow through the sediment, driven by pressure differences at the seafloor, is induced (Ziebis et al., 1996). This effect, however, was not observed in our study. The shape of some microprofiles close to the sediment surface suggests the existence of a Brinkman-Layer, a layer with a thickness in the order of few sediment grains, which is constantly or periodically flushed by bottom water (Morad and Khalili, 2009). This flow could explain part of the different oxygen exchange measurements of the different technologies. Oxygen produced by MPB within the first $\sim$0.5 mm of the sediment could be flushed out and can consequently not be measured with microsensors, while benthic chambers and eddy correlation record this production by measuring in the overlying water (O'Connor and Hondzo, 2008). Planar optodes more or less obstruct the Brinkman layer flow. Therefore, flux measurements with planar optodes might be more accurate than microsensor profiling in permeable sediments. More detailed comparisons between the different technologies are necessary to better constrain the magnitude of this effect.

### 3.5.5. Conclusions

The sediment in the western Kattegat was found to be net heterotrophic during our study, even though the phototrophic community was most likely not light limited under the studied summer conditions. The oxygen dynamic was dominated by fauna activity and macrophytes, while microphytobenthos appeared to play a minor role. The sediment oxygen concentration reacted slowly on changing light conditions, bottom water concentrations and sediment perturbations, while all these factors were found to be highly dynamic. Therefore non-steady state in respect to $O_2$ distribution is likely to be prevalent. The heterogeneity on scales smaller then 1 cm and temporal changes in oxygen penetration depth within hours could mostly be attributed to fauna activity, while microphytobenthos patches below 1 cm were not observed. Decoupling the effects of time and space represents a major challenge in such highly dynamic systems with variability on different time- and space scales. The benthic crawler C-MOVE proved to be a highly versatile and flexible system for seafloor studies in this respect. The simultaneous deployment of the different instruments opened the possibility to study heterogeneity of oxygen distribution and dynamics on very different scales, ranging from millimeters (planar optode) over centimeters (microelectrode profiler with sledge), several hundred meters (operation radius of C-MOVE) to many kilometers (ships range). The concurrent use of these different measurement technologies, complemented by eddy correlation measurements, enabled to identify key processes and the relative importance of fauna, macrophytes and microphytobenthos in benthic oxygen dynamics and mineralization of organic matter.

# References


Aller, R. C., Aller, J. Y., 1998. The effect of biogenic irrigation intensity and solute exchange on diagenetic reaction rates in marine sediments. J. Mar. Res. 56 (4), 905–936.

Barnett, P., Watson, J., Connely, D., 1984. A multiple corer for taking virtually undisturbed samples from shelf, bathysal and abyssal sediments. Oceanlogica Acta 7, 399 – 408.

Berg, P., Risgaard-Petersen, N., Rysgaard, S., 1998. Interpretation of measured concentration profiles in sediment pore water. Limnology and Oceanography 43 (7), 1500–1510.

Berg, P., Røy, H., Janssen, F., Meyer, V., Jørgensen, B. B., Huettel, M., de Beer, D., 2003. Oxygen uptake by aquatic sediments measured with a novel non-invasive eddy-correlation technique. Mar. Ecol. Prog. Ser. 262, 75–83.

Berg, P., Røy, H., Wiberg, P. L., 2007. Eddy correlation flux measurements: The sediment surface area that contributes to the flux. Limnol. Oceanogr 52 (4), 1672 – 1684.

Berg, P., Rysgaard, S., Funch, P., Sejr, M. K., 2001. Effects of bioturbation on solutes and solids in marine sediments. Aquatic Microbial Ecology 26 (1), 81–94.

Canfield, D., Thamdrup, B., Hansen, J., 1993. The anaerobic degradation of organic matter in Danish coastal sediments: iron reduction, manganese reduction, and sulfate reduction. Geochim. Cosmochim. Acta 57 (16), 3867–83.

Canfield, D. E., 1994. Factors influencing organic carbon preservation in marine sediments. Chem. Geol. 114, 315 – 329.

Cartaxana, P., Mendes, C. R., van Leeuwe, M. A., Brotas, V., 2006. Comparative study on microphytobenthic pigments of muddy and sandy intertidal sediments of the tagus estuary. Estuarine, Coastal and Shelf Science 66 (1-2), 225–230.

Christie, M. C., Dyer, K. R., Blanchard, G., Cramp, A., Mitchener, H. J., Paterson, D. M., 2000. Temporal and spatial distributions of moisture and organic contents across a macro-tidal mudflat. Cont. Shelf Res. 20 (10-11), 1219–1241.

Cook, P., Wenzhofer, F., Glud, R., Janssen, F., Huettel, M., 2007. Benthic solute exchange and carbon mineralization in two shallow subtidal sandy sediments: Effect of advective pore-water exchange. Limnol. Oceanogr 52 (5), 1943.

de Beer, D., Wenzhoefer, F., Ferdelman, T., Boehme, S., Huettel, M., van Beusekom, J., Böttcher, M., Musat, N., Dubilier, N., 2005. Transport and mineralization rates in North Sea sandy intertidal sediments, Sylt-Rømø Basin, Wadden Sea. Limnol. Oceanogr 50 (1), 113–127.

De Brouwer, J. F. C., Stal, L. J., 2001. Short-term dynamics in microphytobenthos distribution and associated extracellular carbohydrates in surface sediments of an intertidal mudflat. Mar. Ecol. Prog. Ser. 218, 33–44.

Dyson, K. E., Bulling, M. T., Solan, M., Hernandez-Milian, G., Raffaelli, D. G., White, P. C. L., Paterson, D. M., 2007. Influence of macrofaunal assemblages and environmental heterogeneity on microphytobenthic production in experimental systems. Proceedings of the Royal Society B 274 (1625), 2547.

Ellingsen, K. E., Hewitt, J. E., Thrush, S. F., 2007. Rare species, habitat diversity and functional redundancy in marine benthos. Journal of Sea Research 58 (4), 291–301.

Epping, E., Jørgensen, B., 1996. Light-enhanced oxygen respiration in benthic phototrophic communities. Mar. Ecol. Prog. Ser. 139 (1), 193–203.

Evrard, V., 2007. Assessing the fate of organic matter in subtidal sandy sediments using carbon and nitrogen stable isotopes as deliberate tracers. Phd thesis, University of Utrecht.

Evrard, V., Cook, P. L. M., Veuger, B., Huettel, M., Middelburg, J. J., 2008. Tracing carbon and nitrogen incorporation and pathways in the microbial community of a photic subtidal sand. Aquat. Microbiol. Ecol. 53 (3), 257–269.

Fenchel, T., Glud, R. N., 2000. Benthic primary production and $O_2 - CO_2$ dynamics in a shallow-water sediment: spatial and temporal heterogeneity. Ophelia 53 (3), 159–172.

Floderus, S., 1988. On the spatial distribution of wave impact at the kattegat seabed. Geografiska Annaler 70, 269–272.

Floderus, S., Pihl, L., 1990. Resuspension in the Kattegat: Impact of variation in wind climate and fishery. Estuarine Coastal Shelf Sci. 31 (4).

Forster, S., Huettel, M., Ziebis, W., 1996. Impact of boundary layer flow velocity on oxygen utilisation in coastal sediments. Marine ecology progress series. Oldendorf 143 (1), 173–185.

Gattuso, J. P., Gentili, B., Duarte, C., Kleypas, J., Middelburg, J., Antoine, D., 2006. Light availability in the coastal ocean: impact on the distribution of benthic photosynthetic organisms and their contribution to primary production. Biogeosciences 3 (4), 489–513.

Glud, R., Ramsing, N., Gundersen, J., Klimant, I., 1996. Planar optrodes: a new tool for fine scale measurements of two-dimensional $O_2$ distribution in benthic communities. Mar. Ecol. Prog. Ser. 140 (1-3), 217–226.

Glud, R., Wenzhöfer, F., Tengberg, A., Middelboe, M., Oguri, K., Kitazato, H., 2005. Distribution of oxygen in surface sediments from central Sagami Bay, Japan: In situ measurements by microelectrodes and planar optodes. Deep Sea Res. Part I 52 (10), 1974–1987.

Glud, R. N., 2008. Oxygen dynamics of marine sediments. Mar. Biol. Res. 4 (4), 243 – 289.

Glud, R. N., Stahl, H., Berg, P., Wenzhöfer, F., Oguri, K., Kitazato, H., 2009. In situ microscale variation in distribution and consumption of $O_2$: A case study from a deep ocean margin sediment (Sagami Bay, Japan). Limnol. Oceanogr 54 (1), 1–12.

Glud, R. N., Tengberg, A., Kühl, M., Hall, P. O. J., Klimant, I., Holst, G., 2001. An in situ instrument for planar $O_2$ optode measurements at benthic interfaces. Limnol. Oceanogr 46 (8), 2073–2080.

Graf, G., Bengtsson, W., Diesner, U., Schulz, R., Theede, H., 1982. Benthic response to sedimentation of a spring phytoplankton bloom: process and budget. Mar. Biol. 67 (2), 201–208.

Grenz, C., Denis, L., Boucher, G., Chauvaud, L., Clavier, J., Fichez, R., Pringault, O., 2003. Spatial variability in sediment oxygen consumption under winter conditions in a lagoonal system in New Caledonia (South Pacific). J. Exp. Mar. Biol. Ecol. 285-286, 33–47.

Guarini, J., Blanchard, G., Bacher, C., Gros, P., Riera, P., Richard, P., Gouleau, D., Galois, R., Prou, J., Sauriau, P., 1998. Dynamics of spatial patterns of microphytobenthic biomass: inferences from a geostatistical analysis of two comprehensive surveys in Marennes-Oléron Bay (France). Mar. Ecol. Prog. Ser. 166, 131–141.

Gundersen, J. K., Jorgensen, B. B., 1990. Microstructure of diffusive boundary layers and the oxygen uptake of the sea floor. Nature 345 (6276), 604–607.

Hansen, L. S., Blackburn, T. H., 1992. Effect of algal bloom deposition on sediment respiration and fluxes. Marine Biology 112 (1), 147–152.

Holst, G., Kohls, O., Klimant, I., König, B., Kühl, M., Richter, T., 1998. A modular luminescence lifetime imaging system for mapping oxygen distribution in biological samples. Sensors Actuators B 51, 163–170.

Janssen, F., Faerber, P., Huettel, M., Meyer, V., Witte, U., 2005. Pore-water advection and solute fluxes in permeable marine sediments (I): Calibration and performance of the novel benthic chamber system Sandy. Limnol. Oceanogr, 768–778.

Jesus, B., Brotas, V., Marani, M., Paterson, D. M., 2005. Spatial dynamics of microphytobenthos determined by pam fluorescence. Estuarine, Coastal and Shelf Science 65 (1-2), 30–42.

Jørgensen, B., 1978. A comparison of methods for the quantification of bacterial sulfate reduction in coastal marine sediments. 1. Measurement with radiotracer techniques. Geomicrobiol. J 1, 11–27.

Jørgensen, B. B., Glud, R. N., Holby, O., 2005. Oxygen distribution and bioirrigation in arctic fjord sediments (Svalbard, Barents Sea). Mar. Ecol. Prog. Ser. 292, 85–95.

Jørgensen, B. B., Revsbech, N. P., 1985. Diffusive boundary layers and the oxygen uptake of sediments and detritus. Limnol. Oceanogr. 30 (1), 111–122.

Kim, K., Kim, D., 2007. Seasonal and spatial variability of sediment oxygen fluxes in the Beobsan intertidal flat of Taean Bay, mid-western Korean Peninsula. Geosciences Journal 11 (4), 323–329.

König, B., Kohls, O., Holst, G., Glud, R., Kühl, M., 2005. Fabrication and test of sol-gel based planar oxygen optodes for use in aquatic sediments. Mar. Chem. 97, 262–276.

Kühl, M., Jørgensen, B. B., 1994. The light field of microbenthic communities: Radiance distribution and microscale optics of sandy coastal sediments. Limnol. Oceanogr. 39 (6), 1368–1398.

Li, Y.-H., Gregory, S., 1974. Diffusion of ions in sea water and in deep-sea sediments. Geochim. Cosmochim. Acta 38 (5), 703–714.

Lorenzen, C., 1967. Determination of chlorophyll and pheopigments: spectrophotometric equations. Limnol. Oceanogr 12 (2), 343–346.

MacIntyre, H., Geider, R., Miller, D., 1996. Microphytobenthos: The ecological role of the "secret garden" of unvegetated, shallow-water marine habitats. I. Distribution, abundance and primary production. Estuaries and Coasts 19 (2), 186–201.

Middelburg, J. J., Duarte, C. M., Gattuso, J. P., 2005. Respiration in coastal benthic communities. Respiration in aquatic ecosystems 1 (9), 206–225.

Middleburg, J. J., Barranguet, C., Boschker, H. T. S., Herman, P. M. J., Moens, T., Heip, C. H. R., 2000. The fate of intertidal microphytobenthos carbon: An in situ $^{1}3C$-labeling study. Limnol. Oceanogr 45 (6), 1224–1234.

Migné, A., Spilmont, N., Davoult, D., 2004. In situ measurements of benthic primary production during emersion: seasonal variations and annual production in the Bay of Somme (eastern English Channel, France). Cont. Shelf Res. 24 (13-14), 1437–1449.

Miller, D., Geider, R., MacIntyre, H., 1996. Microphytobenthos: The ecological role of the "secret garden" of unvegetated, shallow-water marine habitats. ii. role in sediment stability and shallow-water food webs. Estuaries and Coasts 19 (2), 202–212.

Morad, M., Khalili, A., 2009. Transition layer thickness in a fluid-porous medium of multi-sized spherical beads. Experiments in Fluids 46 (2), 323–330.

Morris, E. P., 2005. Quantifying primary production of microphytobenthos: application of optical methods. Ph.D. thesis, Rijks University.

O'Connor, B. L., Hondzo, M., 2008. Dissolved oxygen transfer to sediments by sweep and eject motions in aquatic environments. Limnol. Oceanogr 53 (2), 566–578.

Precht, E., Franke, U., Polerecky, L., Huettel, M., 2004. Oxygen dynamics in permeable sediments with wave-driven pore water exchange. Limnol. Oceanogr 49 (3), 693–705.

Reimers, C. E., 1987. An in situ microprofiling instrument for measuring interfacial pore water gradients: methods and oxygen profiles from the North Pacific Ocean. Deep Sea Res. Part I 34 (12), 2019–2021, 2023–2035.

Reimers, C. E., Fischer, K. M., Merewether, R., Smith, K. L., Jahnke, R. A., 1986. Oxygen microprofiles measured in situ in deep ocean sediments. Nature 320 (6064), 741–744.

Revsbech, N., 1989. An oxygen microsensor with a guard cathode. Limnol. Oceanogr. 34 (2), 474–478.

Revsbech, N., Sorensen, J., Blackburn, H., Lomholt, J., 1980. Distribution of oxygen in marine sediments measured with microelectrodes. Limnol. Oceanogr. 25 (3), 403–411.

Røy, H., Huettel, M., Jørgensen, B. B., 2005. The influence of topography on the functional exchange surface of marine soft sediments, assessed from sediment topography measured in situ. Limnol. Oceanogr., 106–112.

Røy, H., Hüttel, M., Jørgensen, B. B., 2002. The role of small-scale sediment topography for oxygen flux across the diffusive boundary layer. Limnol. Oceanogr. 47 (3), 837–847.

Rusch, A., Huettel, M., Forster, S., 2000. Particulate organic matter in permeable marine sands-dynamics in time and depth. Estuarine Coastal Shelf Sci. 51 (4), 399–414.

Schulz, H., Zabel, M., 2000. Marine Geochemistry, 1st Edition. Springer, Berlin, Heidelberg.

Smith, K. L., 1978. Benthic community respiration in the NW Atlantic Ocean: In situ measurements from 40 to 5200 m. Mar. Biol. 47 (4), 337–347.

Smith, K. L., Glatts, R. C., Baldwin, R. J., Beaulieu, S. E., Uhlman, A. H., Horn, R. C., Reimers, C. E., 1997. An autonomous, bottom-transecting vehicle for making long time-series measurements of sediment community oxygen consumption to abyssal depths. Limnol. Oceanogr. 42 (7), 1601–1612.

Stockdale, A., Davison, W., Zhang, H., 2009. Micro-scale biogeochemical heterogeneity in sediments: A review of available technology and observed evidence. Earth Sci. Rev. 92 (1), 81–97.

Sundbäck, K., Enoksson, V., Graneli, W., Pettersson, K., 1991. Influence of sublittoral microphytobenthos on the oxygen and nutrient flux between sediment and water: a laboratory continuous-flow study. Mar. Ecol. Prog. Ser. 74 (2), 263–279.

Sundbäck, K., Miles, A., 2000. Balance between denitrification and microalgal incorporation of nitrogen in microtidal sediments, NE Kattegat. Aquat. Microbiol. Ecol. 22 (3), 291–300.

Thamdrup, B., Canfield, D. E. (Eds.), 2000. Benthic Respiration in Aquatic Sediments, 1st Edition. Methods in Ecosystem Science. Springer-Verlag, New York.

Thamdrup, B., Fossing, H., Joergensen, B., 1994. Manganese, iron, and sulfur cycling in a coastal marine sediment, Aarhus Bay, Denmark. Geochim. Cosmochim. Acta 58 (23), 5115–5129.

Underwood, G. J. C., Kromkamp, J., 1999. Primary production by phytoplankton and microphytobenthos in estuaries. In: Adv. Ecol. Res. Vol. 29. Academic Press, pp. 93–153.

Wenzhöfer, F., Glud, R., 2002. Benthic carbon mineralization in the Atlantic: a synthesis based on in situ data from the last decade. Deep-Sea Res. Part I 49 (7), 1255–1279.

Wenzhöfer, F., Glud, R., 2004. Small-scale spatial and temporal variability in benthic $O_2$ dynamics of coastal sediments: Effects of fauna activity. Limnol. Oceanogr 49 (5), 1471–1481.

Ziebis, W., Huettel, M., Forster, S., 1996. Impact of biogenic sediment topography on oxygen fluxes in permeable seabeds. Mar. Ecol. Prog. Ser. 140, 227–237.

# Chapter 4.

# Subseafloor sedimentary life in the South Pacific Gyre

---

Steven D'Hondt[1], Arthur J. Spivack[1], Robert Pockalny[1], Timothy G. Ferdelman[2], Jan P. Fischer[2], Jens Kallmeyer[3], Lewis J. Abrams[4], David C. Smith[1], Dennis Graham[1], Franciszek Hasiuk[5], Heather Schrum[1], and Andrea M. Stancin[5]

Published in PNAS online before print June 26, 2009, doi:10.1073/pnas.0811793106

[1]Graduate School of Oceanography, University of Rhode Island, USA
[2]Max Planck Institute for Marine Microbiology, Bremen, Germany
[3]Department of Geosciences, University of Potsdam
[4]Department of Geography and Geology, University of North Carolina
[5]Department of Geological Sciences, University of Michigan

## 4.1. Abstract

The low-productivity South Pacific Gyre (SPG) is Earth's largest oceanic province. Its sediment accumulates extraordinarily slowly (0.1–1 m per million years). This sediment contains a living community that is characterized by very low biomass and very low metabolic activity. At every depth in cored SPG sediment, mean cell abundances are 3 to 4 orders of magnitude lower than at the same depths in all previously explored subseafloor communities. The net rate of respiration by the subseafloor sedimentary community at each SPG site is 1 to 3 orders of magnitude lower than the rates at previously explored sites. Because of the low respiration rates and the thinness of the sediment, interstitial waters are oxic throughout the sediment column in most of this region. Consequently, the sedimentary community of the SPG is predominantly aerobic, unlike previously explored subseafloor communities. Generation of $H_2$ by radiolysis of water is a significant electron-donor source for this community. The per-cell respiration rates of this community are about 2 orders of magnitude higher (in oxidation/reduction equivalents) than in previously explored anaerobic subseafloor communities. Respiration rates and cell concentrations in subseafloor sediment throughout almost half of the world ocean may approach those in SPG sediment.

## 4.2. Introduction

Life is previously unknown in the subseafloor sediment of the vast low-productivity regions that dominate the open ocean. Past studies have focused on sites relatively close to shore and beneath major upwelling zones (Whelan et al., 1986, Parkes et al., 2000, D'Hondt et al., 2004, Jørgensen et al., 2006) (Fig. 4.1), where biological productivity and organic flux to the seafloor are generally high (Jahnke, 1996). Their subseafloor [greater than 1.5mbelow seafloor (mbsf)] sedimentary communities contain abundant living microbes (Schippers et al., 2005, Sørensen and Teske, 2006, Biddle et al., 2006, Lipp et al., 2008). These communities (Inagaki et al., 2006, Biddle et al., 2008) and their metabolic activities (D'Hondt et al., 2004, Hinrichs et al., 2006) are diverse. Their activities are dominated by fermentation, sulfate reduction, and methanogenesis (D'Hondt et al., 2002). Their principal food source is buried organic matter from the surface world (D'Hondt et al., 2004). The environmental properties of these previously sampled sites differ greatly from environmental properties throughout most of the open ocean, where oceanic productivity and organic flux to the seafloor are very low (Jahnke, 1996). To understand the extent and nature of subseafloor life in the low-productivity heart of the ocean, expedition Knox-02RR surveyed and cored the sediment at 10 sites throughout the South Pacific Gyre (SPG) and at 1 site at its southern margin (Fig. 4.1). The central SPG has been described as Earth's largest oceanic desert (Claustre and Maritorena, 2003). The middle of the gyre is farther from continents and productive oceanic regions than any other site on Earth. It contains the clearest seawater in the world (Morel et al., 2007). Its organic flux to the seafloor is extremely low (Jahnke, 1996). The area of its low-chlorophyll [$\leq$0.14 mg of chlorophyll-a/$m^3$ (chl-a/$m^3$)] region ($5.2 \times 10^7$ $km^2$)

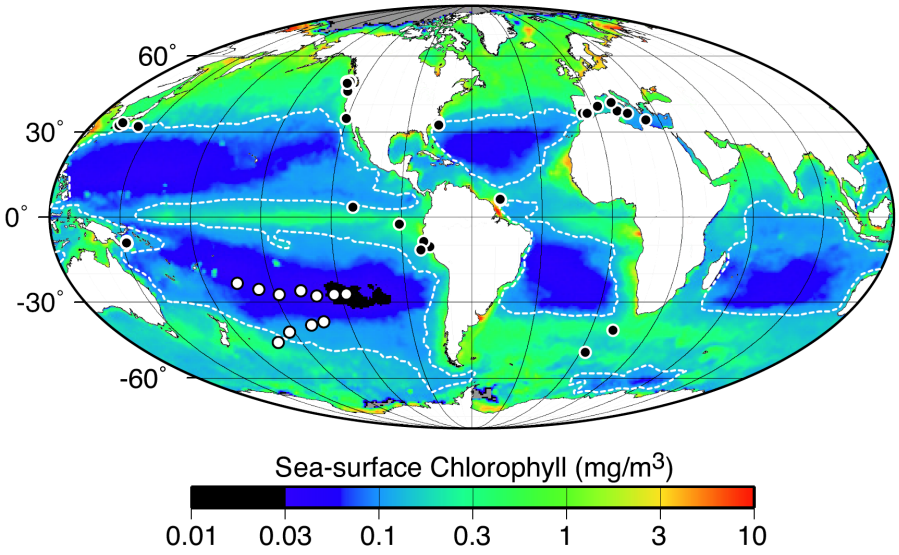


Figure 4.1.: Site locations on a map of time-averaged sea-surface chl-a concentrations (Global SeaWiFS Chlorophyll (mean of September 1997–December 2004)). White dots mark sites analyzed for this study. Black dots mark sites previously analyzed for subseafloor biomass and/or activity (2, 3). Dashed white lines delimit the area in each gyre where the sea-surface chlorophyll-a (chl-a) concentration is $\leq 0.14\,\mathrm{mg\,m^{-3}}$.

is more than twice the area of North America (equal to ≈19,000 Rhode Islands) (Fig. 4.1). Its subseafloor ecosystem has never before been explored.

## 4.3. Results

### 4.3.1. Sedimentation and Organic Burial

The cored sediment ranged in age from 0 to 70Ma and in depth below seafloor from 0 to 9m (Table 4.1). Total sediment thickness ranges from 1 m (SPG-7) to 130m (SPG-12) (determined from 3.5-kHz sonar and seismic reflection profiles). At the deepest water sites in the low chlorophyll region of the SPG (sites SPG-1 to SPG-4 and SPG-9 to SPG-11), the cored sediment is homogeneous brown clay capped by a nearly continuous layer of manganese (Mn) nodules. Discrete horizons of Mn nodules or Mn crust also occur deeper in the cored sediment at SPG-1 and SPG-10. Silt and sand-sized Mn nodules and cosmic debris commonly occur within the brown clay, but fossils, except for scattered ichthyoliths, do not. The cored sediment at the shallowest sites (SPG-6 and SPG-7) is calcareous nanofossil-bearing clay. The sediment at SPG-5 is transitional between these 2 lithologies. Site SPG-12 lies outside the low-chlorophyll region, and its cored sediment is dominantly siliceous ooze with abundant diatom debris and sponge spicules. Mean sedimentation rates are extremely low in the low chlorophyll region of the SPG (Rea et al., 2006) (Table 4.1). In general, they are lowest at sites where the seafloor is below the calcite compensation depth

[≈4500 m below sea level in this region (Seibold and Berger, 1982)] and sea-surface chlorophyll concentrations are below 0.1 mg chl $m^{-3}$. Mean sedimentation rate is higher at our eastern-most sites, where water depth is shallowest (allowing carbonate sediment to accumulate), and at our western-most sites, where sea-surface chlorophyll content is above 0.1 mg chl $m^{-3}$ and the sites were south of the central gyre many tens of millions of years ago. The rate is highest at SPG-12, just outside the central gyre, because of sedimentation of siliceous debris. Mean sedimentation rates within the SPG are among the lowest that occur at the Earth's surface. The highest SPG rates are, respectively, 1 and 2 orders of magnitude lower than rates at equatorial Pacific and Peru Margin sites, where subseafloor life has previously been studied (D'Hondt et al., 2003, Skilbeck and Fink, 2006). Organic carbon burial rates at the sediment surface in the brown clay-dominated sites of the low-chlorophyll region are also extremely low (Table 4.1). The highest of these is more than 1 order of magnitude lower than organic carbon burial rates at sites where subseafloor sedimentary life has previously been studied [e.g., $4.5 \times 10^{-7}$ mol C $cm^{-2}$ annually at equatorial Pacific Ocean Drilling Program (ODP) Sites 1225 and 1226 and $3.1 \times 10^{-6}$ mol C $cm^{-2}$ annually at Peru Margin ODP Sites 1227 and 1230 (D'Hondt et al., 2004)]. Most of the buried organic matter is oxidized in the shallowest portion of the sediment column. Burial of total organic carbon (TOC) below 1.5 mbsf ranges from $4.4 \times 10^{-10}$ to $8.2 \times 10^{-9}$ mol C $cm^{-2}$ annually (Table 4.1). TOC declines very little with increasing depth below the initial few tens of centimeters below seafloor (cmbsf); for example, at SPG-3, it declines from 0.52% at 3 cmbsf to 0.26% at 23 cmbsf and 0.17% at 1.47 mbsf but then declines more slowly to 0.09% at the base of the sediment column (5.17 mbsf). If the TOC burial rate has been relatively constant over the 70million years of sedimentation at SPG-3, the relative constancy of TOC content at depths greater than a few centimeters below seafloor indicates that organic matter at those depths is so recalcitrant or inaccessible that almost none of it has been oxidized since passing through the near-surface zone in its initial few million years after burial.

### 4.3.2. Microbial Biomass

Despite the extraordinarily low rate of organic burial, microbes occur throughout the cored sediment columns (Fig. 4.2), indicating that biomass persists in the sediment for at least 70 million years (compare Fig. 4.2 and Table 4.1). However, cell abundance is extremely low; the average counted concentration at each depth below the seafloor at SPG sites 1–11 is 3 to 4 orders of magnitude lower than the average of all previously explored subseafloor sediment populations at the same depths (Fig. 4.2). Throughout much of the sediment column at these sites, cell concentrations are below the detection limit of standard counts in slurried sediment. Consequently, our counts are based on populations of cells separated from the sediment (Kallmeyer et al., 2008). Although counts of separated cells may slightly underestimate total cell concentrations, there are not significant differences between the results of the 2 techniques at SPG-12, where cell counts are typically above the detection limit of the standard technique. If the counts of separated cells underestimate total cell concentration by 10–30% (Kallmeyer et al., 2008), the effect is not

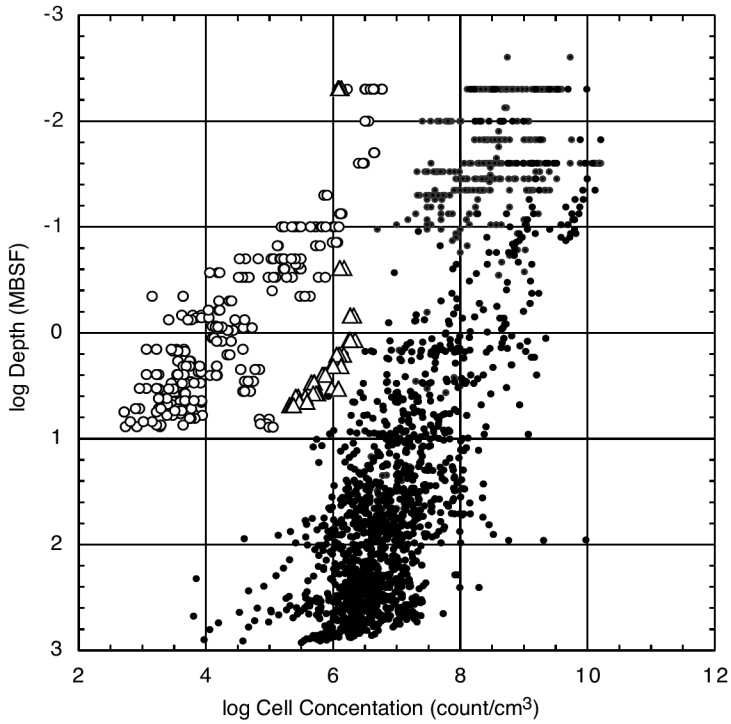


Figure 4.2.: Cell concentrations in subseafloor sediment. White dots mark data from SPG sites SPG-1 to SPG-11, and white triangles mark data from site SPG-12, just outside the gyre (this study). Black dots mark data from all other sites (Parkes et al., 2000, D'Hondt et al., 2004).

significant on the orders-of-magnitude scale that distinguishes the SPG counts from counts of subseafloor populations in other regions (Fig. 4.2).

### 4.3.3. Chemical Evidence of Microbial Activity

Pore water chemistry indicates that $O_2$ is reduced and organic matter is oxidized within the sediment at all the cored sites. At the sites within the low chlorophyll portion of the SPG, dissolved $O_2$ is the principal electron acceptor. It is present throughout the cored sediment columns. Its concentration decreases by tens of micromoles per liter within the initial few tens of centimeters below seafloor and then declines much more slowly with greater depth (Fig. 4.3 Left). In contrast to $O_2$, $NO_3^-$ increases slightly (by a few micromoles per liter at SPG-1 to SPG-4 and at SPG-10 to SPG-11) or exhibits no clear change (at SPG-5 to SPG-9) with depth (Fig. 4.3 Center); the slight increase is attributable to oxidation of buried organic nitrogen. Comparison with sparse data from Deep Sea Drilling Project (DSDP) Leg 92 sites (Gieskes and Boulègue, 1986) in the northern SPG at 20°S suggests that $NO_3^-$ concentrations are probably at or above deep-water concentrations throughout the entire sediment column of the SPG. Just outside the low-chlorophyll region of the SPG, at SPG-12, $O_2$ disappears within 1 mbsf and $NO_3^-$ disappears by 2.5 mbsf. Dissolved $SO_4$ concentration is constant with depth below seafloor

at all 11 sites. This result is not surprising for sites SPG-1 to SPG-11, because $SO_4$ is not reduced where dissolved $O_2$ and $NO_3^-$ are available. Given the absence of dissolved$O_2$ below 1 mbsf and $NO_3^-$ below 2.5 mbsf at SPG-12, the constancy of $SO_4$ with depth indicates that oxidized metals, such as iron and Mn, are the principal electron acceptors at greater depth in the sediment at SPG-12. Alkalinity increases very slightly with depth at 5 sites in the low-chlorophyll region (SPG-2, SPG-4, SPG-7, SPG-9, and SPG- 10) and exhibits no clear trend with depth at the remaining 5 sites in this region (SPG-1, SPG-3, SPG-5, SPG-6, and SPG-11). Alkalinity increases much more strongly with depth at SPG-12 than at any of the sites in the low-chlorophyll region. Alkalinity can be increased by oxic respiration because the carbon dioxide produced will dissolve carbonate if it is present. Nitrate reduction also produces alkalinity. We calculated fluxes of $O_2$ downward into the subseafloor ecosystem and $NO_3^-$ upward at all the sites within the central gyre where the dissolved chemical profiles are stable enough that fluxes can be calculated (Table 4.1). For these calculations, we followed the convention of previous studies by defining the subseafloor ecosystem as beginning at 1.5 mbsf (D'Hondt et al., 2004, 2002). At steady state, these fluxes are nearly equal to the net rate of $O_2$ reduction and the net rate of $NO_3^-$ production by the entire subseafloor sedimentary ecosystem below 1.5 mbsf at each site (these fluxes are not exactly equal to the net subseafloor sedimentary reaction rates because they do not account for fluxes across the sediment/basement interface). The upward $NO_3^-$ flux cannot be calculated (i) at SPG-4 and SPG-6 because no clear trend occurs in their dissolved $NO_3^-$concentration profiles or (ii) at SPG-5 because its dissolved $NO_3^-$ concentration decreases with depth. These $O_2$ fluxes demonstrate that an active microbial community is present in the subseafloor at these sites, despite the very low concentrations of chlorophyll in the overlying ocean and the extraordinarily low rate of organic matter input. The $NO_3^-$ production rates at SPG-1 to SPG-3 and SPG-9 to SPG-11 indicate that this activity is partly fueled by oxidation of nitrogen from buried organic matter. Just outside the central gyre at SPG-12, dissolved $O_2$ disappears well above 1.5 mbsf and the subseafloor ecosystem is characterized by net reduction of $NO_3^-$ rather than net production. The downward flux of $NO_3^-$ past 1.5 mbsf is $2.6 \times 10^{-8}\,\mathrm{mol\,cm^{-2}}$ annually. Because $NO_3^-$ disappears before 2.5 mbsf at SPG-12, this flux fuels respiration for only the shallowest fraction of the subseafloor community at this site.

### 4.3.4. Radiolytic $H_2$ Production

$H_2$ is naturally produced by radiolysis of water in any environment where water is bombarded by $\alpha$-, $\beta$-, and $\gamma$-radiation produced during radioactive decay. Radiolytic $H_2$ has been identified as a significant electron donor in deep continental aquifers where organic products of photosynthesis are largely absent (Lin et al., 2005). It may also be a significant electron donor in marine sediment where organic matter is scarce. Radiolytic $H_2$ production is particularly efficient in deep-sea clays because all the $\alpha$ particles produced in the clay escape from the clay grains and travel through water before being stopped (Blair et al., 2007). We estimate that the radiolytic production of dissolved $H_2$ at these sites is $1 \times 10^{-12}\,\mathrm{mol\,cm^{-3}}$ sediment per year (at SPG-1 to

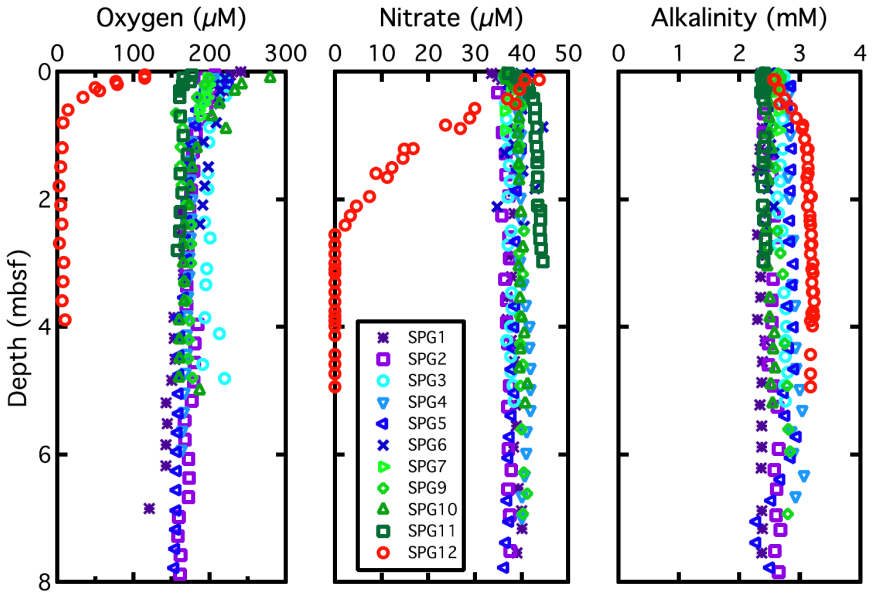


Figure 4.3.: Dissolved chemical concentrations in subseafloor sediment of the SPG sites: $O_2$ (Left), $NO_3^-$ (Center), and alkalinity (Right).

SPG-6) to $1.2 \times 10^{-12}$ mol cm$^{-3}$ sediment per year (at SPG-9 to SPG-11). Total $H_2$ production by this process varies from site to site with thickness of the sediment column; it ranges from $1.6 \times 10^{-8}$ mol $H_2$ cm$^{-2}$ annually at SPG-11 to $8.0 \times 10^{-10}$ mol $H_2$ cm$^{-2}$ annually at SPG-3 (Table 4.1). To assess potential microbial use of radiolytic $H_2$, we calculated the $H_2$ concentrations that would be expected if $H_2$ were not consumed in the sediment column. For these calculations, we considered 2 cases: first, assuming there is a sink for $H_2$ in the underlying basalt and, second, assuming the basalt is impermeable to $H_2$. These 2 cases bracket the range of possibilities for the bottom boundary condition. $H_2$ production, diffusivity, porosity, and tortuosity were assumed to be constant with depth. If radiolytic $H_2$ is not consumed, its peak concentration scales with the square of the thickness of the sediment column. Sites SPG-1 and SPG-3 provide examples of the predicted $H_2$ concentrations. For SPG-1, predicted peak concentration at the base of the cored section (7.81 mbsf) is between 25 and 26 μM. For SPG-3, 5.5 m in length, predicted peak concentration is between 0.32 and 0.64 μM. Measured $H_2$ concentrations are consistently far below these calculated values. No $H_2$ was detected in any of the 154 samples from sites SPG-1 through SPG-11, except for a single sample at SPG-10 (the detection limit ranged from 2–229 nM). The scarcity of $H_2$ at all sites indicates that radiolytic $H_2$ is removed as quickly as it is generated, as expected from *in situ* microbial utilization.

## 4.4. Discussion

### 4.4.1. An Aerobic Subseafloor Ecosystem

In electron (oxidation/reduction) equivalents, $O_2$ fluxes down past 1.5 mbsf in the SPG are nearly equal to the rates at which organic carbon is buried below 1.5 mbsf (Table 4.2). However, the $O_2$ flux slightly exceeds this organic carbonburial rate (by a factor of 2–10) at all but 2 of the sites (Table 4.2). This difference is exacerbated by the evidence from SPG-3 that most of the organic matter below 1.5 mbsf does not get oxidized, even on time scales of many tens of millions of years. The difference between the $O_2$ flux and the TOC burial rate at these sites has several possible explanations: (i) a significant fraction of the $O_2$ may be diffusing through the sediment to the underlying basalt, (ii) the burial rate of organic carbon may have been slightly higher in the very distant past (tens of millions of years ago) than in the past several million years, or (iii) some of the $O_2$ flux oxidizes inorganic chemicals (e.g., reduced iron) in the sediment. The initial explanation likely applies at most, perhaps all, of the sites from SPG-1 to SPG-11, because dissolved $O_2$ concentrations decline very slightly with sediment depth and extrapolations of the concentration profiles predict $O_2$ to be present throughout the entire sediment column at most or all of the sites (Fischer et al., 2007). This explanation is also consistent with estimates of $O_2$ reduction derived from rates of subseafloor $NO_3^-$ production (Table 4.2). These estimates assume that the carbon/nitrogen (C/N) ratio of buried organic matter approximates the Redfield ratio: 106:16. Estimated in this manner, the average organic-fueled $O_2$ reduction rate in the subseafloor sediment of our SPG sites is only about 20% of the average downward $O_2$ flux at the SPG sites and less than half of the average rate of TOC burial below 1.5 mbsf. The inference that porewater is oxic throughout the sediment column in most of the SPG has 2 major implications. First, this subseafloor sedimentary community is predominantly aerobic, unlike previously explored deep subseafloor communities. Second, the flux of $O_2$ through the sediment may sustain aerobic life in the underlying basalt, which ranges in age to more than 100 Ma. These relatively short geochemical profiles do not allow us to quantify precisely how much of the $O_2$ flux is going to sustain microbial respiration in the sediment and how much is going to oxidize the underlying basalt. Precise separation of these 2 rates requires drilling of the entire sediment column at several sites to determine the rate at which dissolved $O_2$ migrates from the sediment to the basalt.

### 4.4.2. Relation to Oceanographic Properties

Even if most of the $O_2$ flux is used to sustain respiration within the sediment at most of the SPG sites, subseafloor sedimentary rates of net respiration are much lower in this region than at all previously explored sites. In electron equivalents, the average $O_2$ flux into the subseafloor ecosystem at the SPG sites ($3.7 \times 10^{-8}$ mol $e^-$ $cm^{-2}$ annually) corresponds to a net respiration rate that is a factor of 5.4 lower than the rate of organic-fueled subseafloor respiration in the lowest activity site previously explored (Peru Basin ODP Site 1231 on the eastern edge of the

SPG) and a factor of 550 less than the rate at the highest respiration site previously explored (Peru Margin ODP Site 1230) [Site 1230 and 1231 rates were taken from the work of (D'Hondt et al., 2004)]. These differences between sites are even greater when $O_2$ reduction is estimated from the rate of subseafloor $NO_3^-$ production (Table 4.2); calculated in this manner, the mean organic-fueled $O_2$ reduction in the subseafloor sediment of our SPG sites ($7 \times 10^{-9}$ mol $e^-$ $cm^{-2}$ annually) is a factor of 28 lower than the rate of organic-fueled respiration at ODP Site 1231 and a factor of 2910 lower than the rate of organic-fueled respiration at Site 1230. Subseafloor cell abundance is also much lower (by 3 to 4 orders of magnitude on average) in the central SPG than at all previously studied sites (Fig. 4.2). These very low cell concentrations and net respiration rates mirror basic oceanographic properties of the SPG. Sea-surface chlorophyll concentrations, organic carbon burial rate, and sediment accumulation rate are all extremely low throughout the region. Sea-surface chlorophyll and productivity are low because the region is far from coastal and other regions of strong upwelling. Organic carbon burial rate is low because sea-surface chlorophyll, biological productivity, and sediment accumulation rates are low.Sedimentation rate is low because (i) the low productivity results in a very low production rate of biogenic debris; (ii) the great distance from shore leads to very low sediment transport from land; and (iii) throughout much of the region, the seafloor is below the carbonate compensation depth, and biogenic carbonate consequently dissolves in the water column and at the seafloor.

### 4.4.3. Potential Reliance on Radiolytic $H_2$ Production

Our calculations indicate that generation of $H_2$ by radiolysis of the interstitial water is a significant electron donor source for this community. In electron equivalents, we estimate the rate of $H_2$ production by water radiolysis at sites SPG-1, SPG-2, SPG-3, SPG-10, and SPG-11 to approach or exceed the rate of organic carbon burial below 1.5 mbsf (Table 4.2). This equivalence implies that radiolysis of water provides roughly half of the electron donors used by the subseafloor sedimentary community at these sites and buried organic matter provides the other half, if all the organic matter is completely used. If less of the organic matter is used, as indicated by the constancy of TOC concentration with depth at SPG-3, radiolytic $H_2$ is the principal electron donor. Although microbial oxidation of this $H_2$ increases gross respiration in this ecosystem, it does not contribute to the net respiration calculated from downward $O_2$ fluxes because the release of $O_2$ by water radiolysis nearly stoichiometrically balances the $O_2$ used to oxidize the $H_2$ ($H_2O \rightarrow 1/2\ O_2 + H_2$). $H_2$ from water radiolysis may be the principal electron donor in this sediment at depths greater than a few meters to a few tens of meters. Buried organic matter is probably the dominant food in the shallowest sediment because it tends to be oxidized at highest rates in shallow sediment and at successively lower rates in deeper (and older) sediment, where only the most recalcitrant or biologically inaccessible organic matter remains. In contrast, radiolytic $H_2$ production will be nearly constant throughout the sediment column if porosity, grain size, and concentrations of radioactive elements remain constant as our estimates assume; consequently, as organic oxidation declines with increasing depth below the seafloor in SPG sediment, $H_2$ from

water radiolysis is likely to become the dominant food source. Recovery of the entire sediment column will ultimately be required to (i) quantify the respective roles of buried organic matter and radiolytic $H_2$ at each depth in the sediment column at each site and (ii) test if $H_2$ from water radiolysis is the dominant electron donor at depth in SPG sediment.

### 4.4.4. Respiration per Cell

Organic-fueled respiration per cell can be independently estimated from $O_2$ fluxes, $NO_3^-$ fluxes, and organic carbon burial rates at 1.5 mbsf (Table 4.2). The first approach assumes that all the downward $O_2$ flux is used for oxidation of organic matter in the sediment. The second approach assumes that a Redfield C/N ratio (106:16) can be used to calculate the rate of organic oxidation from the rate of $NO_3^-$ production ($NO_3^-$ flux upward). The third approach assumes that the organic carbon burial rate has been constant over time. These approaches are subject to different uncertainties. The $O_2$-based rates are overestimates to the extent that $O_2$ migrates through the sediment to the underlying basalt. Uncertainties in estimates from $NO_3^-$ fluxes may result from (i) $NO_3^-$ produced in the sediment diffusing to the underlying basement (as well as to the overlying ocean) and (ii) C/N ratios of buried organic matter differing from the Redfield ratio if organic nitrogen is oxidized faster than organic carbon. Estimates from organic burial rates may be overestimates because they assume that all organic matter is eventually oxidized. Potential gross respiration per cell can be estimated by adding any of the above estimates to the *in situ* rate of radiolytic$H_2$ production per cell (Table 4.2). With any of these approaches ($O_2$ flux, $NO_3^-$ flux, or organic burial rate), gross respiration per cell is above rates necessary to counter aspartic acid racemization and DNA depurination (Price and Sowers, 2004). Respiration per cell appears to be much higher in the oxic SPG sediment than in previously explored anoxic sediment; in electron equivalents, respiration per cell in the anoxic sediment of ODP Leg 201 ranges between $1 \times 10^{-17}$ and $5 \times 10^{-17}$ mol $e^-$ $cell^{-1}$ annually [calculated from fluxes and cell counts of ODP Sites 1226, 1227, 1230, and 1231 (D'Hondt et al., 2004, Wang et al., 2006)]. This result is consistent with the calculation that the energy requirement for biomass synthesis by aerobes is more than 10 times the requirement for biomass synthesis by anaerobes (McCollom and Amend, 2005).

### 4.4.5. Global Implications

These results have direct implications for global patterns of biomass and activity in subseafloor sediment. Several oceanographic properties are at their extreme in the center of the SPG (e.g., sea-surface chlorophyll concentration, distance from continents). The subseafloor sedimentary community of the central SPG is likely to define the low-biomass low-activity end-member for global distributions of subseafloor biomass and respiration. However, the other major ocean gyres resemble the SPG more closely than they resemble the regions where subseafloor life was previously explored. For example, sea-surface chlorophyll concentrations are below 0.14 mg chl/$m^3$ in all the major ocean gyres (Fig. 4.1). Consequently, rates of organic-fueled respiration, cell con-

centrations, and metabolic reliance on radiolytic $H_2$ in subseafloor sediment throughout almost half (48%) of the world ocean may approach the end-member values in SPG sediment.

## 4.5. Materials and Methods

### 4.5.1. TOC Content, Sedimentation Rate, and Burial Rates

TOC was measured at the University of Rhode Island using the technique (Verardo et al., 1990) and a Costech ECS4010 elemental analyzer. For sites SPG-2 to SPG-12, mean sedimentation rates were calculated from crust age and sediment thickness. For SPG-1, mean sedimentation rate was calculated from the 20.1 mbsf depth of the 65-Ma Cretaceous / Paleogene iridium anomaly at DSDP Site 596 (Zhou et al., 1991). Organic carbon burial rates were calculated from TOC content and mean sedimentation rate and adjusted for porosity and wet bulk density. Surface burial of organic carbon is based on TOC content of 0–5 cmbsf at sites SPG-1 to SPG-11 and 10–15 cmbsf at site SPG-12. Burial of organic carbon at 150 cmbsf is based on TOC content of samples taken close to 150 cmbsf (between 143 and 167 cmbsf).

### 4.5.2. Sediment Physical Properties

Wet bulk density, grain density, and porosity were measured on discrete samples using the approach of Blum (1997). Vertical conductivity measurements were performed shipboard with a Brinkmann/Metrohm Conductometer every 5 cm on cores throughout the cored sediment columns. The conductivity probe consisted oft 2-mm-diameter platinum electrodes set 1 cm apart in a plastic block.

### 4.5.3. Cell Counts

At each site, 12–25 sediment samples were taken for shipboard cell counts. Cells were separated from the sediment and counted using the technique of Kallmeyer et al. (2008). At every site, a blank sample was processed by treating 500 µL of 0.2 µm-filtered NaCl solution like a sediment sample through the entire process of cell extraction and counting. Because absolute cell concentrations may not be accurately calculated from regression lines through log-transformed data (Fig. 4.2), average cell counts were calculated from non transformed data. We used data from (Parkes et al., 2000) and (D'Hondt et al., 2003) to calculate average concentrations for previously explored communities.

### 4.5.4. Dissolved Chemical Concentrations

Interstitial waters were extracted from 5-cm long whole rounds of cores using a Manheim-type hydraulic sediment press. Alkalinity titrations were run on a Metrohm 809 Titrando with a Metrohm pH microelectrode, following the method of Gieskes et al. (1991). Based on duplicate analyses of a control sample, precision is 0.5%. Sulfate concentration was quantified with a

Metrohm 861 Advanced Compact IC comprising an 853 $CO_2$ suppressor, a thermal conductivity detector, a 150 × 4.0-mm Metrosep A SUPP 5 150 column, and a 20 µL sample loop. A Metrohm 837 IC Eluent/Sample Degasser was coupled to the system. Based on duplicates, the 95% confidence limit is 0.25%. Nitrate concentrations were analyzed with a Metrohm 844 UV/Vis Compact IC with a 150 × 4.0-mm Metrosep A SUPP 8 150 column. The pooled SD of duplicates is 0.3%. Ex situ dissolved $O_2$ measurements were performed on thermally equilibrated intact whole rounds of cores. At SPG-1 and SPG-2, both custom-made microelectrodes (Revsbech and Jørgensen, 1986) and optodes (Klimant et al., 1995) were used. The optodes, connected to a Microsensor Oxygen Meter Microx TX3 (Presens GmbH), were more stable and were used for measurement at all other sites. Dissolved $O_2$ concentration was determined by inserting a probe radially into the center of the core. Model calculations and radial profiles showed that the $O_2$ concentration in the core center of the core was not affected by ambient air on the time scales of our analyses. For dissolved $H_2$ analyses, samples were collected with sterile 3 mL cutoff syringes. The sample was then extruded directly into a vial, which was immediately filled completely with distilled $H_2O$. A headspace was then created by injecting $H_2$-free gas (500 µL) through the septum while allowing an equal volume of water to escape. The $H_2$ was then given time to diffuse out of the interstitial water (>24 h). Three hundred microliters of the headspace gas was removed and injected into a reduced gas analyzer (Trace Analytic ta3000). The instrument was calibrated with a 100.6-ppm $H_2$ standard (Scott Specialty Gases). Blanks were prepared by using vials with distilled $H_2O$ and the $H_2$-free headspace. The average detection limit was 67 nM $H_2$ (range: 2–229 nM). At SPG-1, the headspace gas was laboratory air. Because these blanks contained too much $H_2$ relative to the samples, we modified the procedure for the remaining sites by using bypass gas [carrier gas ($N_2$) that has passed over the mercury bed to remove traces of $H_2$] for the headspace.

### 4.5.5. Chemical calculations

Dissolved chemical fluxes were calculated using Fick's law, $F = (D/f) * (dC/dx)$, where $dC/dx$ is the gradient of the dissolved chemical concentration profile at 1.5 mbsf, D is the diffusion coefficient for the chemical in free solution, and f is the formation factor (measured as the ratio of the conductivity of seawater to the conductivity of the saturated core). Diffusion coefficients are taken from the method of (Schulz and Zabel, 2000) and corrected for a temperature of 1.5 °C [bottom water temperature in this region (Pickard and Emery, 1982)]. Our electron transport estimates make the following assumptions. Four electrons are accepted by reducing a molecule of $O_2$, and 5 are accepted during reduction of $NO_3^-$ to $N_2$. Eight electrons are donated by oxidizing a molecule of organic nitrogen ($NH_3$) to $NO_3^-$, and 2 are donated by oxidizing an $H_2$ molecule to $H_2O$. Because organic matter is a mix of molecules with carbon in different redox states, the number of electrons donated by oxidizing organic carbon is intermediate between the molecules with the most extreme redox states; because the extreme redox states of organic carbon are carbohydrates [C (0)] and lipids [C (-II)], we assume that 5 electrons are donated by oxidation

of each organic carbon molecule. $H_2$ yields from water radiolysis were calculated as described by Blair et al. (2007). These calculations use the $H_2$ yields of Spinks and Spinks (1990); decay data from Ekstrøm and Firestone (1999); and the stopping power ratios of Aitken (1985) for $\alpha$ -, $\beta$ -,and $\gamma$ -radiation. Potassium-40 abundance was calculated from total potassium according to the method of Wedepohl (1978). The average $^{238}$U, $^{232}$Th, and $^{40}$K concentrations for SPG-1 to SPG-11 were assumed to be equal to the average $^{238}$U, $^{232}$Th, and $^{40}$K concentrations for DSDP Site 595A (SPG-1) [U=12.2 ppm (n=9) and Th=2.9ppm (n=9) (Chan et al., 2006), K=1.56wt% (n=15) (Plank and Langmuir, 1998)]. The average porosity and grain density for SPG-1 to SPG-6 were assumed to be equal to the average measured porosity(82%)and grain density ($2.41\,\mathrm{g\,cm^{-3}}$) for SPG-1 (n=27).The average porosity and grain density for SPG-9 to SPG-11 were assumed to be equal to the average measured porosity (76%) and grain density ($2.43\,\mathrm{g\,cm^{-3}}$) for SPG-9 (n=18). The $H_2$ concentrations that would be expected from radiolytic $H_2$ production if there were no *in situ* $H_2$ utilization were calculated from these radiolytic $H_2$ yields, by analytical solution of the continuity equation, using the same porosity as in the $H_2$ yield calculations, formation factor, and an $H_2$ diffusion coefficient corrected for 1.5 °C.

**Acknowledgements.** The expedition would not have been possible without the extraordinary effort of Captain Tom Desjardins; the crew of the RV Roger Revelle; and Knox-02RR shipboard science party members Rika Anderson, James Dorrance, Alan Durbin, Lee Ellett, Stephanie Forschner, Ruth Fuldauer, Howard Goldstein, William Griffith, Hannah Halm, Robert Harris, Benjamin Harrison, Gregory Horn, Mark Lever, Jon Meyer, Laura Morse, Christopher Moser, Brandi Murphy, Axel Nordhausen, Lucian Parry, Ann Puschell, Justin Rogers, Bruno Soffientino, Melissa Steinman, and Paul Walczak. Coring capabilities were provided by the Oregon State University Coring Facility, directed by Nicklas Pisias and funded by the U.S. National Science Foundation (NSF) Ship Facilities Program. The cored materials and discrete samples from the expedition are curated and stored by the Marine Geological Samples Laboratory at the University of Rhode Island, directed by Steven Carey and funded by the NSF Ocean Sciences Division. This project was funded by the Ocean Drilling Program of the NSF, the National Aeronautics and Space Administration Astrobiology Institute, and the Max Planck Institute for Marine Microbiology.

Table 4.1.: Sediment properties and subseafloor (>1.5 mbsf) biogeochemical fluxes

| Site | lat. | lon. | Basement age (Ma) | water depth ( m) | sed. thickn. (m) | cored sed. (mbsf) | Sed. rate (cm / ky) | Corg content at 0-5 cmbsf (dry weight %) | Corg burial rate 0-5 cmbsf (molC/cm2/yr) | Corg burial rate 150cmbsf (molC/cm2/yr) | Downward O2 flux at 1.5mbsf (mol/cm2/yr) | Upward NO3- flux at 1.5mbsf (mol/cm2/yr) | Radiolytic H2 prod. (mol H2/cm2/yr) |
|---|---|---|---|---|---|---|---|---|---|---|---|---|---|
| SPG-1 | 23°51′ | 165°39′ | 100 | 5697 | 71 | 7.79 | 0.031 | 0.33 | 3.6e-09 | 1.6e-09 | -2.0e-08 | 6.9e-10 | 1.4e-08 |
| SPG-2 | 26°03′ | 156°54′ | 100 | 5127 | 17 | 8.2 | 0.017 | 0.53 | 3.2e-09 | 8.7e-10 | -6.8e-09 | 3.5e-10 | 3.1e-09 |
| SPG-3 | 27°57′ | 148°35′ | 71 | 4852 | 5.49 | 5.49 | 0.008 | 0.42 | 1.2e-09 | 4.4e-10 | -4.1e-09 | 5.4e-10 | 8.0e-10 |
| SPG-4 | 26°29′ | 137°56′ | 33.5 | 4285 | 9 | 7.24 | 0.028 | 0.42 | 4.2e-09 | 1.6e-09 | -5.4e-09 | n.d. | 1.6e-09 |
| SPG-5 | 28°27′ | 131°23′ | 24.1 | 4221 | 17 | 8.05 | 0.069 | 0.36 | 8.8e-09 | 3.8e-09 | -7.6e-09 | n.d. | 3.0e-09 |
| SPG-6 | 27°55′ | 123°10′ | 13.5 | 3738 | 15 | 2.59 | 0.111 | n.d. | n.d. | 7.0e-09 | -2.2e-08 | n.d. | 2.7e-09 |
| SPG-7 | 27°44′ | 117°37′ | 6.1 | 3688 | 1.05 | 1.05 | 0.017 | 0.29 | 1.7e-09 | n/a | n/a | n/a | n/a |
| SPG-9 | 38°04′ | 133°06′ | 39 | 4925 | 20 | 7.05 | 0.051 | 0.38 | 9.5e-09 | 3.8e-09 | -2.8e-09 | 3.0e-10 | 4.5e-09 |
| SPG-10 | 39°19′ | 139°48′ | 58 | 5283 | 21 | 5.63 | 0.037 | 0.56 | 1.0e-08 | 2.0e-09 | -1.2e-08 | 6.0e-10 | 4.8e-09 |
| SPG-11 | 41°51′ | 153°06′ | 75 | 5076 | 67 | 2.98 | 0.089 | 0.51 | 2.2e-08 | 8.2e-09 | -2.4e-09 | 1.6e-09 | 1.6e-08 |
| SPG-12 | 45°58′ | 163°11′ | 73 | 5306 | 130 | 4.98 | 0.178 | 0.34 | 3.0e-08 | 2.7e-08 | n/a | -3.1e-08 | n.d |

Table 4.2.: Rates of subseafloor activities and biogeochemical fluxes (in electron equivalents) per unit area and per cell

| Site | Subseafl. $O_2$ red. rate (mol e-/cm2/yr) | Subseaf. $NO_3^-$ red. rate (mol e-/cm2/yr) | $O_2$ red. rate based on $NO_3^-$ prod. (mol e-/cell/yr) | Organic carbon burial rate at 1.5 mbsf (mol e-/cm2/yr) | Radiolytic $H_2$ prod. rate (mol e-/cm2/yr) | Total cells below 1.5 mbsf | $O_2$ red. rate per cell (mol e-/cell/yr) | $O_2$ red. rate per cell based on net $NO_3-$ prod. (mol e-/cell/yr) | Organic carbon burial rate per cell (mol e-/cell/yr) | Radiolytic $H_2$ prod. rate per cell (mol e-/cell/yr) |
|---|---|---|---|---|---|---|---|---|---|---|
| SPG-1 | 7.9e-08 | n/a | 7.1e-09 | 8.2e-09 | 2.7e-08 | 8.9e-07 | 8.9e-16 | 8.0e-17 | 9.3e-17 | 3.1e-16 |
| SPG-2 | 2.7e-08 | n/a | 3.6e-09 | 4.3e-09 | 6.2e-09 | 2.6e-06 | 1.0e-14 | 1.4e-15 | 1.7e-15 | 2.4e-15 |
| SPG-3 | 1.6e-08 | n/a | 5.6e-09 | 2.2e-09 | 1.6e-09 | 1.7e-06 | 9.6e-15 | 3.2e-15 | 1.3e-15 | 9.3e-16 |
| SPG-4 | 2.2e-08 | n/a | n.d. | 7.8e-09 | 3.2e-09 | 4.7e-06 | 4.7e-15 | n.d. | 1.7e-15 | 6.9e-16 |
| SPG-5 | 3.0e-08 | n/a | n.d. | 1.9e-08 | 6.0e-09 | n.d. | n.d. | n.d. | n.d. | n.d. |
| SPG-6 | 8.9e-08 | n/a | n.d. | 3.5e-08 | 5.4e-09 | n.d. | n.d. | n.d. | n.d. | n.d. |
| SPG-7 | n/a | n/a | n/a | n/a | n/a | n/a | n/a | n/a | n/a | n/a |
| SPG-9 | 1.1e-08 | n/a | 3.0e-09 | 1.9e-08 | 8.9e-09 | 1.5e-06 | 7.6e-15 | 2.1e-15 | 1.3e-14 | 6.1e-15 |
| SPG-10 | 4.8e-08 | n/a | 6.1e-09 | 1.0e-08 | 9.7e-09 | 1.0e-06 | 4.6e-14 | 5.9e-15 | 9.7e-15 | 9.3e-15 |
| SPG-11 | 9.4e-09 | n/a | 1.6e-08 | 4.1e-08 | 3.2e-08 | 7.8e-06 | 1.2e-15 | 2.1e-15 | 5.3e-15 | 4.1e-15 |
| SPG-12 | n/a | -1.30e-07 | n.d. | 1.3e-07 | n.d. | n.d | n.d. | n.d. | n.d. | n.d. |

# References


Aitken, M. J., 1985. Thermoluminescence dating. Academic Press, Orlando, Fl.

Biddle, J. F., Fitz-Gibbon, S., Schuster, S. C., Brenchley, J. E., House, C. H., 2008. Metagenomic signatures of the peru margin subseafloor biosphere show a genetically distinct environment. Proceedings of the National Academy of Sciences 105 (30), 10583–10588.

Biddle, J. F., Lipp, J. S., Lever, M. A., Lloyd, K. G., Sørensen, K. B., Anderson, R., Fredricks, H. F., Elvert, M., Kelly, T. J., Schrag, D. P., 2006. Heterotrophic archaea dominate sedimentary subsurface ecosystems off peru. Proceedings of the National Academy of Sciences 103 (10), 3846–3851.

Blair, C. C., D'Hondt, S., Spivack, A. J., Kingsley, R. H., 2007. Radiolytic hydrogen and microbial respiration in subsurface sediments. Astrobiology 7 (6), 951–970.

Blum, P., 1997. Physical properties handbook - a guide to the shipboard measurement of physical properties of deep-sea cores by the ocean drilling program. Tech. rep., Project Technical Note (Ocean Drilling Program, College Station, TX).

Chan, L. H., Leeman, W. P., Plank, T., 2006. Lithium isotopic composition of marine sediments. Geochemistry Geophysics Geosystems 7, Q06005, 10.1029/2005GC001202.

Claustre, H., Maritorena, S., 2003. The many shades of ocean blue. Science 302 (5650), 1514–1515.

D'Hondt, S., Jørgensen, B., Miller, D., Batzke, A., Blake, R., Cragg, B., Cypionka, H., Dickens, G., Ferdelman, T., Hinrichs, K., 2004. Distributions of microbial activities in deep subseafloor sediments. Science 306 (5705), 2216–2221.

D'Hondt, S., Jørgensen, B., Miller, J. (Eds.), 2003. Controls on Microbial Communities in Deeply Buried Sediments, Eastern Equatorial Pacific and Peru Margin, Sites 1225-1231. Proceedings of the Ocean Drilling Program, Scientific Results, 201. Ocean Drilling Program, College Station, TX.

D'Hondt, S., Rutherford, S., Spivack, A. J., 2002. Metabolic activity of subsurface life in deep-sea sediments. Science 295 (5562), 2067–2070.

Ekstrøm, L., Firestone, R., 1999. World wide web table of radioactive isotopes, database version 2/28/99. available at http://ie.lbl.gov/toi/index.htm, accessed september 19, 2006.

Fischer, J., Ferdelman, T. G., S., D., F., W., Knox-02RR Shipboard Scientific Party, 2007. Extreme oligotrophy in subsurface sediments of the south pacific gyre: Evidence from low oxygen fluxes. Geochimica et Cosmochimica Acta (Suppl S) A281 (71).

Gieskes, J., Boulègue, J., 1986. Interstitial water studies: Leg 92. In: M, L., Rea, D. K., al., e. (Eds.), Initial Reports Deep Sea Drilling Project 92. U.S. Government Printing Office, Washington, pp. 423–429.

Gieskes, J., Gamo, T., Brumsack, H., 1991. Chemical methods for interstitial water analysis aboard JOIDES Resolution,. Tech. rep., Ocean Drilling Program, College Station, TX.

Hinrichs, K. U., Hayes, J. M., Bach, W., Spivack, A. J., Hmelo, L. R., Holm, N. G., Johnson, C. G., Sylva, S. P., 2006. Biological formation of ethane and propane in the deep marine subsurface. Proceedings of the National Academy of Sciences 103 (40), 14684 –14689.

Inagaki, F., Nunoura, T., Nakagawa, S., Teske, A., Lever, M., Lauer, A., Suzuki, M., Takai, K., Delwiche, M., Colwell, F. S., 2006. Biogeographical distribution and diversity of microbes in methane hydrate-bearing deep marine sediments on the pacific ocean margin. Proceedings of the National Academy of Sciences 103 (8), 2815–2820.

Jahnke, R., 1996. The global ocean flux of particulate organic carbon: Areal distribution and magnitude. Global Biogeochemical Cycles 10, 71–88.

Jørgensen, B. B., D'Hondt, S. L., Miller, D. J. (Eds.), 2006. Leg 201 Synthesis: Controls on Microbial Communities in Deeply Buried Sediments. Proceedings Ocean Drilling Program, Scientific Results, 201. Ocean Drilling Program, College Station, TX.

Kallmeyer, J., Smith, D. C., Spivack, A. J., D'Hondt, S., 2008. New cell extraction procedure applied to deep subsurface sediments. Limnology and Oceanography-Methods 6, 236–245.

Klimant, I., Meyer, V., Kühl, M., 1995. Fiber-optic oxygen microsensors, a new tool in aquatic biology. Limnology and Oceanography 40 (6), 1159 – 1165.

Lin, L.-H., Hall, J., Lippmann-Pipke, J., Ward, J. A., Sherwood Lollar, B., DeFlaun, M., Rothmel, R., Moser, D., Gihring, T. M., Mislowack, B., Onstott, T. C., 2005. Radiolytic h2 in continental crust: Nuclear power for deep subsurface microbial communities. Geochem. Geophys. Geosyst. 6, 10.1029/2004GC000907.

Lipp, J. S., Morono, Y., Inagaki, F., Hinrichs, K. U., 2008. Significant contribution of archaea to extant biomass in marine subsurface sediments. Nature 454 (7207), 991–994.

McCollom, T. M., Amend, J. P., 2005. A thermodynamic assessment of energy requirements for biomass synthesis by chemolithoautotrophic micro-organisms in oxic and anoxic environments. Geobiology 3 (2), 135–144.

Morel, A., Gentili, B., Claustre, H., Babin, M., Bricaud, A., Ras, J., Tièche, F., 2007. Optical properties of the "clearest" natural waters. Limnol. Oceanogr 52 (1), 217–229.

Parkes, R. J., Cragg, B. A., Wellsbury, P., 2000. Recent studies on bacterial populations and processes in subseafloor sediments: a review. Hydrogeology 8 (1), 11–28.

Pickard, G. L., Emery, W. J., 1982. Descriptive Physical Oceanography: An Introduction, 4th Edition. Pergamon, New York.

Plank, T., Langmuir, C. H., 1998. The chemical composition of subducting sediment and its consequences for the crust and mantle. Chemical Geology 145 (3-4), 325–394.

Price, P. B., Sowers, T., 2004. Temperature dependence of metabolic rates for microbial growth, maintenance, and survival. Proceedings of the National Academy of Sciences 101 (13), 4631–4636.

Rea, D. K., Lyle, M. W., Liberty, L. M., Hovan, S. A., Bolyn, M. P., Gleason, J. D., Hendy, I. L., Latimer, J. C., Murphy, B. M., Owen, R. M., Paul, C. F., Rea, T. H., Stancin, A. M., Thomas, D. J., 2006. Broad region of no sediment in the southwest pacific basin. Geology 34 (10), 873–876.

Revsbech, N. P., Jørgensen, B. B., 1986. Microelectrodes: their use in microbial ecology. Adv. Microb. Ecol 9, 293–352.

Schippers, A., Neretin, L. N., Kallmeyer, J., Ferdelman, T. G., Cragg, B. A., Parkes, R. J., Jørgensen, B. B., 2005. Prokaryotic cells of the deep sub-seafloor biosphere identified as living bacteria. Nature 433, 861–864.

Schulz, H., Zabel, M., 2000. Marine Geochemistry, 1st Edition. Springer, Berlin, Heidelberg.

Seibold, E., Berger, W. H., 1982. The Seafloor. Springer-Verlag, Berlin, Heidelberg, New-York.

Skilbeck, C. G., Fink, D. (Eds.), 2006. Data report: Radiocarbon dating and sedimentation rates for Holocene - upper Pleistocene sediments, eastern equatorial Pacific and Peru continental margin. Proceedings Ocean Drilling Program, Scientific Results, 201. Ocean Drilling Program, College station, TX, proceedings of the Ocean Drilling Program, Initial Reports.

Sørensen, K. B., Teske, A., 2006. Stratified communities of active archaea in deep marine subsurface sediments. Applied and Environmental Microbiology 72 (7), 4596–4603.

Spinks, J. W. T., Spinks, B., 1990. Introduction to radiation chemistry. John Wiley & Sons, New York.

Verardo, D. J., Froelich, P. N., McIntyre, A., 1990. Determination of organic carbon and nitrogen in marine sediments using the carlo erba na-1500 analyzer. Deep Sea Research Part A 37 (1), 157–165.

Wang, G., Spivack, A. J., D'Hondt, S., 2006. Identification of respiration pathways in deep subseafloor sediments using a co 2 mass-balance model. Astrobiology 6, 230.

Wedepohl, K. H., 1978. Handbook of Geochemistry. Springer-Verlag, Berlin, Heidelberg, New York.

Whelan, J. K., Oremland, R., Tarafa, M., Smith, R., Howarth, R., Lee, C. (Eds.), 1986. Evidence for sulfate-reducing and methane producing microorganisms in sediments from Sites 618, 619, and 622. Vol. 96 of Initial Reports Deep Sea Drillig Project. US Government Printing Office, Washington.

Zhou, L., Kyte, F. T., Bohor, B. F., 1991. Cretaceous/tertiary boundary of dsdp site 596, south pacific. Geology 19 (7), 694–697.

# Chapter 5.

# Oxygen penetration deep into the sediment of the South Pacific Gyre

---

Jan P. Fischer[1], Timothey G. Ferdelman[1], Steven D'Hondt[2], Hans Røy [3], Frank Wenzhöfer[1]

Published in Biogeoscience **6** (2009) 1467-1478

[1]Max Planck Institute for Marine Microbiology, Bremen, Germany
[2]Graduate School of Oceanography, University of Rhode Island, USA
[3]Center for Geomicrobiology, University of Aarhus, Denmark

## 5.1. Abstract

Sediment oxygen concentration profiles and benthic microbial oxygen consumption rates were investigated during an IODP site survey in the South Pacific Gyre. Primary production, particle fluxes and sedimentation rates are extremely low in this ultra-oligotrophic oceanic region. We derived $O_2$ consumption rates from vertical oxygen profiles in sediments obtained on different spatial scales ex situ (in piston cores and multi cores), and *in situ* (using a benthic lander equipped with a microelectrode profiler). Along a transect in the area 24 to 46°S and 165 to 117°W, cores from 10 out of 11 sites were oxygenated over their entire length (as much as 8 m below seafloor), with deep $O_2$ concentrations >150 $\mu mol\,L^{-1}$. This represents the deepest oxygen penetration ever measured in marine sediments. High-resolution microprofiles from the surface sediment layer revealed a diffusive oxygen uptake between 0.1 and 1.3 $mmol\,m^{-2}\,d^{-1}$, equal to a carbon mineralization rate of ∼0.4 - 4.5 $g\,C\,m^{-2}\,yr^{-1}$. This is in the lower range of previously reported fluxes for oligotrophic sediments but corresponds well to the low surface water primary production. Half of the pool of reactive organic matter was consumed in the top 1.5 - 6 mm of the sediment. Because of the inert nature of the deeper sediment, oxygen that is not consumed within the top centimeters diffuses downward to much greater depth. In deeper zones, a small $O_2$ flux between 0.05 and 0.3 $\mu mol\,m^{-2}\,d^{-1}$ was still present. This flux was nearly constant with depth, indicating extremely low $O_2$ consumption rates. Modeling of the oxygen profiles suggests that the sediment is probably oxygenated down to the basalt, suggesting an oxygen flux from the sediment into the basaltic basement.

## 5.2. Introduction

Interpretation of sediment oxygen profiles is a common way to assess benthic carbon cycling since oxygen consumption rates correlate well with remineralization rates in sediments (Bender and Heggie, 1984, Thamdrup and Canfield, 2000). Oxygen concentration profiles thus contain information about the magnitude and vertical organization of carbon turnover. The depth of the oxic-anoxic interface is regulated by the balance between oxygen consumption (aerobic respiration and re-oxidation of the reduced products from anaerobic metabolism) and oxygen transport from the water column (diffusion, advection, bio-irrigation) (Glud, 2008). Due to the low flux of particulate organic matter from the photic zone to the seafloor in ocean gyres, only low rates of carbon mineralization can be sustained, and therefore, deep oxygen penetration can be expected. Wenzhöfer et al. (2001) found an oxygen penetration depth of ∼25 cm in the central South Atlantic. Earlier studies in the central Pacific found oxygen concentrations decreasing with depth only in the top layer and showing very little change with depth below 20 - 40 cm (Murray and Grundmanis, 1980).

The South Pacific gyre (SPG) is the largest oligotrophic marine environment on earth (Claustre and Maritorena, 2003). It is farther away from continents than any other oceanic region, and hence, it has very little aeolian and fluviatile input. The surface water of the SPG is char-

acterized by chlorophyll concentrations below 20 $\mu g\,m^{-3}$ (Ras et al., 2008) and these waters are among the clearest on earth in terms of UV absorption (Morel et al., 2007). The low surface water productivity results in low sedimentation rates that vary between 0.08 and 1.1 $mm\,kyr^{-1}$ (D'Hondt et al., 2009). In general, sediments of the SPG have received little scientific interest since the 1901 expedition of the S.S.Brittania described them as oceanic red-clays with manganese nodules. The whole area is understudied compared to other oceanic regions (Daneri and Quinones, 2001) and little is known about the carbon cycle in the seabed. Since the overall area of oligotrophic subtropical gyres represents up to 60% of the global oceans (Claustre et al., 2008), their importance is evident. A recent study by D'Hondt et al. (2009) provides evidence that SPG sediments harbor subseafloor communities where microbial cell abundances are orders of magnitude lower than in all previously described subseafloor environments at the respective subseafloor depths. D'Hondt et al. (2009) used deep penetrating oxygen profiles coupled with pore water distributions of electron acceptors and metabolic products to demonstrate that extremely low aerobic metabolic activities occur throughout the SPG sediments. In this study, we more carefully investigate those deep oxygen profiles, combine them with microprofiles of the top sediment layer and explore these data in terms of depth-resolved oxygen consumption rates via mathematical modeling.

To investigate the oxygen flux in oligotrophic sediments, *in situ* and ex situ measurements with microsensors were performed using a free-falling benthic lander (Reimers et al., 1986, Wenzhöfer and Glud, 2002) and a multi-coring device, respectively. The high-resolution $O_2$ profiles obtained from the uppermost active first centimeters were used to calculate the diffusive oxygen uptake of the sediment. Additionally, a special set-up for onboard measurements of oxygen concentrations in long piston and gravity cores was developed. Combining these methods enabled an integrated picture of the respiration rates in the first decimeters of the sediment down to several meters. Extrapolating the profiles down to the basalt and the application of a reaction-diffusion model gave further insight into $O_2$ consumption in deeper layers. The rates of benthic carbon mineralization of the ultra-oligotrophic sediments of the SPG are discussed in comparison to other oligotrophic environments.

## 5.3. Material and Methods

### 5.3.1. Study site

During the KNOX-02RR expedition (17 December 2006 - 27 January 2007), we sampled sediment cores at 11 stations within the region 24°S to 46°S and 165°W to 117°W (Fig. 5.1). The cruise track can be divided into two transects. A northern transect at a latitude of 24°S to 27°S, proceeds from older crust (∼100 Ma) to younger (∼6 Ma) and at the same time from the outer portion of the gyre to its center. The southern transect at latitude of 38°S to 45°S leads out of the gyre towards older crust (∼75 Ma) (Fig. 5.1). Bottom water temperatures in this region are between 1.2 and 1.4°C, the salinity is 34.7 and bottom water oxygen content is ∼220 $\mu mol\,L^{-1}$ (derived

from the database of the International Council for the Exploration of the Sea, ICES) which corresponds to 63% saturation at the sea surface (Weiss, 1970). To gain a comprehensive picture of oxygen profiles in low-activity sediments, different methods were used for their investigation at different spatial scales. Oxygen profiles in the top few centimeters of the sediments were measured with microelectrodes profiling top down, both *in situ* with a benthic lander and ex situ in recovered cores. To investigate deeper sediment layers, oxygen concentrations were measured ex situ with needle-shaped optodes through drilled holes in piston core liners.

### 5.3.2. *in situ* measurements

A free falling, programmable benthic lander was used to measure oxygen profiles in the top centimeters *in situ* with high resolution (Archer et al., 1989, Wenzhöfer and Glud, 2002). The lander was equipped with a microelectrode profiler enabling profiling in 100 µm steps down to 5 cm. On-board sensor calibration prior to the deployment was performed with air-saturated and anoxic seawater at *in situ* temperature. The obtained profiles were used to calculate diffusive fluxes into the sediment, using Fick's first law of diffusion (Berner, 1980). Since the diffusive boundary layer (DBL) could not accurately be determined from the profiles, the diffusive flux (DOU) was calculated from gradients just below the sediment surface:

$$DOU = -\phi D_s \left.\frac{\partial C}{\partial z}\right|_{z=0} = -\frac{D_0}{F} \left.\frac{\partial C}{\partial z}\right|_{z=0} \tag{5.1}$$

where $\phi$ represents the porosity and $D_s$ is the sediment diffusion coefficient (corrected for tortuosity). The molecular diffusion coefficient of oxygen in free solution $D_0$=1.13 $\times$ $10^{-9}$ $m^2$ $s^{-1}$ was taken from (Schulz and Zabel, 2000) and corrected for *in situ* salinity and temperature (Li and Gregory, 1974). We did not determine the sediment porosity directly. Instead, we measured the formation factor $F$ as the ratio of the electric resistivity of the bulk sediment to the resistivity of the unrestricted porewater (Fig. 5.2). Conductivity was determined with a Brinkman / Metrohm Conductometer every 5 cm in the center of split piston cores. The probe consisted of two 2 mm ∅ platinum electrodes spaced 1 cm apart. All calculations were done using an average sediment formation factor $F$ of 1.69. In subsequent equations, we express $D_0/F$ as $\phi D_s$ for consistency with the literature. The lander was deployed at station 2, 5, 7 and 10. However, due to technical problems, *in situ* microprofiles could be obtained only at station 10.

### 5.3.3. Ex situ measurements on multi-cores

To study the top sediment layer in more detail, sediment was recovered using a Multiple Corer (Barnett et al., 1984). These cores appeared undisturbed with intact microstructure at the sediment surface. Immediately after recovery, the sealed tubes were stored at 4°C. Small rotating magnets ensured well-mixed overlying waters and prevented a too large DBL to develop (Glud et al., 1994, Rasmussen, 1992). Due to technical limitations, oxygen profiles were measured only at 4 out of the 11 stations with Clark-Type microelectrodes (Revsbech, 1989), a custom-made picoamperemeter, an A/D converter (DAQPad-6020E, National Instruments) and a motorized

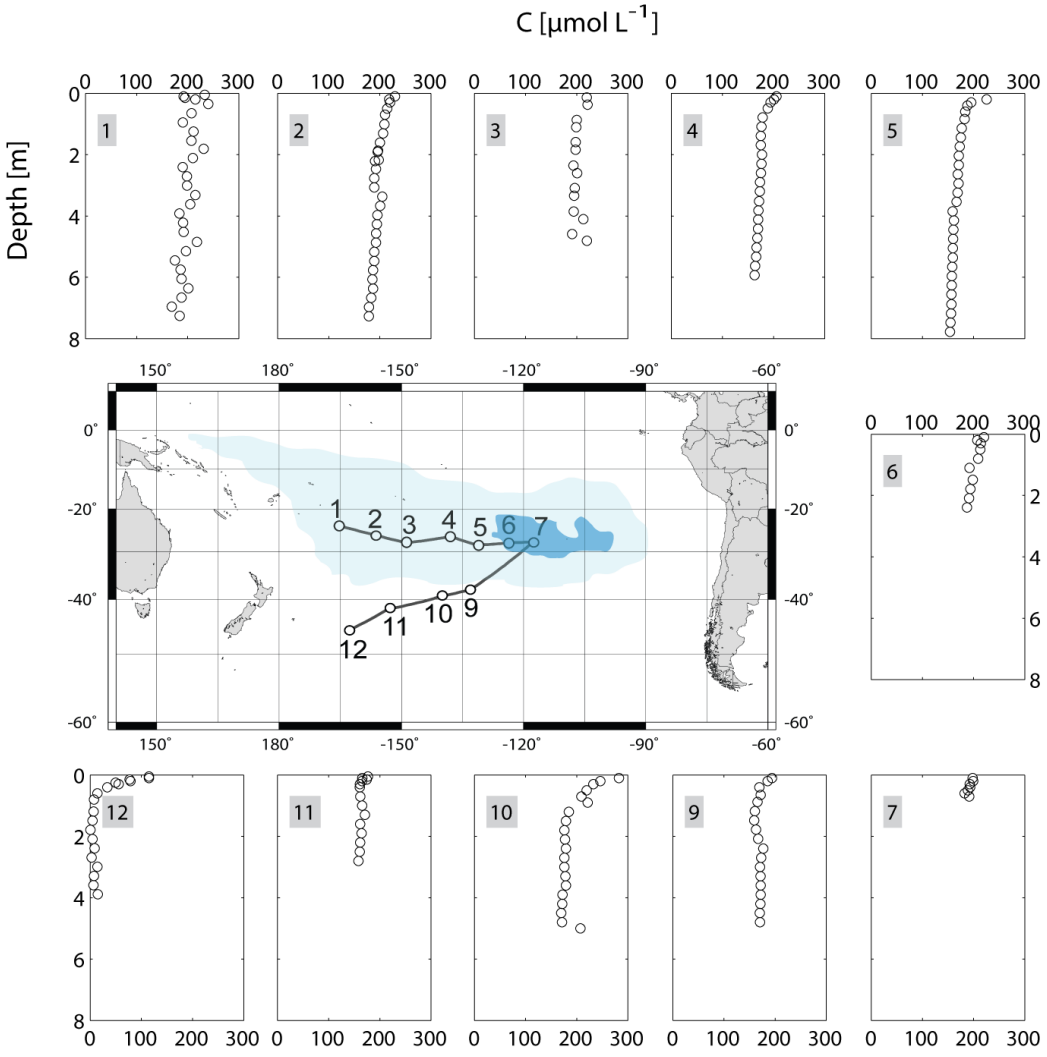


Figure 5.1.: Sampling stations in the South Pacific (middle) and deep oxygen profiles at the respective positions. The shaded areas depict surface chlorophyll concentrations below 0.1 (light blue) and 0.03 (dark blue) mg m$^{-3}$, respectively. The chlorophyll concentration of the remaining sampling area was between 0.1 and 0.25 mg m$^{-3}$ (averaged SeaWiFS remote sensing data).

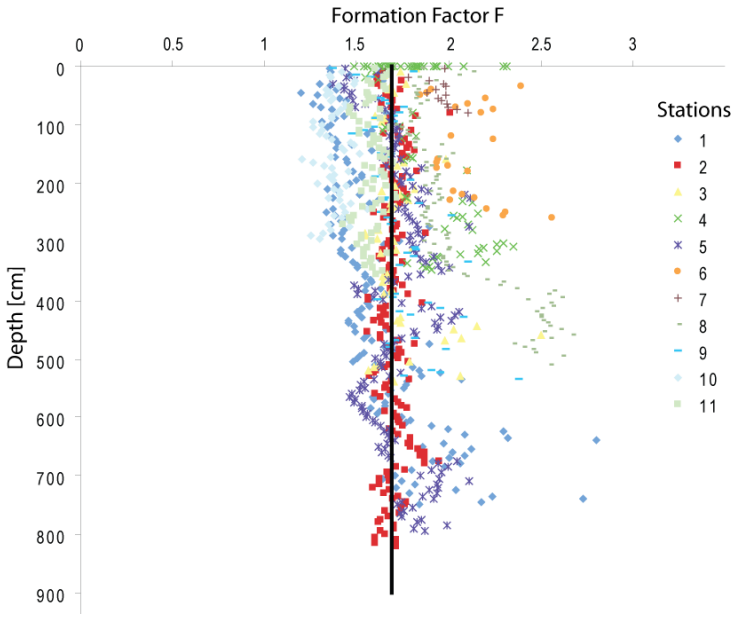


Figure 5.2.: Sediment formation factors as calculated from conductivity measurements on cores of all stations. The black line represents the average value of 1.69.

stage (VT-80, Micos GmbH, Germany). The calculation of DOUs was carried out as described in section 5.3.2. It is known that ex situ measurements of oxygen profiles are biased by core recovery artifacts, tending to underestimate the oxygen penetration depth and to overestimate the calculated benthic flux (Glud et al., 1994). Sediment decompression and warming as well as enhanced availability of labile organic matter are possible explanations. These findings result from investigations in highly productive areas with high gradients and low oxygen penetration depths. Since our measurements were performed in low-productivity regions with deep oxygen penetration and low microbial activities, only little differences between *in situ* and ex situ results are to be expected.

### 5.3.4. Ex situ measurements on piston cores

We compared measurements with clark-type microelectrodes and needle optodes on both-, piston cores and trigger cores (which operate like gravity cores) of Station 1 and 2 and found no significant difference in the oxygen profiles (data not shown). However, the signals of the optodes were found to be more stable and precise. Since optodes are also mechanically more robust, they were used for all subsequent measurements. Oxygen concentrations in one piston core were measured per station. The optode itself consisted of a fiber optic cable (125 µm ∅), glued into a stainless steel capillary that was reinforced by another stainless steel tube into which the capillary was fit (Klimant et al., 1995, Wenzhöfer et al., 2001). The fiber tip was polished using lapping film with decreasing grain size, down to 0.5 µm (3M Inc.). The sensing dye consisted of 2% platinum(II) mesotetra (pentafluorophenyl) porphyrin (Frontier Scientific, Inc.) in a polystyrene matrix. To

coat the fiber tip, the mixture was dissolved in chloroform and applied under a microscope using a micromanipulator. Optode readout was done using a MICROX TX3 (PreSens Precision Sensing GmbH) optode meter. A two-point calibration was done using anoxic and air-saturated seawater at room temperature about every 2 h. Conversion of the measured fluorescence lifetime of the optode to oxygen values was done internally by the instrument, using a modified Stern-Vollmer equation.

After recovery, the piston cores were cut into sections of 150 cm and the ends were sealed with PVC caps and adhesive tape. The cores were allowed to thermally equilibrate for at least 24 h in the lab at 20 °C before the measurements started. The raised temperature decreases the solubility of oxygen within the porewater of the sediment. If supersaturation was reached, a change in oxygen concentration would have been the result. However, the oxygen solubility at 20 celsius and salinity of 35 is 231 µmol $L^{-1}$. This is below the bottom water concentration at all sites. Therefore, oversaturation could not occur. Since the volumetric $O_2$ consumption rates in the deeper layers were very low, we assume that small variation in this rate due to warming will not affect our measurements on the time scales involved. Immediately prior to each measurement, two 6 mm ∅ holes were drilled through the core liner in close vicinity to each other using a spiral drill with a stop unit to prevent drill penetration into the sediment. The self-made fiber sensor was inserted through one of the holes into the center of the core and a temperature probe for thermal compensation was inserted through the second hole. Over the first 50 cm of the piston core, measurements were done in 10 cm intervals, while the remaining core was measured in 20 - 30 cm intervals. After insertion of the optode into the center of the core, the sensor was allowed to equilibrate for about 15 min, before the optode readout was averaged over 5 min. A randomized order of measurements along the core prevented measurement drift artifacts. To ensure that the center of the core was unaffected by ambient air that diffused into the core after recovery, radial microsensor profiles with a clark-type microsensor were done on a core that was left in the lab for 32 h . In a distance of about 2 cm from the core liner, the oxygen profile leveled-off, showing that the center of the 10 cm ∅ core was undisturbed (data not shown).

### 5.3.5. Modeling

Our model analysis of the oxygen profile is based upon steady-state mass balance of oxygen in the pore water. We used different parameterizations of a 1-dimensional reaction-diffusion model to analyze different aspects of the data. Since bioturbation and sedimentation can be neglected in the SPG, the 1-D-model can be formulated as

$$\phi D_s \frac{\partial^2 C}{\partial z^2} - R_{\text{surf}} - R_{\text{deep}} = 0 \tag{5.2}$$

where $\phi$ is the porosity, $D_s$ the sediment diffusion coefficient ($\phi D_s$ was measured as $D_0/F$, s. section 5.3.2), $C$ the oxygen concentration, $z$ is the depth within the sediment and $R_{\text{surf}}$ and $R_{\text{deep}}$ are terms describing the $O_2$ consumption rate close to the sediment surface (labile organic carbon) and deep within the sediment (refractory organic carbon). There was no clear trend in

the formation factor with depth and the scatter in the measurements was relatively high (Fig. 5.1). Therefore, we used an average (constant) formation factor of 1.69 for all calculations. Since it is likely that the first meter of the piston cores was disturbed during coring (Buckley et al., 1994, Skinner and McCave, 2003), we excluded these data points from our analysis of the deep oxygen profiles.

In order to obtain upper and lower bounds for rates deep within the sediment at each site, we varied $R_{\mathrm{deep}}$ and the oxygen flux $F_d$ at the lower boundary of the domain $z_{\mathrm{max}}$, which was set to the depth of the deepest data point. The use of a mean value of the topmost three data points for $C_0$ was chosen to account for scatter in the data. We assumed that $R_{\mathrm{deep}}$ remained constant with depth and since the surface sediment layer was not included in this modeling step, $R_{\mathrm{surf}}$ was set to zero. We used the symbolic math software Maple (Maplesoft, Inc.) to obtain an analytical solution for the oxygen concentration $C$ at depth $z$ (in meters below $C_0$) with the given boundary conditions:

$$C(z) = \frac{1}{2}\frac{R_{\mathrm{deep}}}{\phi D_s}z^2 + \frac{z}{\phi D_s}\left(F_d - R_{\mathrm{deep}}z_{\mathrm{max}}\right) + C_0 \tag{5.3}$$

The goodness of fit was evaluated by calculating generalized $R^2$ values for all tested combinations of $F_d$ and $R_{\mathrm{deep}}$ as the sum of squares of the distances of the data points to the fitted model at the respective depths, normalized to the squared distances of the points to the mean of all values ($R^2$=1-SSR/SST, Schabenberger and Pierce (2001)). To incorporate the high-resolution microprofiles in the model (Eq. 5.2), $R_{\mathrm{deep}}$ was set to constant values, found in the model calibration for the deep sediment described above. A depth-dependent $O_2$ consumption rate was assumed to account for the much higher respiration in the top layer, decreasing exponentially with depth:

$$R_{\mathrm{surf}}(z) = R_{\mathrm{max}}e^{-\alpha z} \tag{5.4}$$

The bottom water concentration $C_0$ was used as top boundary condition whereas a fixed flux ($F_d$) to the basalt was chosen as bottom boundary condition. As analytical solution of equation 5.2 and 5.4 with these boundary conditions, we obtained:

$$C(z) = \frac{1}{\phi D_s}\left(\frac{R_{\mathrm{max}}e^{-\alpha z}}{\alpha^2} + \frac{R_{\mathrm{deep}}z^2}{2} + z\left(\frac{R_{\mathrm{max}}e^{-\alpha z_{\mathrm{max}}}}{\alpha} - R_{\mathrm{deep}}z_{\mathrm{max}} + F_d\right) - \frac{R_{\mathrm{max}}}{\alpha^2}\right) + C_0 \tag{5.5}$$

A simultaneous variation of $R_{\mathrm{max}}$ and $\alpha$ was performed to fit the model to the complete dataset, including microsensor and piston core measurements. The flux to the basalt was set to zero for this study ($F_d = 0$). For a more intuitive interpretation of the fit parameter $\alpha$, the depth $z_{\mathrm{half}}$ at which the rate drops to half the surface rate $R_{\mathrm{max}}$ can be calculated from $\alpha$ as:

$$z_{\mathrm{half}} = -\frac{\ln(0.5)}{\alpha} \tag{5.6}$$

Since the system is not electron-acceptor limited, this can be regarded as the depth where half of the reactive organic matter is used up. To compare the integrated $O_2$ consumption rates in

the surface with the integrated rates deeper in the sediments, the flux to the surface layer was calculated as

$$F_{\mathrm{surf}} = \int_{z=0}^{\infty} R_{\mathrm{surf}}(z)dz \qquad \text{with Eq. (4.4), this simplifies to} \qquad F_{\mathrm{surf}} = \frac{R_{\max}}{\alpha} \tag{5.7}$$

and the integrated deep uptake as

$$F_{\mathrm{deep}} = R_{\mathrm{deep}} z_s \tag{5.8}$$

with $z_s$ being the thickness of the sediment at the respective station.

### 5.3.6. Calculation of carbon input

Several empirical models have been proposed for the calculation of the carbon flux to oceanic sediments from primary production in surface waters (Berger et al., 1987, Betzer et al., 1984, Pace et al., 1987, Suess, 1980, e.g.). Specific models for oligotrophic regions, however, do not exist. The model composed by Antia et al. (2001) was used in this study ($J_{\mathrm{POC\_A}} = 0.1 PP^{1.77} z^{-0.68}$ ) since it represents an average of the cited models, where $PP$ is the surface water primary production in $\mathrm{gC\,m^{-2}\,yr^{-1}}$ and $z$ the water depth in meters. Primary production values were estimated from SeaWiFs remote sensing data, converted into integrated annual primary productivity by the IMCS Ocean Primary Productivity Team (Rutgers, State University of New Jersey) using the algorithms from Behrenfeld and Falkowski (1997). To convert the measured oxygen fluxes into fluxes of labile organic carbon ($J_{\mathrm{POC\_R}}$) we used a respiratory quotient ($O_2$:C) of 1.3.

## 5.4. Results and Discussion

Biogeochemical processes in sediments can be divided into transport phenomena and reaction processes. In general, important vertical transport processes in marine sediments are bioturbation/bioirrigation, advection and molecular diffusion (Berg et al., 2001). Since we found very few traces of macrobenthos in the SPG, bioturbation and bioirrigation are likely to be negligible for solute transport; the low permeability of clay sediments (Spinelli et al., 2004) found at all stations also excludes any appreciable advection. Therefore, molecular diffusion is the dominant transport process in these oligotrophic sediments, and together with biogeochemical reactions (e.g. respiration), controls the penetration of oxygen into the sediment.

### 5.4.1. Benthic carbon fluxes

Microsensor oxygen profiles of the uppermost sediment layer were measured ex situ in recovered sediment cores at Stations 4 - 7 and *in situ* at Station 10 (Fig. 5.7, right panels). A general trend of decreasing oxygen fluxes toward the center of the gyre was observed (Table 5.1), varying between $0.12\,\mathrm{mmol\,m^2\,d^{-1}}$ (Station 6) and $1.32\,\mathrm{mmol\,m^2\,d^{-1}}$ (Station 4). However, the value at station 4 appears exceptionally high, especially compared to station 10. Here, farthest away from the center of the gyre and with the highest surface productivity, higher rates than closer

Table 5.1.: Sampling positions, waterdepth [m], sediment thickness [m], diffusive oxygen uptake (DOU) and fluxes of particulate organic matter as calculated from primary production ($J_{POC\_A}$) or using the oxygen fluxes ($J_{POC\_R}$). Units: DOU: mmol $m^{-2}$ $d^{-1}$ PP, $J_{POC\_A}$, $J_{POC\_R}$: gC $m^{-2}$ $yr^{-1}$. Sediment thicknesses after D'Hondt et al. (2009).

| Stat. | Lat. | Lon. | W. depth | Sed. Thick. | bottom W. O2 | DOU | $J_{POC\_R}$ | PP | $J_{POC\_A}$ |
|---|---|---|---|---|---|---|---|---|---|
| 1 | 23°51′ | 165°39′ | 5697 | 71 | 203 | – | – | 77 | 0.61 |
| 2 | 26°03′ | 156°54′ | 5127 | 17 | 228 | – | – | 83 | 0.75 |
| 3 | 27°57′ | 148°35′ | 4852 | 5.5 | 218 | – | – | 86 | 0.83 |
| 4 | 26°29′ | 137°56′ | 4285 | 9.4 | 217 | 1.32 | 4.46 | 72 | 0.66 |
| 5 | 28°27′ | 131°23′ | 4221 | 16.5 | 220 | 0.45 | 1.51 | 77 | 0.75 |
| 6 | 27°55′ | 123°10′ | 3738 | 15 | 221 | 0.12 | 0.40 | 70 | 0.69 |
| 7 | 27°45′ | 117°37′ | 3688 | 1.5 | 202 | 0.26 | 0.88 | 66 | 0.69 |
| 9 | 38°04′ | 133°06′ | 4925 | 19.8 | 205 | – | – | 118 | 1.90 |
| 10 | 39°19′ | 139°48′ | 5283 | 21.4 | 227 | 0.23 | 0.79 | 113 | 1.60 |
| 11 | 41°51′ | 153°06′ | 5076 | 67 | 213 | – | – | 130 | 1.90 |
| 12 | 45°58′ | 163°11′ | 5306 | 130 | 205 | – | – | 157 | 2.49 |

to the center would have been expected. It has to be noted that station 10 represents the only *in situ* measurement and ex situ measurements tend to overestimate DOU (Glud, 2008, e.g.). However, locally enhanced consumption rates can also not be excluded.

The measured oxygen fluxes are slightly lower compared to previously reported fluxes from oligotrophic sediments in the Atlantic (>0.3 mmol $m^{-2}$ $d^{-1}$ (Wenzhöfer and Glud, 2002, Wenzhöfer et al., 2001)), however, an older study by Smith (1978) reported oxygen fluxes in the NW Atlantic as low as 0.02 mmol $m^{-2}$ $d^{-1}$. The fluxes reported here are higher than some fluxes measured in the central equatorial Pacific (0.09 - 0.68 mmol $m^2$ $d^{-1}$ (Hammond et al., 1996) and 0.013 - 0.22 mmol $m^{-2}$ $d^{-1}$ (Murray and Grundmanis, 1980)) even though there is a lower primary production in the surface-water of the SPG. However, the coarse sampling resolution of several centimeters by Murray and Grundmanis (1980) and Hammond et al. (1996) very likely underestimates the oxygen consumption at the sediment-water interface. Reimers et al. (1984) report microelectrode measurements in the central Pacific with values between 0.2 and 0.8 mmol $m^{-2}$ $d^{-1}$, supporting this assumption.

Since the vast majority of organic matter that reaches the seafloor is ultimately oxidized, oxygen fluxes can be used to calculate organic carbon fluxes (Jahnke, 1996). Converting our measured oxygen fluxes into carbon equivalents, assuming a respiration coefficient of 1.3 resulted in carbon fluxes ($J_{POC\_R}$) between 0.40 and 4.46 gC $m^{-2}$ $yr^{-1}$ with a mean of 1.61 gC $m^{-2}$ $yr^{-1}$ (Table 5.1). These carbon fluxes are in the same order of magnitude as fluxes reported for the deep North Pacific (Murray and Kuivila, 1990). These carbon fluxes ($J_{POC\_R}$) generally confirm the extrapolated estimates of Jahnke (1996) for the SPG which were based on a rather

simple extrapolation procedure. The decrease of fluxes towards the center of the gyre parallels a decrease in surface water primary production, indicating that the benthic mineralization is primarily fueled by the export of organic matter from surface waters.

Using primary production estimates from ocean color data (Behrenfeld and Falkowski, 1997) and an empirical model for carbon export to deep waters (Antia et al., 2001) permits an alternative estimation of the particulate organic carbon ($J_{\mathrm{POC\_A}}$) fluxes to the sediment. Given the high discrepancies generally found between POC fluxes, calculated from ocean color data and sediment trap measurements (Gehlen et al., 2006), the fluxes from remote-sensing PP generally agree with the fluxes derived from our oxygen profiles ($J_{\mathrm{POC\_R}}$). At stations 4, 5 and 7, $J_{\mathrm{POC\_R}}$ exceeds $J_{\mathrm{POC\_A}}$ by 21-85%, while at stations 6 and 10, $J_{\mathrm{POC\_A}}$ is 74% and 103% larger, respectively. Generally, $J_{\mathrm{POC\_A}}$ shows a lower variability between the stations on the northern transect than $J_{\mathrm{POC\_R}}$. Differences between $J_{\mathrm{POC\_R}}$ and $J_{\mathrm{POC\_A}}$ were not correlated to surface chlorophyll concentrations or sedimentation rates. One cause for the remaining differences may be the assumption that the formation factor remains constant with depth, and hence one ignores the porosity gradient in the surface layer. Another, and maybe more likely, explanation for the discrepancy may be that the empirical algorithms used to correlate chlorophyll a content with ocean color are based mostly on data points in the Northern Hemisphere with few points from oligotrophic gyres (Claustre and Maritorena 2003). Although quantification of primary production by remote sensing has improved, oligotrophic regions are still poorly represented and empirical models for carbon export fluxes are poorly constrained (e.g. Gehlen et al., 2006). The presence of a very large pool of dissolved organic matter in the SPG (Raimbault et al., 2008) can furthermore skew the results and lead to overestimation of primary production estimates derived from remote sensing (Claustre and Maritorena, 2003). Additionally, Dandonneau et al. (2003) argue that floating particles can cause significant artifacts in chlorophyll sensing in oligotrophic waters. All these factors could lead to increasing overestimations of $J_{\mathrm{POC\_A}}$ towards the center of the gyre. While the limited number of sampling stations in our study and uncertainties about the porosity gradient in the first millimeters of the sediment does not allow a final conclusion about the magnitude of cross-gyre differences in carbon mineralization, the overall average magnitude of carbon mineralization at the seafloor for this region has, for the first time, been experimentally constrained.

### 5.4.2. Coupling surface and deep respiration

The low sedimentation rates in the SPG prevents labile organic carbon from reaching deeper sediment layers, and thus respiratory activity strongly drops with depth, and the gradient in the oxygen concentration rapidly decreases as can be seen from the microprofiles (Fig. 5.7, right panels). The measured $O_2$ fluxes at the sediment-water interface are not exceptionally low compared to other oligotrophic open-ocean sites (Hammond et al., 1996, Murray and Grundmanis, 1980, Suess, 1980, Wenzhöfer and Glud, 2002). Nevertheless, because of the inert nature of the deeper sediment, any oxygen that escapes consumption in the surface layers is free to diffuse

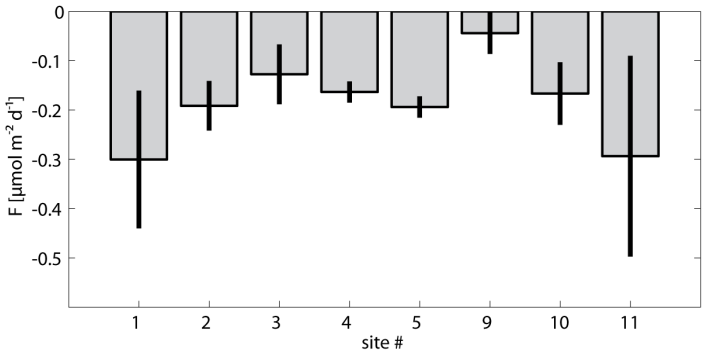


Figure 5.3.: Deep fluxes calculated from linear fits of the measured oxygen profiles on piston cores. Error bars represent 90% confidence intervals. Stations 6 was omitted due to the low number of data points below 1 m.

downwards and oxygenate deep layers. All piston cores within the central gyre were oxygenated over their entire length (up to 8 m, Fig. 5.1). The only station where oxygen did not penetrate to the base of the core is Station 12, farthest away from the center of the gyre, where oxygen penetrated about 1 m into the sediment. Generally, the piston cores showed a drop in oxygen concentration within the first meter from bottom water concentration (220 µmol $L^{-1}$) to 170 - 180 µmol $L^{-1}$. However, in the microsensor profiles, both-, ex situ and *in situ*, this same initial drop in concentration was already observed within the first few centimeters. The considerably greater interval over which this decrease occurred in the piston cores (∼1 m) most likely resulted from the coring process, mixing the top section of the cores (Buckley et al., 1994, Skinner and McCave, 2003).

The downward oxygen flux within the deep piston cores was constrained in two ways. First, we simply fitted a linear trend to the oxygen profile below 1 mbsf to obtain an estimate of the downward oxygen flux $F_d$ ($R_{deep}$=0). A decrease of $F_d$ towards the center of the gyre is suggested (Fig. 5.3), yet it is statistically not significant.

In a second step, we fitted a 1-D diffusion-reaction model (Eq. 5.3) to the deep profiles below 1 mbsf (Fig. 5.4) while varying the respiration rate ($R_{\mathrm{deep}}$) and the downward flux ($F_d$) at the lower boundary provides lower and upper constraints on the respiration rate. Figure 5.5 shows combinations of the parameter $R_{\mathrm{deep}}$ and $F_d$ that lead to the fits shown in Figure 5.4. Reasonably good fits could be obtained for $O_2$ consumption rates between zero and $\sim$ 30 µmol $m^{-3}$ $yr^{-1}$. Downward fluxes are likely to be below 0.3 µmol $m^{-2}$ $d^{-1}$ but above 0.05 µmol $m^{-2}$ $d^{-1}$ except for stations 6 and 9, where lower fluxes appear to be possible (Fig. 5.5). Note however that these fluxes and consumption rates are very small and, as shown in Figure 5.5, the downward flux $F_d$ correlates strongly with the oxygen consumption rate $R_{\mathrm{deep}}$, which makes that these two parameters are not well constrained. Additionally, different scatter in the data lead to values of $R^2$ of the best fitting model between 0.23 at station 9 and 0.91 at station 5.

Extrapolation of 10 exemplary profiles obtained from the range of well fitting parameters down

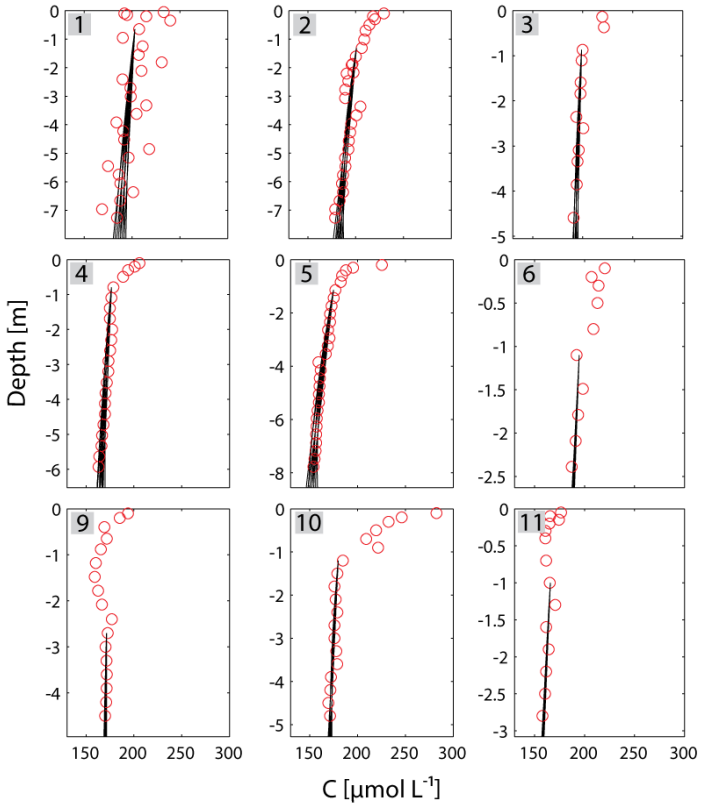


Figure 5.4.: Best fitting model runs for 9 different stations (black lines) as a result of a variation of the constant respiration rate $R_{\text{deep}}$ and the flux at the lower boundary $Fd$. Please note the different scales on the depth axis.

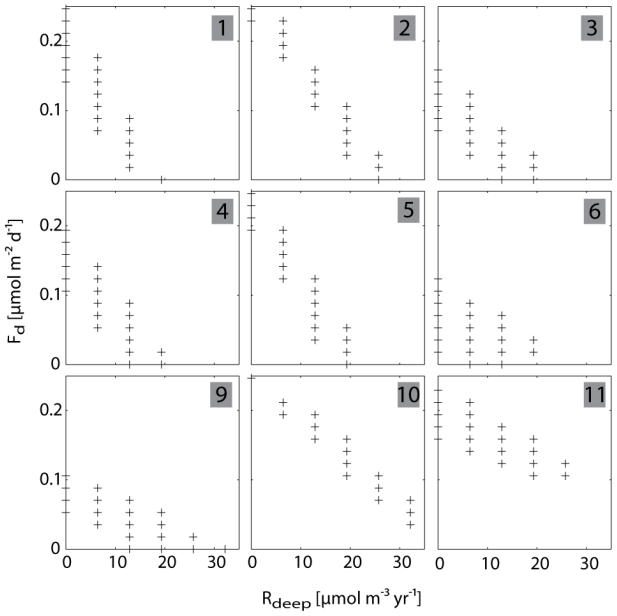


Figure 5.5.: Parameter combinations for the best fitting profiles of figure 5.4 and 5.6

to the basalt for each site, suggests the presence of oxygen within the entire sediment column (Fig. 5.6). Exceptions are station 1 and 11, where oxygen might have reached zero within the sediment. The complete oxygenation of the sediment column excludes all other electron acceptors from use and the low overall respiration rates deep in the sediment effectively stretch the zone over which the aerobic degradation of organic matter occurs to several meters.

The whole oxygen profile, including surface and deeper layers was modeled for all stations, where surface microsensor profiles were available (Stations 4-7 and 10), assuming exponentially decreasing rates in the top centimeters plus a constant term accounting for the deep aerobic respiration (Fig. 5.7).

A similar approach to model sediment $O_2$ profiles was taken by Hammond et al. (1996) for central Pacific sediments. However, they assumed a sum of two exponentially decreasing respiration terms and applied the model to coarse resolution porewater measurements of the top centimeters only. We found the model to be in excellent accord with the data ($R^2$>0.94) for all 5 stations. The exponential term can be explained by a pool of reactive organic matter which is being exploited by the microbial community, following first order reaction kinetics. Half of the reactive organic matter was consumed in depths ($z_{\mathrm{half}}$), varying between 1.3 mm (Station 4) and 6 mm (Station 10) (Fig. 5.7). Given that the sedimentation rate is in the order of 0.1 to 1 mm kyr$^{-1}$ (D'Hondt et al., 2009), a low rate constant for organic carbon oxidation can be expected and intraanual variations in sediment oxygen uptake are unlikely (Sayles et al., 1994).

By integrating the exponentially decreasing respiration rate $R_{\mathrm{surf}}$(z) over the whole sediment thickness using the best fitting parameter combinations, the integrated $O_2$ consumption in the

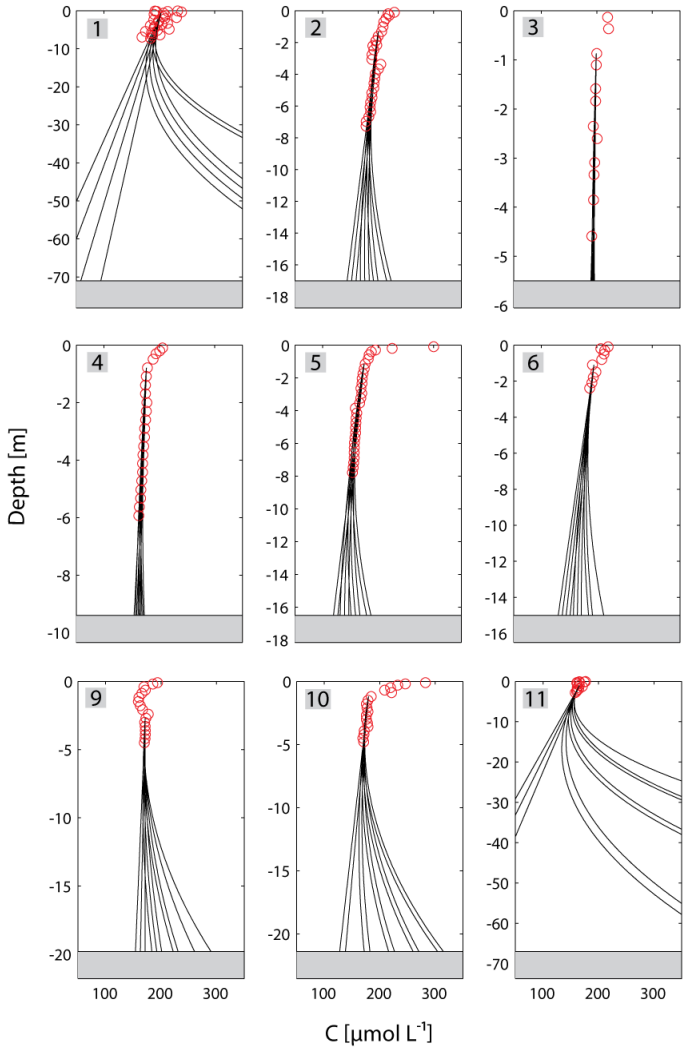


Figure 5.6.: Extrapolated profiles of oxygen concentration of 9 different stations down to the basalt (grey bar). Circles indicate measured oxygen concentrations; solid lines depict the extrapolations for different parameter constellations for the deep respiration rate and the flux (for further information see text)

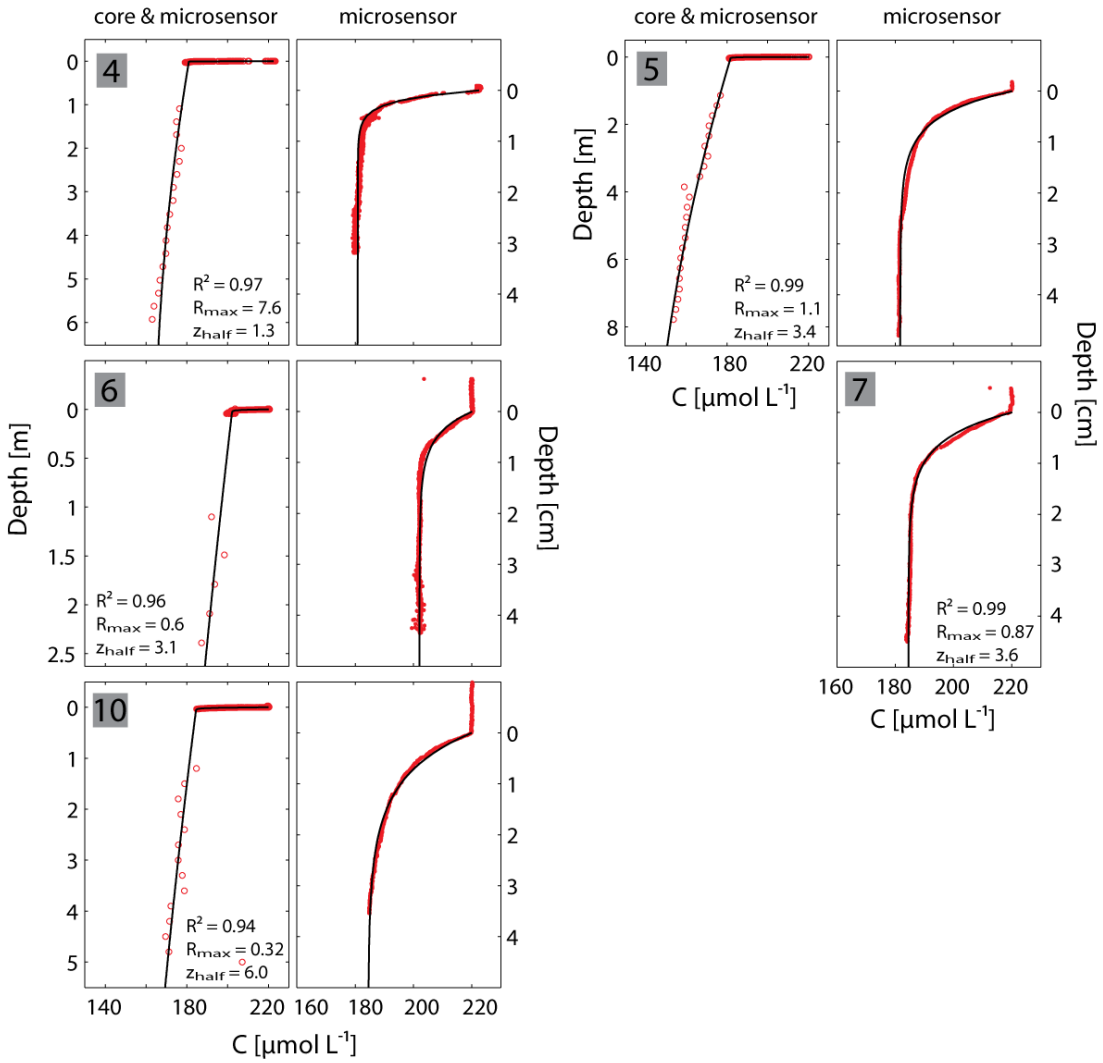


Figure 5.7.: Composed profiles of Stations 4-7 and 10, using data from piston core measurements and microprofiler (red symbols) and fitted model with exponentially decreasing respiration rates with depths for the upper sediment layer plus constant offset, accounting for deep respiration (solid line). The left panels show the composed profiles, whereas the right panels represent a magnification of the top 5 cm, showing microsensor data and model result only. For station 7, no deep measurements (below 1 m) were available. Units: $R_{\max}$ [nmol cm$^{-3}$ s$^{-1}$]; $z_{\text{half}}$ [mm].

Table 5.2.: Best fitting parameters of the combined surface and deep oxygen uptake model (Fig. 5.7, Eq. 5.5). The values for $F_{\mathrm{surf}}$ represent the total flux of oxygen due to the exponential (surface) term while $F_{\mathrm{deep}}$ are the respective fluxes due to the constant (deep) term (s. text for details).

| Stat. | $R_{\mathrm{deep}}$ [$\mu$mol m$^{-3}$ yr$^{-1}$] | $R_{\mathrm{max}}$ [$\mu$mol m$^{-3}$ s$-1$] | $z_{\mathrm{half}}$ [mm] | $F_{\mathrm{surf}}$ [mmol m$^{-2}$ d$-1$] | $F_{\mathrm{deep}}$ [$\mu$mol m$^{-2}$ d$^{-1}$] |
|---|---|---|---|---|---|
| 4 | 7.88 | 7.59 | 1.3 | 1.26 | 0.20 |
| 5 | 6.31 | 1.06 | 3.4 | 0.45 | 0.29 |
| 6 | 7.88 | 0.59 | 3.1 | 0.23 | 0.32 |
| 7 | 7.88 | 0.88 | 3.6 | 0.39 | 0.03 |
| 10 | 3.15 | 0.32 | 5.9 | 0.25 | 0.18 |

upper sediment layer is calculated ($F_{\mathrm{surf}}$, Eq. 5.7). It is 3-4 orders of magnitude higher compared to the deeper sediment as calculated by the integrated rate $R_{\mathrm{deep}}$ ($F_{\mathrm{deep}}$, Eq. 5.8) (Table 5.2). Given the small values of $z_{\mathrm{half}}$ (Table 5.2), more than 99.9% of the total oxygen that enters the sediment is consumed in the top few centimeters of the sediment and only a very small proportion is taken up by the deep subsurface or enters the basaltic basement. Since the DOU values (Table 5.1) were obtained by linear interpolation of the oxygen profiles within the top millimeter below seafloor, small differences to the summarized surface- and deep fluxes as obtained by the model were found.

The deep $O_2$ consumption can be fueled by slow degradation of highly refractory organic matter, up to millions of years old. The small decline of total organic carbon with depth in the deeper layers as reported by D'Hondt et al. (2009) would agree well with this. In this case, the low respiration term would not be constant but declining with such a low decrease with depth that it is not significantly different from a constant term. Another explanation for the relatively constant deep respiration would be the radiolysis of water due to radioactive decays in sediment grains (Blair et al., 2007, D'Hondt et al., 2009, Jørgensen and D'Hondt, 2006). This process, reported for continental rock by Lin et al. (2005), would split water in hydrogen and hydroxyl radicals. The hydrogen could act as electron donor while the hydroxyl radicals could further react to molecular oxygen. If this reaction is stoichiometric, the whole process is completely cryptic and is not reflected in the oxygen profiles at all, since the produced hydrogen and oxygen could be recombined microbially to water. If the hydroxyl radical, however, does not completely form molecular oxygen but further reacts with organic material or mineral surfaces, the additionally stimulated respiration could account for the constant respiration rate over depth that we observed. The bioavailability of refractory organic matter can be enhanced by reaction with the highly reactive hydroxyl radicals formed by radiolysis, stimulating deep respiration. A similar process is well known for the degradation of organic matter with ultraviolet light (Benner and Biddanda, 1998, Moran and Zepp, 1997, Zafiriou, 2002).

### 5.4.3. Basement fluxes

Previous studies have shown the possibility of seawater flowing through cracks and voids of the basalt that underlies marine sediments, and thus act as a source or sink of dissolved substances (D'Hondt et al., 2004). Extrapolations of our oxygen profiles show the possibility of fluxes across the sediment / basalt interface (Fig. 5.6). In a scenario with higher respiration rates, which still provides acceptable fits of the data (Fig. 5.4 & 5.5), this could lead to fluxes from the basalt to the sediment. However, for stations 3 and 4, where the piston core measurements reached close to the basalt, and hence the extrapolation procedure is the most reliable, such an efflux seems to be unlikely. The sediments from Stations 1 - 11 are geochemically similar and microbial cell numbers are comparable for these sites. Furthermore, high volumetric respiration rates are not supported by nitrate and alkalinity data (D'Hondt et al., 2009). Thus, a net flux of oxygen through the sediment into the basement at each site constitutes the most likely scenario, and leads to the question of possible sinks within the basalt. Oxygen could either be transported away by fluid flow within cracks and voids in the basalt (Fisher, 1998) or it could be reduced. One possibility would be the existence of a chemolitotrophic community within the basalt (Edwards et al., 2005, Stevens, 1997). Such communities were previously described for the flanks of the mid-ocean ridges (Ehrhardt et al., 2007, Huber et al., 2006) but their existence under the ocean basins remains controversial (Cowen et al., 2003). Drilling into the basalt under the SPG is necessary to further address this issue.

### 5.4.4. Regional and global relevance

Our sample sites cover a large part of the SPG. Therefore, we calculate that the total area of completely oxygenated sediments in this region is at least 10 - 15 million $km^2$, thus accounting for 3 - 4% of the global marine sediments. Murray and Grundmanis (1980) also found oxygen below 50 cm in equatorial Pacific sediments (hence outside of the SPG). Like the profiles obtained here, their oxygen profiles did not reach zero values but showed rather constant concentrations below an initial drop in the first several centimeters. Taking these findings into account, the fully oxygenated area is likely to be much larger, when including the deeply oxygenated sediment further north. Since the vast majority of all oxygen profiling measurements so far has been done in highly productive coastal areas or at mid-ocean ridges (Seiter et al., 2005, Wenzhöfer and Glud, 2002), it is likely that deep oxygen penetration also occurs in other low-productivity regions on earth, e.g. the North Pacific. Wenzhöfer et al. (2001) measured an *in situ* oxygen penetration depth of ∼25 cm in the Atlantic; comparable ex situ oxygen penetration depths were measured by Rutgers Van Der Loeff et al. (1990). Estimated carbon mineralization rates from the subtropical Atlantic gyre are in the order of 1.5 - 2 $gC\,m^{-2}\,yr^{-1}$ (Wenzhöfer and Glud, 2002) and compare well with rates from our sites (Tab. 1). However, they are based only on few *in situ* measurements. Considering only the central sites (Station 6 and 7) rates differ by a factor 2, highlighting the extreme setting of the central SPG as an ultimate oceanic desert.

## 5.5. Conclusions

The aim of this work was to measure and analyze oxygen fluxes and consumption rates in sediments of the South Pacific Gyre, the most oligotrophic oceanic region on earth, and to obtain information about the magnitude and spatial organization of carbon turnover. While the oxygen flux to the sediment is not extraordinary low compared to other oligotrophic sites, we found strong indications for oxygen penetrating down to the basalt in nearly the whole region. Oxygen consumption rates decrease strongly within the first few centimeters of the sediment and oxygen that is not reduced within this upper sediment horizon is free to diffuse further downwards. Even in the deeper layers, there is still a small and constant flux of oxygen.

**Acknowledgements.** The authors would like to thank all participants of the KNOX-02RR cruise and the crew of the R/V Roger Revelle for their expert work. We particularly thank Franciszek Hasiuk and Andrea Stancin for the shipboard resistivity measurements used to calculate formation factor. Axel Nordhausen's technical assistance on board was most helpful. Without the work of Ingrid Dohrmann, Gabriele Eickert, Paul Färber, Volker Meyer, Ines Schröder and Cäcilia Wiegand this study would not have been possible; Moritz Holtappels helped with the analytical solution of the model. We thank two reviewers for their helpful comments; especially Filip Meysman's effort helped a lot to improve the manuscript. We thank the Integrated Ocean Drilling Program of the US National Science Foundation for funding the expedition. We also thank the Max Planck Society and the German National Science Program (DFG) IODP program for funding the lead author's participation in the expedition and for sponsoring our post-cruise research. The service charges for this open access publication have been covered by the Max Planck Society.

# References


Antia, A., Koeve, W., Fischer, G., Blanz, T., Schulz-Bull, D., Scholten, J., Neuer, S., Kremling, K., Kuss, J., Peinert, R., 2001. Basin-wide particulate carbon flux in the Atlantic Ocean: Regional export patterns and potential for atmospheric $CO_2$ sequestration. Global Biogeochemical Cycles 15 (4), 845–862.

Archer, D., Emerson, S., Smith, C. R., 1989. Direct measurement of the diffusive sublayer at the deep sea floor using oxygen microelectrodes. Nature 340 (6235), 623–626.

Barnett, P., Watson, J., Connely, D., 1984. A multiple corer for taking virtually undisturbed samples from shelf, bathysal and abyssal sediments. Oceanlogica Acta 7, 399 – 408.

Behrenfeld, M., Falkowski, P., 1997. A consumer's guide to phytoplankton primary productivity models. Limnology and Oceanography 42 (1), 1479–1491.

Bender, M. L., Heggie, D. T., 1984. Fate of organic carbon reaching the deep sea floor: a status report. Geochimica et Cosmochimica Acta 48 (5), 977–986.

Benner, R., Biddanda, B., 1998. Photochemical transformations of surface and deep marine dissolved organic matter: Effects on bacterial growth. Limnology and Oceanography 43 (6), 1373–1378.

Berg, P., Rysgaard, S., Funch, P., Sejr, M. K., 2001. Effects of bioturbation on solutes and solids in marine sediments. Aquatic Microbial Ecology 26 (1), 81–94.

Berger, W. H., Fischer, K., Lai, C., Wu, G., 1987. Ocean productivity and organic carbon flux. i. overview and maps of primary production and export production. University of California, San Diego, SIO Reference 87-30, 67pp.

Berner, R., 1980. Early Diagenesis: A Theoretical Approach, 1st Edition. Princeton Series in Geochemistry. Princeton University Press.

Betzer, P., Showers, W., Laws, E., Winn, C., Ditullio, G., Kroopnick, P., 1984. Primary productivity and particle fluxes on a transect of the equator at 153∘W in the Pacific Ocean. Deep-sea research. Part A 31 (1), 1–11.

Blair, C. C., D'Hondt, S., Spivack, A. J., Kingsley, R. H., 2007. Radiolytic hydrogen and microbial respiration in subsurface sediments. Astrobiology 7 (6), 951–970.

Buckley, D. E., MacKinnon, W. G., Cranston, R. E., Christian, H. A., 1994. Problems with piston core sampling: Mechanical and geochemical diagnosis. Marine Geology 117 (1-4), 95–106.

Claustre, H., Huot, Y., Obernosterer, I., Gentili, B., Tailliez, D., Lewis, M., 2008. Gross community production and metabolic balance in the South Pacific Gyre, using a non intrusive bio-optical method. Biogeosciences 5, 463–474.

Claustre, H., Maritorena, S., 2003. The many shades of ocean blue. Science 302 (5650), 1514–1515.

Cowen, J. P., Giovannoni, S. J., Kenig, F., Johnson, H. P., Butterfield, D., Rappe, M. S., Hutnak, M., Lam, P., 2003. Fluids from aging ocean crust that support microbial life. Science 299 (5603), 120–123.

Dandonneau, Y., Vega, A., Loisel, H., du Penhoat, Y., Menkes, C., 2003. Oceanic rossby waves acting as a 'hay rake' for ecosystem floating by-products. Science 302 (5650), 1548–1551.

Daneri, G., Quinones, R., 2001. Undersampled ocean systems: a plea for an international study of biogeochemical cycles in the Southern Pacific Gyre and its boundaries. US JGOFS Newsletter 11 (1), 9.

D'Hondt, S., Jørgensen, B., Miller, D., Batzke, A., Blake, R., Cragg, B., Cypionka, H., Dickens, G., Ferdelman, T., Hinrichs, K., 2004. Distributions of microbial activities in deep subseafloor sediments. Science 306 (5705), 2216–2221.

D'Hondt, S., Spivack, A. J., Pockalny, R., Ferdelman, T. G., Fischer, J. P., Kallmeyer, J., Abrams, L. J., Smith, D. C., Graham, D., Hasiuk, F., Schrum, H., Stancin, A. M., 2009. Subseafloor sedimentary life in the South Pacific Gyre. Proceedings of the National Academy of Sciences 106 (28), 11651–11656.

Edwards, K. J., Bach, W., McCollom, T. M., 2005. Geomicrobiology in oceanography: microbe-mineral interactions at and below the seafloor. Trends in Microbiology 13 (9), 449–456.

Ehrhardt, C. J., Haymon, R. M., Lamontagne, M. G., Holden, P. A., 2007. Evidence for hydrothermal archaea within the basaltic flanks of the East Pacific Rise. Environmental Microbiology 9 (4), 900–912.

Fisher, A., 1998. Permeability within basaltic oceanic crust. Reviews of Geophysics 36 (2), 143–182.

Gehlen, M., Bopp, L., Emprin, N., Aumont, O., Heinze, C., Ragueneau, O., 2006. Reconciling surface ocean productivity, export fluxes and sediment composition in a global biogeochemical ocean model. Biogeosciences 3 (4), 521–537.

Glud, R. N., 2008. Oxygen dynamics of marine sediments. Marine Biology Research 4 (4), 243 – 289.

Glud, R. N., Gundersen, J. K., Revsbech, N. P., Jørgensen, B. B., 1994. Effects on the benthic diffusive boundary layer imposed by microelectrodes. Limnology and Oceanography 39, 462–467.

Hammond, D. E., McManus, J., Berelson, W. M., Kilgore, T. E., Pope, R. H., 1996. Early diagenesis of organic material in equatorial Pacific sediments: stoichiometry and kinetics. Deep Sea Research Part II 43 (4-6), 1365–1412.

Huber, J. A., Johnson, H. P., Butterfield, D. A., Baross, J. A., 2006. Microbial life in ridge flank crustal fluids. Environmental Microbiology 8 (1), 88–99.

Jahnke, R., 1996. The global ocean flux of particulate organic carbon: Areal distribution and magnitude. Global Biogeochemical Cycles 10, 71–88.

Jørgensen, B. B., D'Hondt, S., 2006. A starving majority deep beneath the seafloor. Science 314 (5801), 932–934.

Klimant, I., Meyer, V., Kühl, M., 1995. Fiber-optic oxygen microsensors, a new tool in aquatic biology. Limnology and Oceanography 40 (6), 1159 – 1165.

Li, Y.-H., Gregory, S., 1974. Diffusion of ions in sea water and in deep-sea sediments. Geochimica et Cosmochimica Acta 38 (5), 703–714.

Lin, L.-H., Hall, J., Lippmann-Pipke, J., Ward, J. A., Sherwood Lollar, B., DeFlaun, M., Rothmel, R., Moser, D., Gihring, T. M., Mislowack, B., Onstott, T. C., 2005. Radiolytic $H_2$ in continental crust: Nuclear power for deep subsurface microbial communities. Geochemistry, Geophysics, Geosystems 6.

Moran, M. A., Zepp, R. G., 1997. Role of photoreactions in the formation of biologically labile compounds from dissolved organic matter. Limnology and Oceanography 42 (6), 1307–1316.

Morel, A., Gentili, B., Claustre, H., Babin, M., Bricaud, A., Ras, J., Tièche, F., 2007. Optical properties of the "clearest" natural waters. Limnology and Oceanography 52 (1), 217–229.

Murray, J., Kuivila, K., 1990. Organic matter diagenesis in the northeast Pacific: transition from aerobic red clay to suboxic hemipelagic sediments. Deep-Sea Research Part I 37 (1), 59–80.

Murray, J. W., Grundmanis, V., 1980. Oxygen consumption in pelagic marine sediments. Science 209 (4464), 1527–1530.

Pace, M. L., Knauer, G. A., Karl, D. M., Martin, J. H., 1987. Primary production, new production and vertical flux in the eastern Pacific Ocean. Nature 325 (6107), 803–804.

Raimbault, P., Garcia, N., Cerutti, F., 2008. Distribution of inorganic and organic nutrients in the South Pacific Ocean - evidence for long-term accumulation of organic matter in nitrogen-depleted waters. Biogeosciences 5 (2), 281–298.

Ras, J., Claustre, H., Uitz, J., 2008. Spatial variability of phytoplankton pigment distributions in the Subtropical South Pacific Ocean: comparison between in situ and predicted data. Biogeosciences 5, 353–369.

Rasmussen, H., J. B. B., 1992. Microelectrode studies of seasonal oxygen uptake in a coastal sediment: Role of molecular diffusion. Marine Ecology Progress Series 81 (3), 289–303.

Reimers, C. E., Fischer, K. M., Merewether, R., Smith, K. L., Jahnke, R. A., 1986. Oxygen microprofiles measured in situ in deep ocean sediments. Nature 320 (6064), 741–744.

Reimers, C. E., Kalhorn, S., Emerson, S. R., Nealson, K. H., 1984. Oxygen consumption rates in pelagic sediments from the Central Pacific: First estimates from microelectrode profiles. Geochimica et Cosmochimica Acta 48 (5), 903–910.

Revsbech, N., 1989. An oxygen microsensor with a guard cathode. Limnology and Oceanography 34 (2), 474–478.

Rutgers Van Der Loeff, M. M., Meadows, P. S., Allen, J. A., 1990. Oxygen in pore waters of deep-sea sediments [and discussion]. Philosophical Transactions of the Royal Society of London. Series A 331 (1616), 69–84.

Sayles, F. L., Martin, W. R., Deuser, W. G., 1994. Response of benthic oxygen demand to particulate organic carbon supply in the deep sea near Bermuda. Nature 371, 686–689.

Schabenberger, O., Pierce, F. J., 2001. Contemporary statistical models for the plant and soil sciences. CRC Press, p. 343.

Schulz, H., Zabel, M., 2000. Marine Geochemistry, 1st Edition. Springer, Berlin, Heidelberg.

Seiter, K., Hensen, C., Zabel, M., 2005. Benthic carbon mineralization on a global scale. Global Biogeochemical Cycles 19 (1).

Skinner, L. C., McCave, I. N., 2003. Analysis and modelling of gravity- and piston coring based on soil mechanics. Marine Geology 199 (1-2), 181–204.

Smith, K. L., 1978. Benthic community respiration in the NW Atlantic Ocean: In situ measurements from 40 to 5200 m. Marine Biology 47 (4), 337–347.

Spinelli, G., Giambalvo, E. G., Fisher, A. T. (Eds.), 2004. Hydrologic properties and distribution of sediments. Hydrogeology of the Oceanic Lithosphere. Cambridge University Press, Cambridge, UK.

Stevens, T., 1997. Lithoautotrophy in the subsurface. FEMS Microbiology Reviews 20 (3-4), 327–337.

Suess, E., 1980. Particulate organic carbon flux in the oceans - surface productivity and oxygen utilization. Nature 288 (5788), 260–263.

Thamdrup, B., Canfield, D. E., 2000. Benthic respiration in aquatic sediments. In: Sala, O. E., Jackson, R. B., Mooney, H. A., Howarth, R. W. (Eds.), Methods in ecosystem science. Springer-Verlag, New York.

Weiss, R., 1970. The solubility of nitrogen, oxygen, and argon in water and seawater. Deep Sea Research A 17, 721 – 735.

Wenzhöfer, F., Glud, R., 2002. Benthic carbon mineralization in the Atlantic: a synthesis based on in situ data from the last decade. Deep-Sea Research Part I 49 (7), 1255–1279.

Wenzhöfer, F., Holby, O., Kohls, O., 2001. Deep penetrating benthic oxygen profiles measured in situ by oxygen optodes. Deep-Sea Research Part I 48 (7), 1741–1755.

Zafiriou, O., 2002. Sunburnt organic matter: Biogeochemistry of light-altered substrates. Limnology and Oceanography Bulletin 11 (4), 69–74.

# Concluding Remarks and Perspectives

Oxygen is a key element in the global biogeochemical cycles and oxygen fluxes in marine sediments can be used to determine carbon mineralization rates. Almost all reducing equivalents from organic carbon oxidation in marine sediments finally end up reducing molecular oxygen. This happens either directly during aerobic respiration or indirectly by reoxidation of reduced compounds released by anaerobic processes. This thesis presents studies on oxygen distribution and oxygen dynamics in marine sediments on different spatial scales and in contrasting environments. It comprises laboratory and field studies as well as the development of novel measurement technology.

In **Chapter 2** a new high resolution planar optode (HiPO), based on the combination of fiber optics with $O_2$ imaging technology is described. This technique enables the concurrent imaging of light and oxygen distributions within sediments. By means of this method, light-driven microscale heterogeneities of oxygen concentrations in photic sediments can be investigated. Since the HiPO also exhibits increased accuracy in oxygen imaging compared to conventional planar optodes, it is particularly suited to calculate rates of production and respiration by mathematical modeling of the transient $O_2$ concentration field. The technique was successfully used to study the coupling between autotrophic and heterotrophic communities in sandy sediments and their dependence on local light conditions. Pronounced heterogeneities in the distribution of respiration and photosynthesis rates existed and were clearly correlated to the likewise patchy scalar irradiance within the sediment. Changes in the illumination were reflected by immediate changes in the oxygen distribution. In contrast to this fast response of the microbial community to changing light conditions, several hours were still needed to re-establish steady-state conditions in the sediment oxygen distributions.

**Chapter 3** reports on benthic oxygen dynamics in shallow, subtidal photic sands of the Kattegat at water depths of $\sim$10 m. Sandy subtidal sediments are largely understudied with respect to oxygen dynamics and especially benthic primary production is poorly constrained. The different methods that exist to determine benthic oxygen fluxes *in situ* all act on different characteristic time and length scales. In order to decouple spatial and temporal variability in this highly dynamic system planar optodes, microsensors, incubation chambers and an eddy correlation instrument were deployed simultaneously. Considerable spatial variability was present

on scales ranging from centimeters to kilometers, often correlated with faunal activity. Primary production by microphytobenthos was detected but benthic oxygen dynamics were dominated by the influence of fauna and macroalgae. The sediment was net heterotrophic at all observed light conditions. Strong changes in incident light and mechanical perturbations of the sediment resulted in transient oxygen concentrations within the sediment, sometimes lasting for several hours. Non-steady state situations in these sandy sediments are thus likely to be prevalent. This is an important finding that should be taken into account if microsensor-derived oxygen fluxes are used to quantify benthic carbon mineralization, since especially the calculation of depth-resolved respiration rates from microprofiles relies on the steady-state assumption. While this study yielded data about short-term variability, it also raises questions about changes in benthic mineralization on time scales of days to months. It is a great technological and logistic challenge to approach these questions.

A contrasting environment to the highly productive and dynamic coastal sediment was found in the South Pacific Gyre, the most oligotrophic marine environment on earth, as described in **Chapter 4 and 5**. For the first time, benthic mineralization rates were constrained by oxygen flux measurements and were found to be in the order of 0.4 - 1.5 $\mathrm{gC\,m^{-2}\,yr^{-1}}$ for a region of about 10 - 15 million $\mathrm{km^2}$. At all study sites faunal activity was negligible and POC fluxes were so low that almost all bioavailable organic carbon was oxidized in a thin surface layer of the sediment. Volumetric respiration rates dropped several orders of magnitude within these upper five centimeters as revealed by mathematical modeling of microprofiles. Deeper in the sediment, microbial cell numbers were exceptionally low but the per-cell respiration rates exceeded those of more active deep-sea sediments. The downward diffusion of oxygen overran oxygen consumption by microbial respiration and in consequence, oxygen was measured even at eight meter below the seafloor. The difference between sampling sites that were hundreds of kilometers apart was notably small in this respect. Extrapolations of the oxygen distribution in the deep profiles suggested completely oxic sediment and an $O_2$ flux to the underlying basalt bedrock for a large region within the South Pacific. Recent measurements in the subtropical North Atlantic showed similar results, underlining the global importance of these oligotrophic regions (pers. communication Timothy G. Ferdelman and Hans Røy). Given the large area of the subtropical gyres, it is not unlikely that almost half of the global ocean sediments show very deep oxygen penetration.

There are still large undersampled regions like the Arctic Ocean and the Subtropical Gyres. Here, benthic mineralization rates are poorly constrained. Therefore, exploratory studies (**Chapter 4 and 5**) are still needed to complete global carbon flux budgets. Furthermore, even in the well-studied regions, little is known about the spatial variability of benthic carbon mineralization on scales ranging from millimeters to kilometers. This implies a high risk that extrapolations are carried out from findings that are not representative. Temporal variability of carbon fluxes to the seafloor on different timescales has also been investigated only for a few sites, further complicating up-scaling attempts. Mathematical models of early diagenetic processes, being appropriate to investigate the temporal response of marine sediments to changes in organic

matter input, are not able to tackle the driving forces that determine these changes (e.g., fluxes of organic matter, benthic primary production and light regime, benthic activity patterns). To overcome these limitations, long-term *in situ* monitoring, complemented with studies on different spatial scales (**Chapter 3**) seems to be the natural next step. While suitable sensors for the monitoring of physical parameters are widely available, only few chemical sensors are applicable for long-term use to this point. The fast developing field of optical sensing is most promising in this respect. Currently, new optode materials with enhanced performance and durability emerge on the market. A combination of fiber optics with imaging technology allows the parallel use of hundreds of fiber-optodes; a working example of such an instrument has been developed as a by-product of this thesis. By this approach, long-term data for benthic and pelagic oxygen dynamics could be easily attained, particularly if methods of *in situ* calibration are developed. Together with the evolution of low power consuming microcomputers, and modern composite structural materials, autonomous, small and smart instruments for multi-parameter long-term measurements come into reach. These instruments would allow combined monitoring of benthic oxygen exchange and other biogeochemical parameters like pH, $H_2S$, $pCO_2$, $Ca^{2+}$ over extended periods of time and with high spatial coverage and thus help to improve the knowledge about spatio-temporal dynamics of benthic biogeochemical processes.

# Appendix A.

# Two-dimensional mapping of photopigments distribution and activity of Chloroflexus-like bacteria in a hypersaline microbial mat

---

Ami Bachar[1], Lubos Polerecky[1], Jan P. Fischer[1], Kyriakos Vamvakopoulos[1], Dirk de Beer[1], Henk M. Jonkers[1,2]

Published in FEMS Microbiology Ecology **65** (2008) 434-448

**Abstract**

Pigment analysis in an intact hypersaline microbial mat by hyperspectral imaging revealed very patchy and spatially uncorrelated distributions of photopigments Chl *a* and BChl *a*/c, which are characteristic photopigments for oxygenic (diatoms and cyanobacteria) and anoxygenic phototrophs (Chloroflexaceae). This finding is in contrast to the expectation that these biomarker pigments should be spatially correlated, as oxygenic phototrophs are thought to supply the Chloroflexaceae members with organic substrates for growth. We suggest that the heterogeneous occurrence is possibly due to sulfide, which production by sulfate-reducing bacteria may be spatially heterogeneous in the partially oxic photic zone of the mat. We furthermore mapped the near infra-red light controlled respiration of Chloroflexaceae under light and dark conditions and found that Chloroflexaceae are responsible for a major part of oxygen consumption at the lower part of the oxic zone in the mat. The presence of Chloroflexaceae was further confirmed by FISH probe and 16S rRNA gene clone library analysis. We assume that species related to the genera Oscillochloris and 'Candidatus Chlorothrix', in contrast to those related to Chloroflexus and Roseiflexus, depend less on excreted photosynthates but more on the presence of free sulfide, which may explain their presence in deeper parts of the mat.

[1]Max Planck Institute for Marine Microbiology, Bremen, Germany
[2]Delft University of Technology, Delft, The Netherlands

# Appendix B.

# Presentations and Field Trips during my PhD study

## B.1. Oral presentations

- **Innovative Technologies for high resolution measurements of biogeochemical processes**
  J. P. Fischer, F. Wenzhöfer
  Visit of a Chinese delegation at AWI and MARUM, March 9, 2006 Bremerhaven, Germany

- **Benthic Primary Production in subtidal Sands: Variability on different scales**
  J. P. Fischer and F. Wenzhöfer
  11th International Symposium on Microbial Ecology (ISME-11), August 20-25, 2006 Vienna, Austria

- **Benthic Oxygen Dynamics in the photic zone - spatial organization of $O_2$ production and respiration measured in high resolution 2D**
  J. P. Fischer and F. Wenzhöfer
  ASLO 2007 Aquatic Sciences Meeting, February 4-9, 2007 Santa Fe, New Mexico

- **Benthic biogeochemical studies in coastal marine sediments on different spatial and temporal scales using the mobile sensor platform C-MOVE**
  F. Wenzhöfer, C. Waldmann, J. P. Fischer, M. Bergenthal, H. Røy
  ASLO 2007 Aquatic Sciences Meeting, February 4-9, 2007 Santa Fe, New Mexico

- **Extreme oligotrophy in subsurface sediments of the South Pacific Gyre: Evidence from low oxygen fluxes**
  J. P. Fischer, T. Ferdelman, S. D'Hondt, F. Wenzhöfer, and KNOX-02RR Shipboard Scientific Party
  Goldschmidt 2007, August 19-24, 2007 Cologne, Germany

- **Deep oxygen penetration in ultra-oligotrophic South Pacific Sediments**
  J. P. Fischer, T. Ferdelman, S. D'Hondt, F. Wenzhöfer, and KNOX-02RR Shipboard Sci-

entific Party
International Workshop on Microbial Life under Extreme Energy Limitation 'The Starving Majority', October 21-24, 2007 Aarhus, Denmark

## B.2. Poster presentations

- **Distribution and quantification of benthic primary production in sandy coastal sediments**
  J. P. Fischer, F. Wenzhöfer, R. N. Glud
  ASLO 2005 Summer Meeting, June 19-24, 2005 Santiago de Compostella, Spain

- **Benthic Oxygen Dynamics in the photic zone - spatial organization of $O_2$ production and respiration measured in high resolution 2D**
  J. P. Fischer and Frank Wenzhöfer
  Visit of the MPI advisory board, Febrary 2008

- **Oxygen dynamics in ultra-oligotrophic sediments of the South Pacific Gyre**
  J. P. Fischer, T. Ferdelman, S. D'Hondt, F. Wenzhöfer, and KNOX-02RR Shipboard Scientific Party
  Visit of the MPI advisory board, Febrary 2008

## B.3. Research Cruises / Field trips

- WATT cruise 04A, German Wadden Sea, 26 October - 6 November, 2004
- Helsingør, Field trip, April 2005
- Sylt, Field trip, April 2006
- F/S Heincke, Cruise He 254, Kattegat, July 4-13, 2006
- R/V Roger Revelle, Cruise KNOX-02RR, South Pacific, 17 December 2006 - 27 January 2007
- F/S Meteor, Cruise M76/2, Namibia, 17 May - 04 June, 2008

# Danksagung

Sehr viele Menschen haben auf die eine oder andere Art zum Zustandekommen dieser Arbeit beigetragen und ich bin sehr dankbar dafür. Zunächst möchte ich Frank Wenzhöfer dafür danken, dass er mich in jeder Hinsicht unterstützt hat und mir den Freiraum einräumte auch unkonventionelle Ideen zu verfolgen. Antje Boetius danke ich für ihre Unterstützung und für die Energie, mit der sie sich für ihre Gruppe einsetzt und dafür, dass sie diese Arbeit begutachtet hat. Dieter Wolf-Gladrow danke ich für seine Bereitschaft das Erstgutachten zu übernehmen und für Diskussionen und Hilfe bei Berechnungen.

Viele Menschen am Max-Planck-Institut für marine Mikrobiologie waren zunächst Kollegen und sind im Laufe der Jahre zu Freunden geworden. Mit Simone Böer und Gunter Wegener hatte ich die besten Büro"mitbewohner" die ich mir vorstellen kann. Hans Røy danke ich für die anregenden Gespräche über unsere vielen gemeinsamen wissenschaftlichen und privaten Interessen. Besonders danke ich auch Rita Dunker, Janine Felden, Moritz Holtappels, Felix Janssen, Anna Lichtschlag und Marc Viehweger für die spannende und entspannende Zeit, die ich mit ihnen verbracht habe.

Für Unterstützung und kreative Umsetzung eigentlich unmöglicher technischer Ideen in kürzester Zeit danke ich Axel Nordhausen, Marc Viehweger, Volker Asendorf, Paul Färber, Volker Meyer, Georg Herz, Alfred Kutsche, und Harald Osmers.

Keine einzige Mikrosensormessung wäre ohne die Unterstützung von Gabriele Eickert, Cecila Wiegand, Ingrid Dohrman, Karin Hohman und Ines Schröder möglich gewesen, die die Senoren gebaut haben. Bernd Stickford hat auch noch die abseitigste Literatur besorgt. Für Anmerkungen zu den Manuskripten danke ich Simone Böer, Rita Dunker, Stefanie Grünke, Moritz Holtappels, Felix Janssen, Hans Røy, Daniel Santillano und Gunter Wegener sowie allen meinen Koautoren und ganz besonders Frank. Dirk de Beer und Timothy Ferdelman danke ich für viele anregende Diskussionen. Bedanken möchte ich mich auch bei den Mitgliedern meines *Thesis Committees*, Dieter Wolf-Gladrow and Heribert Cypionka, für ihre Anregungen und die aufgebrachte Zeit. Prof. Ulrich Fischer, Christina Bienhold und Katrin Schmidt danke ich für ihre Bereitschaft, an meinem Prüfungsausschuss mitzuwirken.

Sehr dankbar bin ich auch meinen Freunden und ganz besonders meinen Eltern für all ihre Unterstützung auf so vielen verschiedenen Ebenen.

# Erklärung

Hiermit versichere ich, dass ich die vorliegende Arbeit

- ohne unerlaubte fremde Hilfe angefertigt habe,
- keine anderen als die von mir angegebenen Quellen und Hilfsmittel benutzt habe, und
- die den benutzten Werken wörtlich oder inhaltlich entnommenen Stellen als solche kenntlich gemacht habe

Bremen, 08. September, 2009